DEVICE ENGINEERING FOR ENHANCED EFFICIENCY FROM PLATINUM(II) PHOSPHORESCENT OLEDs

Minghang Li, B.S.

Dissertation Prepared for the Degree of

DOCTOR OF PHILOSOPHY

UNIVERSITY OF NORTH TEXAS

August 2010

APPROVED:

Nigel Shepherd, Major Professor
Mohammad Omary, Co-Major Professor
Rick Reidy, Committee Member
Jincheng Du, Committee Member
Mohammed El Bouanani, Committee Member
Narendra Dahotre, Chair of the Department of Materials Science and Engineering
Costas Tsatsoulis, Dean of the College of Engineering
James D. Meernik, Acting Dean of the Robert B. Toulouse School of Graduate Studies

Li Minghang, Device Engineering for Enhanced Efficiency from Platinum(II) Phosphorescent OLEDs. Doctor of Philosophy (Materials Science and Engineering), August 2010, 193 pp., 133 figures, 20 tables, 204 chapter references.

Phosphorescent organic light emitting diodes (PHOLEDs) based on efficient electrophosphorescent dopant, platinum(II)-pyridyltriazolate complex, bis[3,5-bis(2-pyridyl)-1,2,4-triazolato]platinum(II) ($Pt(ptp)_2$) have been studied and improved with respect to power efficiency, external efficiency, chromacity and efficiency roll-off. By studying the electrical and optical behavior of the doped devices and functionality of the various constituent layers, devices with a maximum EQE of 20.8±0.2 % and power efficiency of 45.1±0.9 lm/W (77lm/W with luminaries) have been engineered. This improvement compares to devices whose emission initially could only be detected by a photomultiplier tube in a darkened environment. These devices consisted of a 65 % bis[3,5-bis(2-pyridyl)-1,2,4-triazolato]platinum(II) ($Pt(ptp)_2$) doped into 4,4'-bis(carbazol-9-yl)triphenylamine (CBP) an EML layer, a hole transporting layer/electron blocker of 1,1-bis[(di-4-tolylamino)phenyl]cyclohexane (TAPC), an electron transport layer of 1,3,5-tris(phenyl-2-benzimidazolyl)-benzene (TPBI), and a LiF/Al cathode. These devices show the acceptable range for warm white light quadrants and qualify to be called "warm white" even w/o adding another emissive layer.

Dual EML devices composed of neat $Pt(ptp)_2$ films emitting orange and CBP: $Pt(ptp)_2$ film emitting blue-green produced a color rendering index (CRI) of 59 and color coordinates (CIE) of (0.47,0.49) at 1000Cd/m² with power efficiency of 12.6±0.2 lm/W and EQE of 10.8±0.2 %. Devices with two blue fluorescent emission layers as singlet filters and one broad yellow emission layer from CBP: $Pt(ptp)_2$ displayed a CRI of 78 and CIE of (0.28,0.31) at 100Cd/m² with maximum power efficiency of 6.7±0.3 lm/W and EQE of 5.7±0.2%.

ACKNOWLEDGMENTS

There are a number of people whom I am indebted a tremendous amount of thanks to and would like to acknowledge.

First and foremost, I would like to thank my main advisor Dr. Nigel Shepherd and co-advisor Dr. Mohammad Omary for their supervision, advice, guidance and support during the course of my doctoral research here in UNT. Their dedication to research and their students, and, their knowledge of science and people has impressed and encouraged me in many aspects in the past four years. I am lucky to have them both as mentors. I am also particularly grateful and thankful to my colleague Ming-Te Lin for the great work we achieved and experienced together.

Secondly, I am thankful to my committee members Drs. Jincheng Du, Rick Reidy and Mohammed El Bouanani for serving in my dissertation panel. To the members of MTSE departmental staff: Wendy Agnes, Joan Jolly, Lindsay Quinn, April Porter, John Sawyer and David Garrett, thank you so much! The friendship and help of Unnat Bhansali, Huiping Jia(UTD), Fangling Kuo, Mohammad Maneshian, Shailesh Vidhate, Koffi Dagnon, Sandeep Manandhar, Arun Devaraj, Antariksh Singh, Benedict Mensah, Eric Osei-Yiadom, Maia and Bill Bischof are very much appreciated.

Thirdly and most importantly, I thank my parents, Weiguo Li and Jiru Wang whose solid support, continuous encouragement, unconditional love and sacrifice made this happen. I would like to thank my husband Xudong Ruan for his love, everyday support and understanding, my unborn baby boy Binghua Ruan and all my cousins for their encouragement and care in their own special ways. I love them and owe them more than they know.

Lastly, I would like to thank the Almighty Lord for protecting, reinforcing and giving me inspiration throughout the course of this research work.

TABLE OF CONTENTS

Page

LIST OF TABLES

Page

LIST OF FIGURES

Page

CHAPTER 1

INTRODUCTION

1.1 Motivation

With the promise of being ten times more efficient than incandescent lighting, organic light emitting diodes (OLEDs) can potentially change the way we light our homes and businesses. Significant potential advantages of OLEDs over current fluorescent lamps and incandescent bulbs include low power consumption, no mercury content, suitability for flexible substrates, and low cost with relatively easy fabrication.

White light can be achieved by a variety of ways including combining red, green and blue emission from in three separate layers, mixing red, green and blue dopants in a single emissive layer, and down converting blue emission with yellow phosphors. The limitations of all of these strategies include lengthy processing procedures, the possibility of energy transfer from the higher emission energy dopants to the lower emission energy dopants, unbalanced exciton distributions in the three separate layers, limited power and external quantum efficiencies for fluorescent materials, huge efficiency roll-offs for phosphorescent materials at higher current density and brightness, and voltage dependent color instability etc. Most recently, platinum (II) phosphorescent materials have attracted attention due to their unique photochemical and structural characteristics and suitability for white OLED applications. Their attractive features include a variety of emissive excited states, broad emission spectra, and, efficiency and color stability. However there is still a significant need for improved performance of platinum (II) based OLEDs in terms of both efficiency and

stability for future applications. It was reported by Forrest's group that by combining the monomer and excimer emission from platinum (II)(2-(4',6'-difluoro-phenyl)pyridinato-N,$C^{2'}$) (2,4-pentanedionate) (FPt1) with the blue emission from a fluorescent dopant (FIrpic), broad emission with a color rendering index (CRI) of 78, a peak external quantum efficiency (EQE) of 4.0±0.4 % and peak power efficiency (PE) of 4.4±0.4 lm/W could be obtained 78[1]. Pt(N^C^N) complexes and (PtL2Cl): N^C^N-coordinated terdentate ligands based on 1,3-dipyridylbenzene have been synthesized and reported by Williams, Cocchi, Kalinowski and co-workers. A color rendering index of 90 with an external quantum efficiency of 6.5% was achieved [2] by using Mtdata: 4,4',4″-tris(*N*-(3-methylphenyl)-*N*-phenylamino)triphenylamine as an electron donor and PtL2CL as electron acceptor. Jabbour's group has reported that by incorporating the broad excimer emission of platinum(II) [2-(4′,6′-difluorophenyl)pyridinato-*N*,N,$C^{2'}$)](2,4-pentanedionato) (FPt) with a novel host material together with judicious engineering of the device structure, external quantum efficiency can be improved from 5.7% (5.2 lm/W, 11.8 Cd/A) to 15.9% (12.6 lm/W, 37.8 Cd/A) at 500 Cd/m² with a maximum CRI 75 [3]. Doping concentration is essential to controlling the relative monomer/excimer emission ratio and CRI of all of these devices. Device performance based on platinum(II) emission is very sensitive to the host material, device structure and layer thicknesses. Therefore, smart engineering for enhanced efficiencies of platinum(II) phosphorescent OLEDs is very important. A new phosphorescent complex, bis[3,5-bis(2-pyridyl)-1,2,4-triazolato]platinum(II)= $Pt(ptp)_2$ has been synthesized and evaluated in white organic light emitting diodes to quantify its performance compared to other Pt(II) complexes. Key comparison metrics were power and external quantum efficiency,

CRI, and efficiency roll-off at high device current and brightness.

1.2 Major Contributions of Dissertation

By varying the doping level in x% $Pt(ptp)_2$:CBP thin films, the ratio of monomer to excimer emission could be adjusted. This phenomenon was observed in both the photoluminescence and electroluminescence behaviors. Near white OLEDs with peak external quantum and power efficiencies of 13.16±0.04 % (at 178 Cd/m²) 27.80±0.16 lm/W (at 14 Cd/m^2) were demonstrated. The corresponding efficiency numbers at a practical brightness of 1000 Cd/m^2, were 12.40±0.07 %, and 21.10±0.12 lm/W respectively. The $Pt(ptp)_2$ dopant level in these devices was 65%, N,N'-dicarbazolyl-3,5-benzene(mCP) was the electron/exciton blocker layer, the CIE coordinates were (0.44,0.51), and the CRI was 49 at 1000 Cd/m^2.

By studying and comparing the electrical and optical behavior of the devices doped at different concentration levels and thickness effects, devices were engineered for optimal exciton confinement and recombination. These structures consisted of an emissive layer (EML) with 65 % bis[3,5-bis(2-pyridyl)-1,2,4-triazolato]platinum(II) ($Pt(ptp)_2$) doped into 4,4'-bis(carbazol–9-yl)triphenylamine (CBP), a hole transporting layer/electron blocker of 1, 1-bis[(di-4-tolylamino)phenyl]cyclohexane (TAPC), an electron transport layer of 1,3,5-tris(phenyl-2-benzimidazolyl)-benzene (TPBI) and a LiF/Al cathode. These structures exhibited the highest peak EQE of 20.8 ±0.2 % at 247 Cd/m², power efficiency of 45.1±0.9 lm/W at 28.6 Cd/m². The corresponding numbers at 1000 Cd/m² were 19.3±0.7% and 32.6±1 lm/W respectively.

Dual EML devices composed of a neat $Pt(ptp)_2$ layer emitting orange and CBP:

$Pt(ptp)_2$ layer emitting blue-green were studied in an attempt to developed "balanced white". However, these devices could only be categorized as "warm" due to a deficiency of blue emission. At 1000Cd/m², a power efficiency of 12.6±0.2 lm/W, EQE of 10.8±0.2 %, CRI of 59 and CIE of (0.47, 0.49) were achieved. Dual EML devices using Mtdata and CBP as host produced more balanced white emission with a CRI of 63 at 13V, and CIE of (0.37,0.49). By combing fluorescent emission from BCzVBi and yellow broad-band phosphorescent emission from CBP: $Pt(ptp)_2$ device with two blue fluorescent emission layers as singlet filters, a CRI of 78, and CIE of (0.28,0.31) at 100Cd/m² , and a maximum power efficiency of 6.7±0.3 lm/W and EQE of 5.7±0.2 % were obtained.

1.3 Organization of Dissertation

This dissertation has six main chapters. This chapter, Chapter 1, provides an introduction and summary for the whole work. Chapter 2 presents a background of OLEDs operation as well as a general overview of the current research and development status of OLED materials and devices. In Chapter 3 the structural, chemical and photoluminescence properties of $Pt(ptp)_2$ thin films are presented. Chapter 4 reports the results of optimizing $Pt(ptp)_2$ device structures for higher power and quantum efficiency. The results of device chromacity tuning for more balance white emission is documented in Chapter 5. In Chapter 6, conclusions and future work are presented and discussed.

1.4 References

[1]B. W. D'Andrade, J. Brooks, V. Adamovich, M. E.Thompson, S. R. Forrest, Adv. Mater

14,1032(2002).

[2] J. Kalinowski, M. Cocchi, D. Virgili, V. Fattori and J. A. G. Williams, Adv. Mater **19**, 4000 (2007).

[3] E. L. Williams, K. Haavisto, J. Li, and G. E. Jabbour, Adv. Mater **19**, 197(2007)

CHAPTER 2

LITERATURE REVIEW

2.1 Introduction

Electroluminescence (EL), by definition, is the nonthermal generation of light resulting from application of an electric field to, or driving a current through a substance [1], normally a semiconductor. There are two basic methods for obtaining EL. For In the first mechanism light is generated by electron and hole injection, and subsequent recombination at a semiconductor p-n junction [2]. This is the mechanism exploited in semiconductor LEDs, lasers and organic light emitting diodes (OLEDs). In the second type of EL, light is generated by impact excitation of a luminescent center embedded in a wide bandgap semiconductor host by high-energy electrons [1]. Ac thin-film EL, ac powder EL device, dc EL device and dc powder EL device are all categorized in this group.

Below, an overview of the historical development of electroluminescence technology as well as a brief discussion of OLED technology progress is given. Important Figures of Merit to electrically and optically characterize OLEDs are reviewed. This is followed by a review of the interesting device architectures that are used for balancing carrier transport and chromatic tuning. The basic physical property requirements for organic molecular light emitting materials are also covered. The physical processes for achieving light emission are discussed. Finally a review of the limitations and problems in the current OLED technology is presented.

2.2 Historical Review of Electroluminescence Technologies

Electroluminescence technology has undergone a tremendous revolution since its discovery by Henry Round in 1907 who obtained light emission by passing a current though a silicon carbide detector. The item "Electroluminescence" was first used by Georges Destriau in 1936, who obtained the emission of light from zinc sulfide powders under an applied voltage. After that, the attempt to create a commercial ceramic electroluminescent lamp by GTE Sylvania necessitated a fundamental understanding of EL device physics [3]. The first practical form of a thin film electroluminescent device was discovered by Vlasenko and Popkov in 1960. The device was composed of a crystalline electroluminescent phosphor sandwiched between two dielectric layers as Fig 2.1 shows [3].

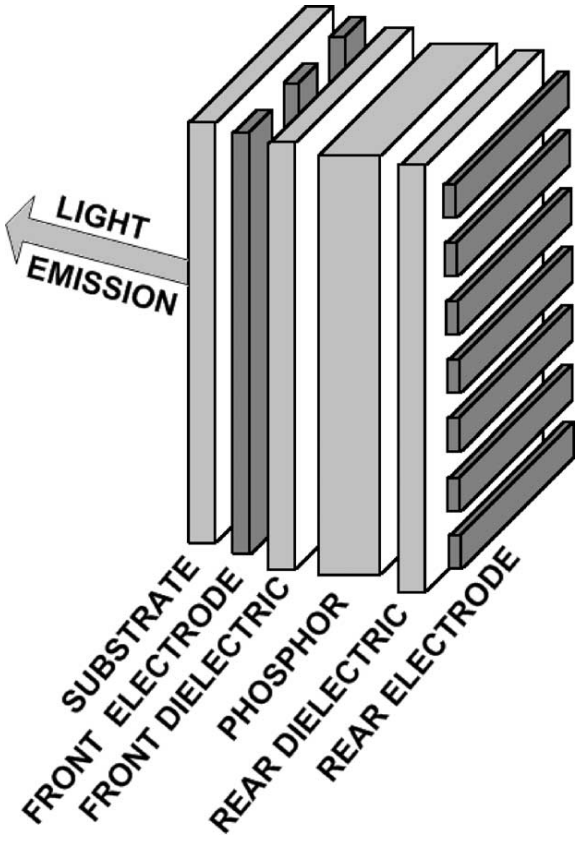

Figure 2.1 Schematic of a TEFL device. Reproduced from Reference [3].

It took this technology almost two decades, and, the development of blue phosphor SrS: Cu, SrS: Se between 1993 and1997 [4] to overcome the limitation of monochrome emission.

Since the early 1960s the field of integrated optics and optoelectronics has undergone very rapid development as a result of extensive use of semiconductor epitaxial growth technology such as MBE and MOCVD. Semiconductors, due to their bandgap structure, give a variety of electrical and optical properties suitable for a range of electronics and optoelectronics. The first commercial GaAsP light- emitting diodes (LED) were introduced in 1962. Nowadays, in some portions of the visible region, the efficiency of some GaAs-based LEDs exceeds that of the filtered fluorescent lamps of the same color and is a factor of 3 of white fluorescent lamps. Inorganic semiconductor light emitting diodes experienced very rapid growth as a result of the increased fundamental understanding of their band structures. With regard to bandgap type, semiconductors can be categorized into two groups: direct and indirect semiconductors. In direct bandgap semiconductors the minimum of the conduction band occur at the same k values with the maximum of the valence band. On the other hand, in indirect bandgap semiconductors, the minimum of the conduction band is not aligned with the maximum of the valence band. Fig 2.2 is the energy gap versus lattice constant and emission wavelength for a range of III-V ternary and quaternary compounds. Especially, InGaAs, InGaAsP, and InAlGaAs are good candidates for light sources such as LEDs, because they are direct bandgap and have very high radiative recombination efficiencies.

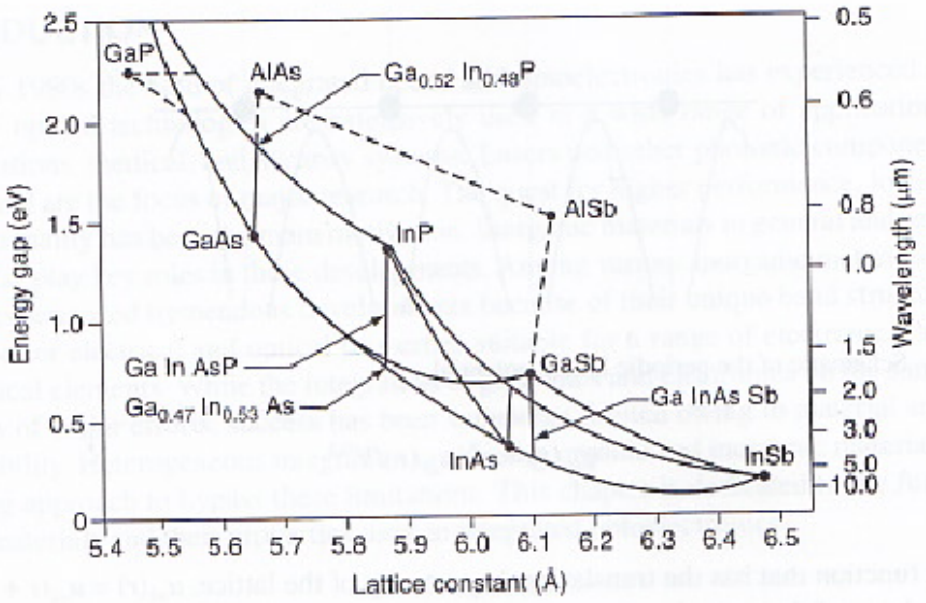

Figure 2.2 Energy gap versus lattice constant versus emitting wavelength for III-V semiconductor. Reproduced from Reference [2]

The simplest LED devices are composed of a p-n junction being separated by a junction plane. When the two sides are in contact as in Fig 2.3, majority carriers which are holes in the p-type material will diffuse into n-type material, leaving negative space charges behind. On the other hand, majority carriers which are electrons in the n-type material will diffuse into p-type material, leaving positive space charges behind. In the forward bias, holes will be injected into the p-type part and electrons will be injected into the n-type part. If the applied voltage is high enough, the injected electron and holes will diffuse to the space charge zone and recombine to produce photons. In direct bandgap semiconductors, radiative recombination dominates which leads to light emission. On the other hand, for the indirect gap materials the probability for radiative recombination is low, and injected charge recombine without producing light.

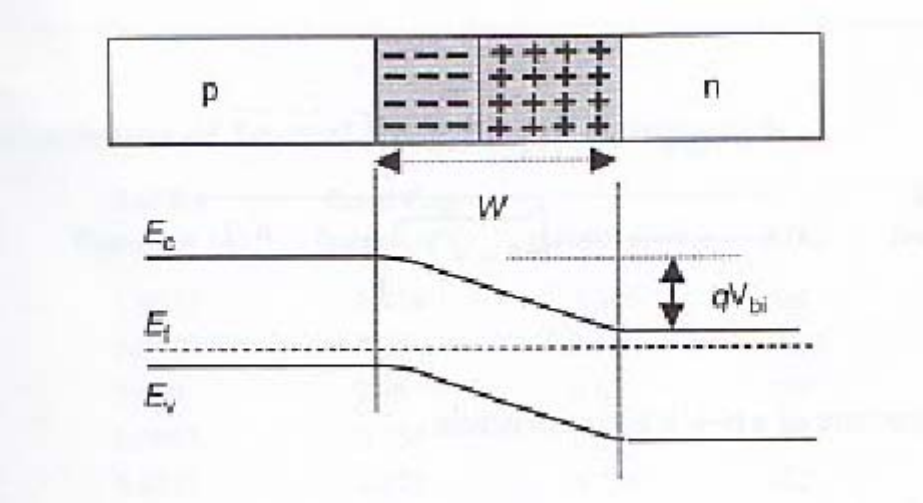

Figure 2.3 A p-n junctions for LED application. Reproduced from reference [2].

The advent of OLED technology electroluminescence (EL) technology has generated a good deal of interest. Organic EL, by definition, is the electrically driven emission of light from a noncrystalline organic material. The first bi-layer organic light emitting device which required a moderate driving voltage and produced promising luminous efficiency was announced by C.W.Tang and his team at Kodak in 1987 [13]. In Fig 2.4, hole transport layer (HTL) materials is introduced to create a heterojunction which facilitates hole-injection and simultaneously enhances the probability of exciton formation and recombination near the interface region.

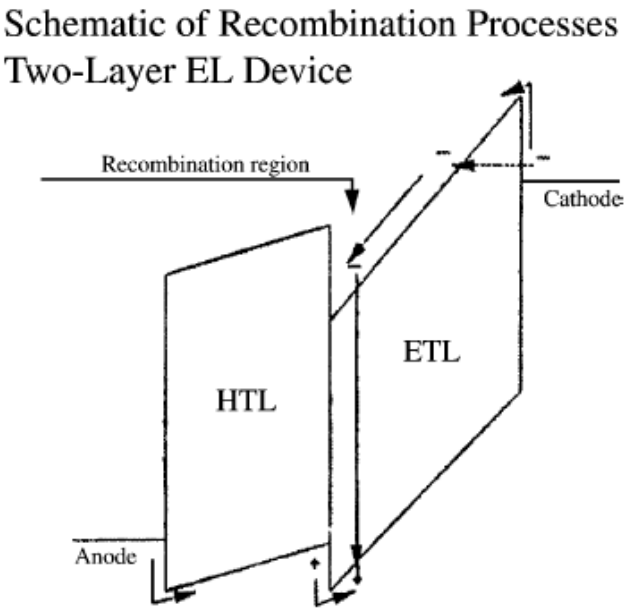

Figure 2.4 Energy level diagram of a bi-layer OLED. Reproduced from reference [5].

Shortly after Tang's device, a conducting polymer-based LED was introduced by Friend's [6, 7] group at Cambridge. Since then, several groups working on OLEDs and PLEDs have been exerting their efforts for improving luminous and power efficiency, chromatic tuning, device stability, etc. with the goal of achieving full-color displays, and commercial general lighting.

2.3 Perspective: Comparison of Inorganic and Organic Electroluminescence

Among semiconductor light emitting devices can be placed in either of two groups which are characterized by the emitting material. Namely, inorganic EL devices and organic EL devices. Inorganic EL, by definition, is the electrically driven emission of light from crystalline inorganic material. Due to the presence of a periodic crystalline structure and a well-defined density of states, band-type transport is dominant in inorganic LEDs [2].

Compared to inorganic solids, there are no well-defined, continuous density of states in organic materials, which are instead characterized by their, highest occupied molecular orbital (HOMO), and lowest unoccupied molecular orbital (LUMO). Electronic transport is accomplished by electrons hopping along LUMOs close to cathode side and holes along HOMO close to anode side.

To date, inorganic LED have been used in a wide range of applications from indicators and numeric alphanumeric displays to automotive interior and telecommunication applications(telephone screens and backlighting) [8]. Semiconductor lasers are widely used in various commercial and defense applications. Compact lasers with very low threshold current, high spectral purity, high power, and high beam quality have been demonstrated over a wide wavelength range[8]. The best external quantum efficiency achieved among these devices exceeds 50% [9]. Table 2.1 is a LED material and wavelength chart from the LEDtronics company [10]. The whole visible range is covered by these diodes, and shows the potential of solid state lighting to replace incandescent lamps. Large radiative emission efficiency LED materials are good candidates for this application.

Table 2.1. LED materials and wavelength chart from LEDtronics.

Peak Wave length (nm)	Dominant Wave length (nm)	Color Name	Nominal Fwd Voltage (V_f@20ma)	Intensity (mcd) 5mm LEDs (For Reference)	Radiant Power mW/sr	LED Die Material
843	N/A	Infrared	1.7	N/A	86mW@50mA	GaAIAs/

						GaAs
654	641	Ultra Red	1.9	1000mcd@20mA	13mW@20mA	GaAIAs/GaAlAs
640	625	HE Red	2.0	220mcd@20mA	1.8mW@20mA	GaAsP/GaP
634	624	Super E.Red	2.2	8000mcd@20mA	45mW@20mA	InGaAIP
616	610	Super Orange	2.0	2000mcd@20mA	7mW@20mA	InGaAIP
609	604	Orange	2.0	220mcd@20mA	0.7mW@20mA	GaAsP/GaP
598	593	Super Yellow	2.0	5000mcd@20mA	10mW@20mA	InGaAIP
592	589	Super P.Yellow	2.3	4000mcd@20mA	8mW@20mA	InGaAIP
582	584	Yellow	2.1	170mcd@20mA	0.3mW@20mA	GaAsP/GaP
3000K	N/A	Warm White	3.3	5500mcd@20mA	17mW@20mA	InGaN
6000K	N/A	Pale White	3.3	5500mcd@20mA	17mW@20mA	InGaN
8000K	N/A	Cool White	3.3	5800mcd@20mA	23mW@20mA	InGaN
575	573	Super	2.0	1800mcd@20m	3mW@20mA	InGaAIP

		L.Green		A		
563	569	HE Green	2.3	210mcd@20mA	0.03mW@20mA	GaP/GaP
563	564	Super P.Green	2.1	400mcd@20mA	0.6mW@20mA	InGaAIP
557	560	Pure Green	2.2	140mcd@20mA	0.2mW@20mA	GaP/GaP
522	528	Aqua Green	3.4	15,000mcd@20mA	30mW@20mA	InGaN
501	502	Blue Green	3.4	4300mcd@20mA	16mW@20mA	InGaN
455	460	Super Blue	3.2	3000mcd@20mA	61mW@20mA	InGaN
425	447	Ultra Blue	4.0	250mcd@20mA	5mW@20mA	SiC/GaN
402	420	Ultra Violet	3.8	39mcd@20mA	53mW@20mA	SiC/GaN

Reproduced from reference [10].

Despite tremendous progress in the performance of III-V-based LED technology, the rate of commercialization for solid state lighting is slow and due to cost as well as competition with existing incandescent and fluorescent lamps. For flat-panel displays, the drive circuitry and diode costs make high-resolution and large area screens extremely expensive. Also MBE and MOCVD, both of which are considered expensive and required advanced technical knowhow, are the most widely used methods to prepare inorganic EL thin films by far. Compared to other technologies, organic light emitting diodes can be fabricated

by wet solution processing and dry thermal evaporation, both of which are considerably cheaper than MBE or MOCVD. The potential advantages over other technologies are obvious: low cost, easy fabrication, solution processable [9], light weight, and low power consumption and flexible substrate applications.

2.4 Historical Review and Progress in OLED Research and Technology

2.4.1 The First Bilayer OLED Device

In the 1960s, organic electroluminescence was observed in single crystal anthracene and tetracene doped anthracene by M. Pope and H. P. Kallmann. The first organic electroluminescent device, which required very high operating voltages was demonstrated in the same paper[11]. In separate attempts by Helfrich and Schneider, ~ 100 V or above was required to inject charges into the organic crystals. Although they announced a high external quantum efficiency of ~5% could be achieved by this type of device, less than 0.1%W/W power-conversion efficiency led to limited interest for practical application [12]. In 1987, Tang and Van Slyke's report on a double-organic-layer electroluminescent device was a major breakthrough of organic electroluminescent devices [13].

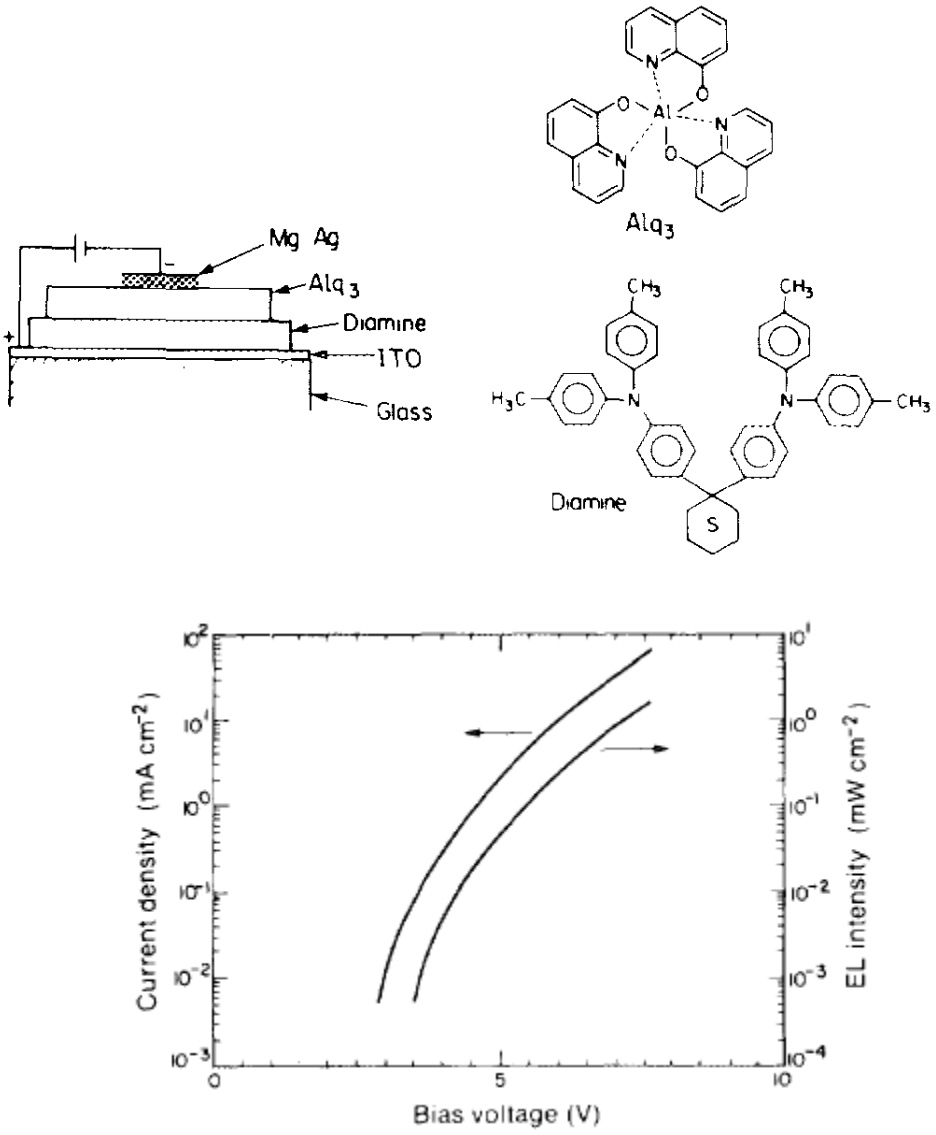

Figure 2.5 First bi-layer OLED configuration and its I-V characteristics

This structure which is shown in Fig 2.5, used diamine as the hole transport layer and Alq3 as both the electron transport and emitting layer. The applied voltage necessary for producing brightness above 1000 Cd/m^2 was significantly reduced to below 10V. The peak power efficiency was 1.5lm/W. Since the first commercial 64X256-pixel OLED display car stereos was produced by Pioneer Corp in 1997, more and more OLEDs have been produced and immense research efforts have been devoted to improving the color gamut, luminance

efficiency and device reliability. Those efforts include electrode modifications, synthesis of new organic materials, and device structures [13].

2.4.2 Electrode Modifications

Electrode modifications are performed to ensure minimal interface barriers for electron and hole injection into the organic layers i.e., to ensure better workfunction alignment between the injecting and receiving layers. Because ITO is the most common material used as the anode and is in direct contact with organic material, the surface characteristics of ITO directly affect the electrical and optical behavior of the device. Anode modification can be sorted into several approaches: plasma pretreatment of the ITO, modification by organic additives, and, inorganic and hybrid materials. The as-received ITO substrates usually have a workfunction of about 4.5eV, while the HOMO level of HTL or emissive layer (EML) material is ordinarily below 5.0eV. Thus, there is a large interface barrier between the anode and organic layer [15,16]. Reducing the barrier between the Femi level of the anode and the organic layer is critical for a low device turn-on voltage. Traditional methods such as Ultra-Violet Ozone, oxygen plasma, acid treatment and thermal annealing are all well investigated and developed for the purpose of increasing work function of ITO. More recently, very thin metal coated on ITO by e-beam evaporation, for example, Au, Sn, Pb, Pt, has been demonstrated to increase the work function of ITO by 0.6eV or more, and the contact with hole transport materials such as N,N'-Bis(3-methylphenyl)- N,N'-bis(phenyl)-benzidine (TPD) is nearly ohmic leading to dramatically improved hole injection current[17][18]. OLEDs using an ultra thin metal oxide layer including Al_2O_3 [19],

CuOx [20], Tb_4O_7, ZnO, Y_2O_3, Nb_2O_5, and Pr_2O_3 [21] have all exhibited higher luminous efficiency and lower turn on voltage. Cathode modification includes Alkali metals fluorides such as LiF [22], CsF [23], NaF [24], which act as buffer layers and can lower the turn on voltage and increase the luminous efficiency. The lower turn on voltage may attribute to surface dipole formation and electron extraction enhancement. Nanoscale interfacial modification layers, for example, Ca(acac)2 [25], Langmuir-Blodgett films[26] , have also been investigated and developed as electrode modification methods. These mechanisms include enhancing electron injection, preventing luminescence quenching from cathode and increasing the barrier for hole injection, etc.

2.4.3 The Design of EL Materials

The design of EL materials for use in OLEDs is one of the most important factors for optimal device performance, as is the case for all electronic and optical devices.

Charge carriers can combine to form excitons either in the singlet or in the triplet manifold of the molecule. By harvesting both triplet and singlet exciton, phosphorescent material can achieve nearly 100% internal EL efficiency [30][31]. One of the critical advancements in the development of OLED display technology can be attributed to the discovery of the guest-host doped emitter system [28]. This is because a single host material can be used together with a variety of highly fluorescent guest dopants leading to a gamut of electroluminescence with high efficiencies. Another advantage of the doped emitter system in OLEDs is the transfer of electrogenerated excitons from host to highly emissive and stable dopants which increases the possibility radiative decay [29]. Energy transfer from host to

dopant by excitons and only singlet states are harvested by fluorescent material which only represents 25% of the total excited states, the rest of 75% are wasted as shown in Fig 2.6. Phosphorescent material instead by harvesting all four possible spin orientations of excitons (1 singlet and 3 triplets), 100% IQE can be achieved.

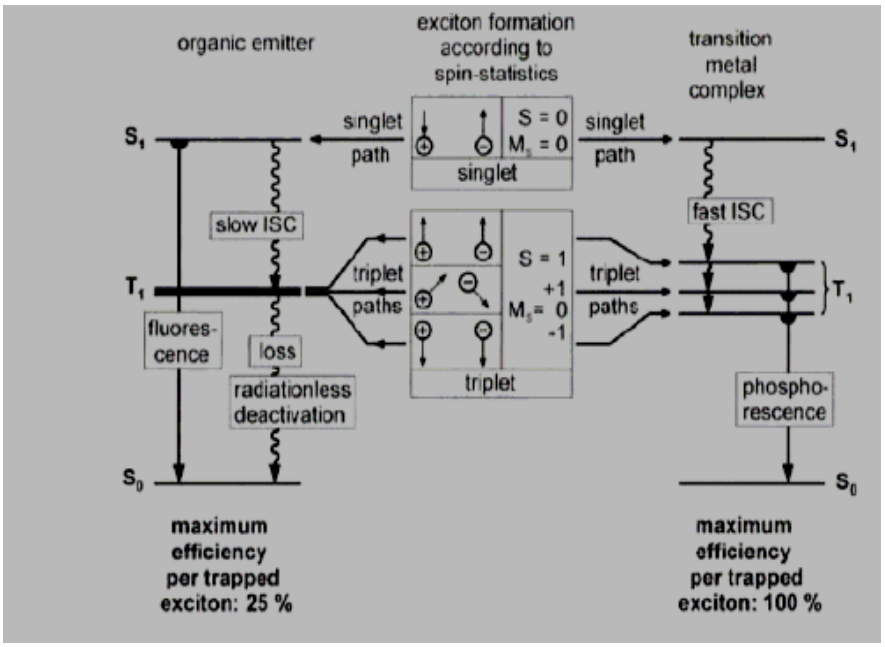

Figure 2.6 Explanation of triplet harvesting phenomenon to achieve higher efficiencies [30]

2.4.4 Outcoupling Improvement

External quantum efficiency is proportional to internal quantum efficiency as well as outcoupling efficiency. Light which is generated from the light emitting layer travels in all directions and be subjected to two possibilities: escape from the device or be trapped by in the multilayer stack due to internal reflection and differences in refractive index. Most of the light generated is are either trapped in the organic layers or emitted out from the edge of an OLED device. It is known that the fraction of light escaped from the substrate is,

$\eta_{cp,ext} = \frac{1}{2n_{org}^2}$. For the purpose of application of ITO as anodes in OLEDs, refractive index (n) of glass is around 1.5, and only 20% of the total emitted light is outcoupled in the direction of the viewer. Light out-coupling techniques have been implemented to enhance the external efficiency of OLEDs including shaped substrate technique [32], micro-lens arrays [33] and two-dimensional photonic crystal structure [34], etc.

2.5 Important Figures of Merit to Characterize OLEDs Electrically and Optically

2.5.1 Threshold Voltage

Threshold voltage can be determined from the LED or OLED's IV curve, and is the intercept of the current curve in the linear regime with the voltage axis. In the Fig 2.7, V_t is the threshold voltage.

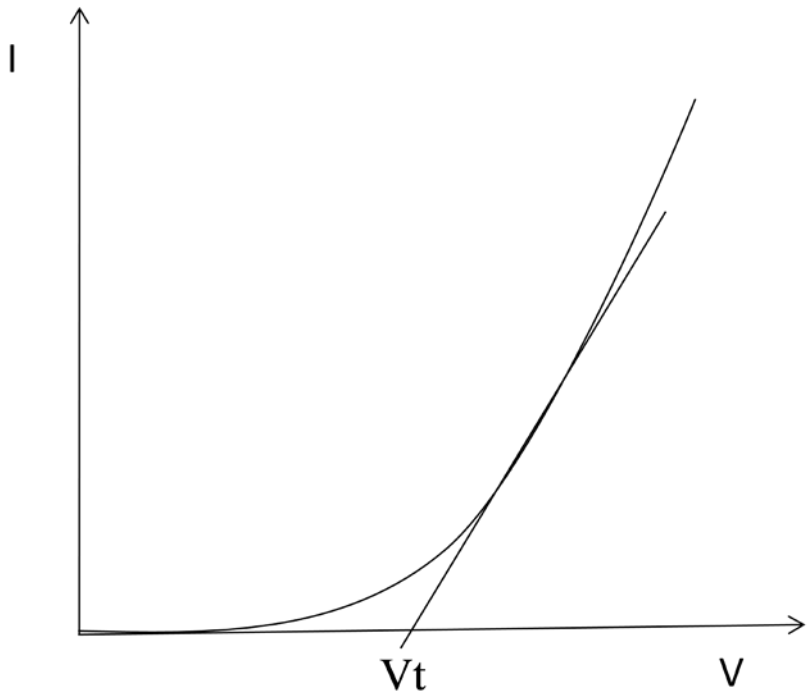

Figure 2.7 Typical IV curve in LED and OLED

2.5.2 Radiance and Luminance [70]

Radiance, by definition, is a measure of flux density per unit solid viewing angle expressed in W/cm^2/sr. Radiance is independent of distance for an expected area source, because the sampled area increases with distance, cancelling inverse square losses. The radiance, shown in Fig 2.8, L,of a diffuse (Lambertian) surface is related to the radiant existence (flux density), M, of a surface by the relationship : L=M/π. Some luminance units (asb,L,fL)already contain π in the denominator, allowing simpler conversion to illuminance units[70].

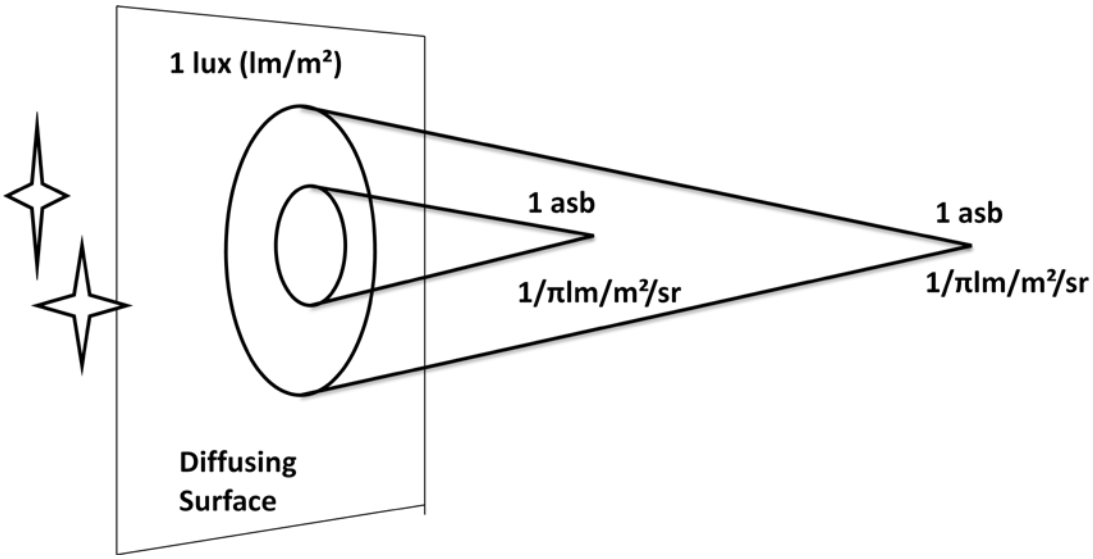

Figure 2.8 Radiance. Reproduced from Reference [70]

Luminance is a photometric measure of the luminous intensity per unit area of light travelling in a given direction. It describes the amount of light that is emitted from a particular area, and falls within a given solid angle

Luminance is defined by $L_V = \frac{d^2F}{dAd\Omega\cos\theta}$

Where

L_v is the luminance (cd/m^2),

F is the luminous flux or luminous power (lm),

θ is the angle between the surface normal and the specified direction

A is the area of the surface (m^2),and

Ω is the solid angle (sr).

2.5.3 Internal Quantum Efficiency and External Quantum Efficiency [71]

The internal quantum efficiency, η_{int}, defined as the ratio of the number of photons produced within an EL device to the number of electrons flowing through the external circuit[71] or

$$\eta_{int} = \frac{\#\text{of photons emitted from active region per second}}{\#\text{of electrons injected into LED/OLED per second}}$$

Similarly, external quantum efficiency η_{ext} is defined as

$$\eta_{ext} = \frac{\#\text{of photons emitted into free space per second}}{\#\text{of electrons injected into LED/OLED per second}}$$

The external quantum efficiency gives the ratio of usable photons emitted out of the device to the number of injected electrons.

$$\eta_{ext} = \eta_{int}\ \eta_{ph} = \gamma\, \eta_{ex}\, \Phi_p\, \eta_{ph}\ [72]$$

Where η_{ph} is the light out-coupling efficiency, η_{ex} is the fraction of total excitons formed which result in singlet excitons (from spin statistics , η_{ex} ~1/4 for fluorescent molecular dyes, and 1 for phosphorescent materials), γ is the electron hole charge balance factor or in other words, the fraction of injected charge carriers forming excitons, and Φ_p is the quantum yield (the photoluminescence efficiency) of the dopant. Because only singlets are radiative in fluorescent materials, η_{ex} ~1/4 , η_{ext} is limited to 5%, assuming η_{ph}

~$1/2n^2$~20% for a glass substrate with index of refraction n=1.5. In contrast, both singlets and triplet can be radiative by using high efficiency phosphorescent materials, and η_{int} can approach 100%, in which case η_{ext} ~20% can be expected [72]. External quantum efficiency is commonly calculated from experimental data by

$$\eta_{ext} = \frac{5.0 \times 10^3}{(h\nu)\varphi(\lambda)} LE$$

Where

LE is the luminous efficiency

$h\nu$ is the photon energy (in eV) of the emission

$\varphi(\lambda)$ is the photonic luminosity function

2.5.4 Luminous Efficiency and Power Efficiency

Luminous efficiency /power efficiency is the ratio of luminous flux (in lumens) to power (usually measured in Amps or watts). For OLED application, it is defined as the ratio of luminous flux emitted from the device to the electric current or power consumed by driving a current through it, and thus describes how well the amount of electricity can be converted into an amount of light.

$$\text{Luminous efficiency LE (cd/A)} = \frac{L}{j}$$

$$\text{Power efficiency PE (lm/W)} = \frac{\pi * L}{jV}$$

Where

L is the luminance

j is the current density

V is the applied voltage

2.5.5 CIE and CRI

CIE and CRI are both quantitative methods for evaluating chromaticity.. In the study of the spectral distribution of phosphors, one of the first mathematically defined color spaces was the CIE 1931 XYZ color space. It was created by the International Commission on Illumination (CIE) in 1931[73] by plotting on a two-dimensional graph with three values (x, y and z=1-x-y coordinates). Primary color for blue (λ=435.8nm), green(λ=546.1nm),and red(λ=700nm) were used as monochromatic sources in the 1931 CIE system.

The tristimulus values for a color with a spectral power distribution I(λ) are given in terms of the standard observer by

$$Y = \int_0^\infty I(\lambda)\,\overline{y}(\lambda)\,d\lambda \quad X = \int_0^\infty I(\lambda)\,\overline{x}(\lambda)\,d\lambda$$

$$Z = \int_0^\infty I(\lambda)\,\overline{z}(\lambda)\,d\lambda$$

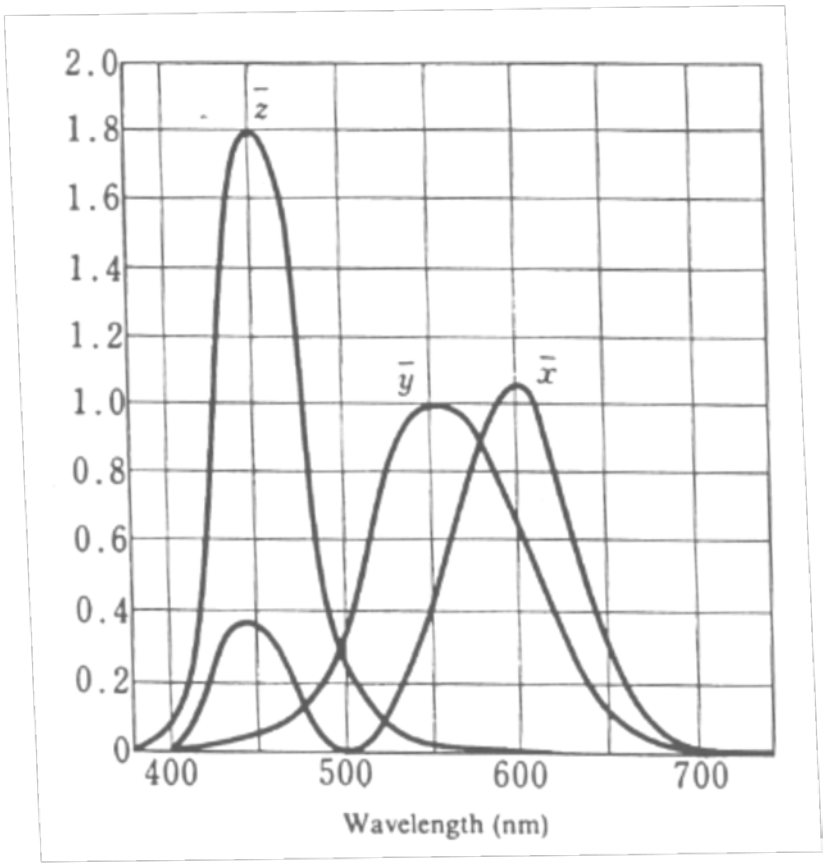

Figure 2.9 Red(x), green(y),and blue(z) tristimulus curves. Reproduced from Reference [73].

The derived color space specified by x, y, and Y is known as the **CIE xyY** color space and is widely used to specify colors in practice.

The chromatic coordinates are calculated from

$$x=\frac{X}{X+Y+Z},\ y=\frac{Y}{X+Y+Z},\ z=\frac{Z}{X+Y+Z}=1-x-y$$

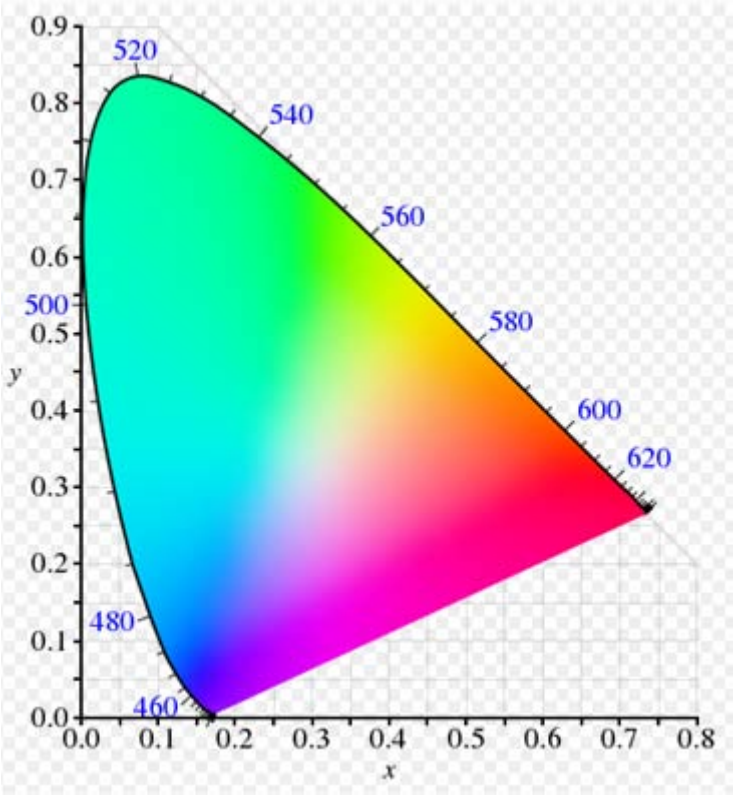

Figure 2.10 1931 Commission de L'Eclariage chromaticity diagram. Reproduced from reference [73].

The color rendering index (CRI) (sometimes called color rendition index), is a quantitative measure of the ability of a light source to reproduce the colors of various objects faithfully in comparison with an ideal or natural light source.

2.6 Organic Light Emitting Diode Structures

2.6.1 Monochrome Structures

Monochrome OLEDs emit primarily a single color and can contain two or multiple layers. Multiple layer emitting devices may contain fluorescent dyes or phosphorescent dyes in their emitting layers.

Fig 2.11 shows a typical, well-designed stack of an OLED. It consists of a series of

thin layers which are either solution-processed or vacuum-deposited. Under forward bias, holes are injected from a transparent anode, which is composed of a non-stoichiometric composite of SnO2(10-20%) and In2O3(90%-80%), called ITO. Adjacent to this anode layer, a hole injection/transport layer(HTL) with its HOMO energy matching the workfunction of the transparent anode is normally used for balanced hole transport to the EML. On the other hand, an electron injection layer (EIL)/electron transport layer (ETL) with its LUMO energy matching the workfunction of the cathode needs to be suitably chosen to facilitate a well-balanced electron transport into EML from the other side. It has been shown that an ultrathin LiF layer with appropriate thickness will increase the electron injection capacity from the cathode to organic layer [35] and also keeps the ETL from chemical reactions with the cathode materials [36]. Apparently, although the efficiency of hole and electron transport to EML must be high, it is also important to achieve the balance of electron and hole transport to avoid ohmic losses and maximize the OLED device efficiency. Ohmic losses can be avoided by inserting a electron-blocker layer [37] between HTL and EML and/or and hole blocking layer[38] between ETL and EML. The LUMO of EBL can prevent electrons from leaving EML. At the opposite side, the HOMO of HBL can prevent holes from leaving EML. As a result of spatially confining electrons and holes to the emissive layer, the device efficiency can be dramatically increased. However; high charge densities can be built up at the interfaces and lead to unfavorable device lifetime and carrier transport characteristics [39].

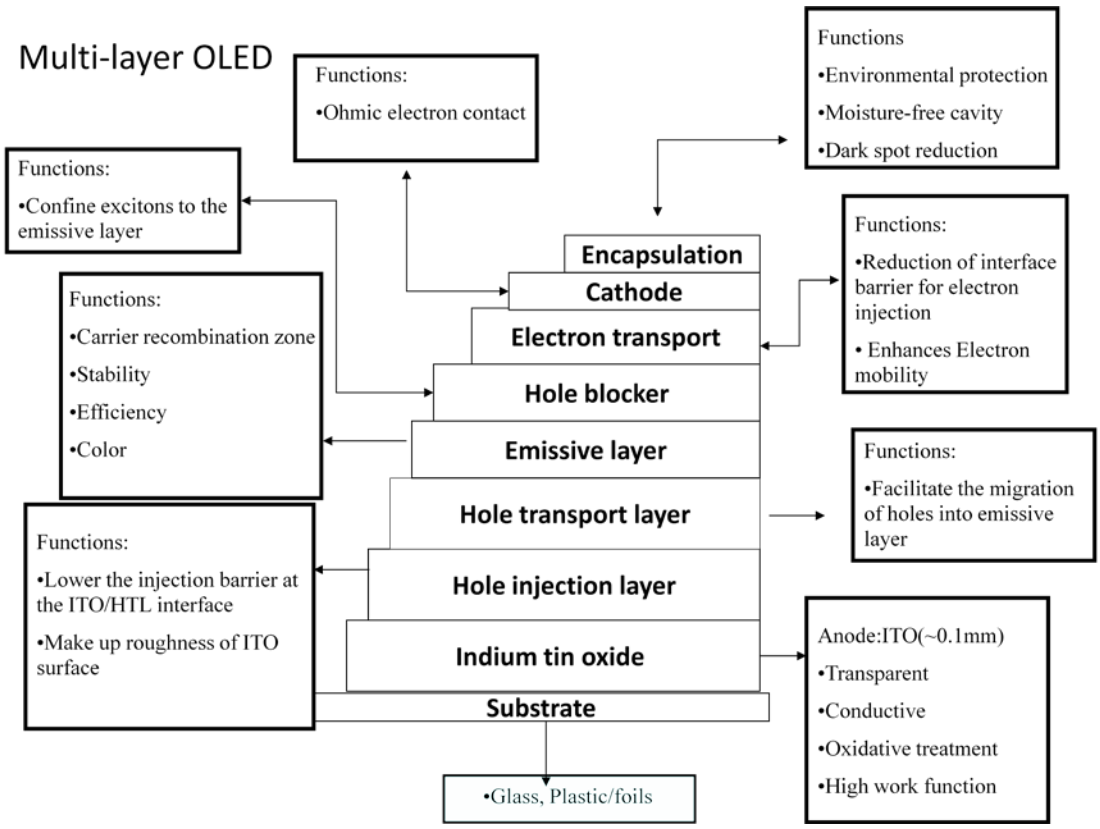

Figure 2.11 A typical multiple layer OLED

The structures of OLEDs can be categorized into three groups as shown in Fig 2.12. One is the bottom-emitting structure in which light emission takes place from the substrate side. Another one is the top-emitting architecture in which light is achieved from the topside of the device. The third one is the transparent light-emitting structure in which the light output is omni-directional since both the cathode and the anode are transparent. The bottom-emitting device has been widely used by many research groups as a preferred device structure since it is based on the transparent ITO which is commercial available. The development of top-emitting devices on the other hand have been highly required for applications in active-matrix displays. Transparent light emitting diodes which have greater than 70% transparency when turned off provide the potential for high resolution displays and interesting applications

such as skylights during the day time, the general lighting devices during the night time.

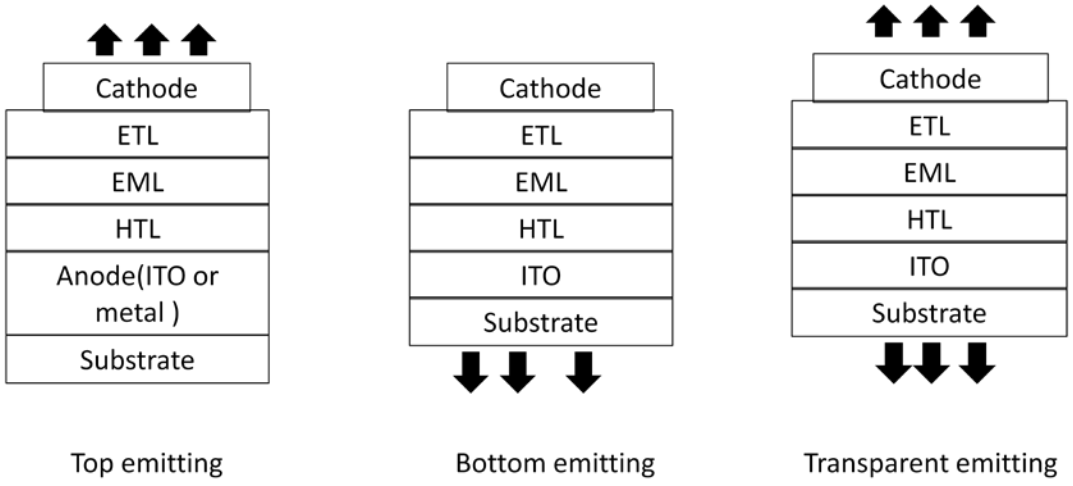

Figure 2.12 OLED structures

Stacked OLED devices(SOLEDs)

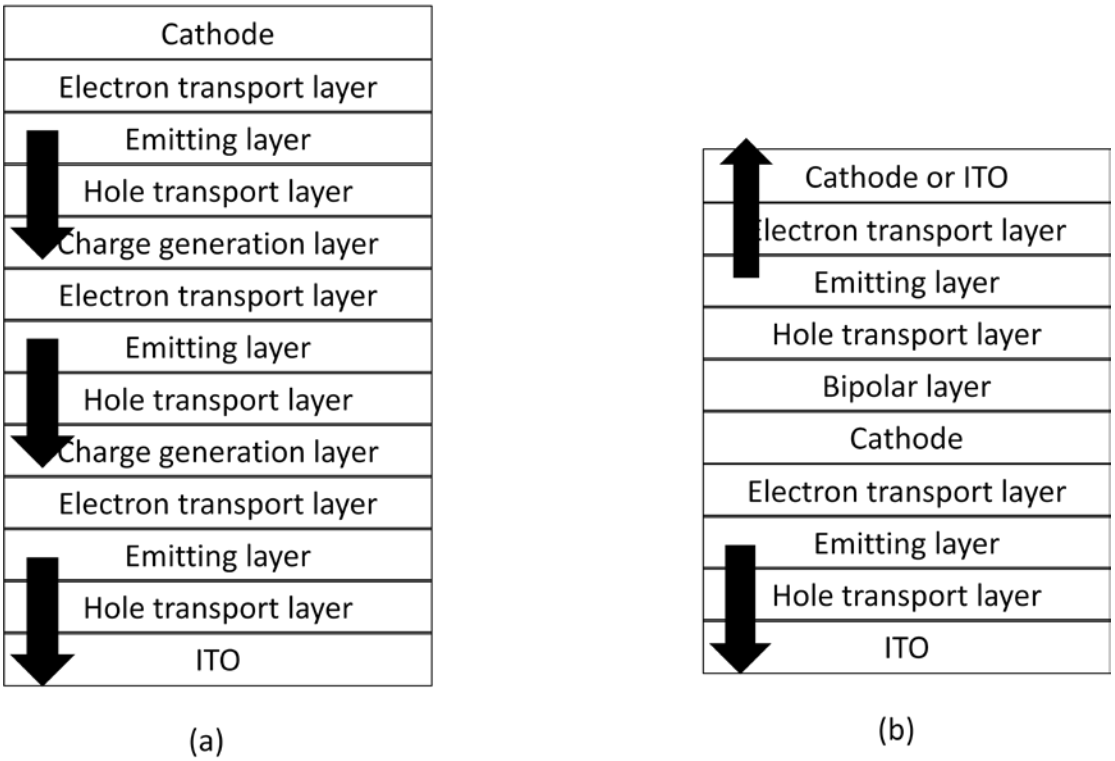

Figure 2.13 SOLED structure

Higher brightness and therefore higher current densities are required in OLEDs for general lighting applications. However two major problems may occur: first, device opto-electrical property degradation rates increase as the current density increases. Second,

efficiency roll-off occurs at higher voltages and current densities. OLEDs connected in series as shown in Fig 2.13(a) can solve this problem, because the current goes through the whole circuit, and each cell only withstands a fraction of the applied voltage, and the relative current densities are smaller. For the both top and bottom emitting OLEDs shown in Fig 2.13(b), a transparent common cathode called a "bipolar electrode" is needed, which can be used as an anode for one side and a cathode for the other side. Table 2.2 is the comparison of several different bipolar electrodes.

Table 2.2 Bipolar electrodes

	As cathode	As anode	Thermal evaporation or Sputtering?
Mg:Ag/ITO [10]	Good	Good	Both
CuPc/ITO/CuPc [11]	Not good	Good	Both
Mg:Ag/IZO [12]	Good	Good	Both
LiF/Al/Au [13]	Good	Not good	Thermal evaporation Only
LiF/Al/Ag (This paper)	Good	Very good	Thermal evaporation Only

Reproduced from [40]

For the bottom-only emitting SOLEDs, either ultrathin metal or metal oxide can be used as the interconnection layer of the two adjacent cells. However, because of the limited optical transmission of the ultrathin all metal electrodes, metal- oxide charge generation layers (e.g. MnO3[41]) have been developed and widely used to inject electrons into the EIL of one cell, and holes into HILof the other cell. It is reported that "OLEDs emitting at 5000

units can have lifetimes exceeding several thousand hours [2]".

2.6.2 Structure Strategy for WOLED Applications

White organic light emitting devices are one of the most promising candidates for future solid-state general lighting. Strategies that are applied for the WOLED application can be categorized into three major groups. White color can be achieved by combining blue, red and green emission from one triple-doped [46-51] or three single doped emissive layers [54]. By doping three different dopants into a wide bandgap common host, a high color rendering index necessary for general lighting applications can be achieved[55]. However, this method is problematic, since the energy transfer efficiency from host to each dopant can be different and energy steadily transfers from the higher energy dopant to lower energy dopant. Therefore, a careful adjustment of each dopant concentration is needed to achieve a well-balanced white color. Another problem for this approach is the color stability is low. Using different dopants in physically separate emissive layers is an alternative method to avoid this energy transfer problem, however, exciton diffusion may still occur in between these layers. The difficulty in achieving balanced charge recombination and exciton confinement in each of these separate layers makes this strategy more complicated. The increased number of layers also leads to fabrication reproducibility issues. Another approach for generating white color relies on emission of complementary colors (i.e., blue and yellow) from a double-doped [56] or two single doped emissive layers[41-45]. Devices have been fabricated and evaluated using fluorescent, phosphorescent, and a combination of both as emitters. Similar to the previous approach, energy transfer as well as exciton diffusion problem still exist even

though the device fabrication is simplified. The third method is taking advantage of exciplex [52], or, using both monomer and excimer emissions [53] from a single phosphorescent dopant to further simplify the OLED architecture. Due to the low luminescence efficiency of the exciplexes, devices using this method achieve no more than 0.6lm/W power efficiency, which is not practical for general lighting applications. Therefore, the most promising way to achieve balanced white with simple device architectures is by using a broad emitter that combines both monomer and excimer emission.

2.7 Organic Electroluminescent Device Materials

2.7.1 General Requirement of OLED Materials

Multilayer OLED devices are made of a series of evaporated organic and metal thin films. Most of the organic materials sublimes in the 200ºC-500ºC .A multiple source thermal evaporator is required for OLED fabrication as shown in Fig 2.14.

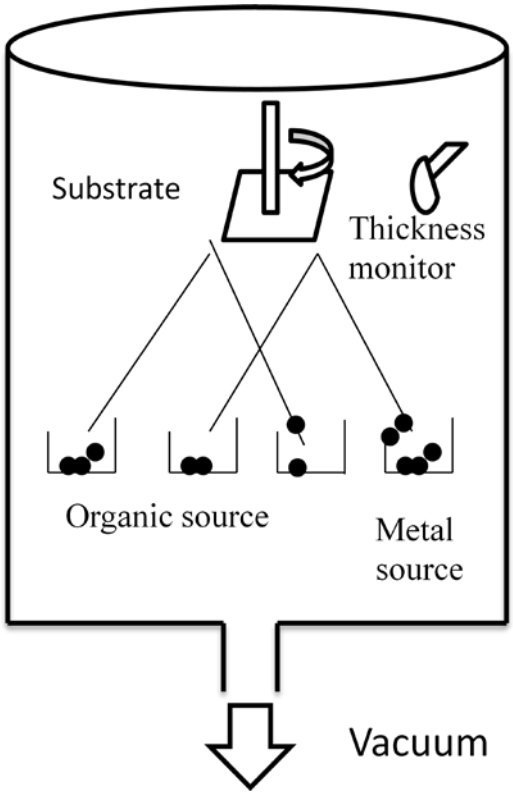

Figure 2.14 Multiple source evaporator for OLED

The organic materials used for an OLED device must meet several general requirements:

1. Suitability for vacuum deposition: Good thermal stability, in other words, sublimation without decomposition is required.

2. Sufficiently high glass transition temperature: “avoiding crystallization of the layer material within the desired lifetime of the device” [57].

2.7.2 Anodes and Cathodes

OLEDs require a transparent conducting oxide metal to facilitate hole injection from the electrode to the homo of the organic material. ITO has been most commonly chosen as transparent anode. Thin films of ITO can be deposited on glass or plastic substrates by

several ways including vacuum evaporation, sputtering, chemical vapor deposition[62] [63], pulsed laser deposition[64] ,spray pyrolysis[65] and sol-gel reaction[66]. Some of the comparison is shown in the below in Table 2.3. It is reported that conduction polymer such as PEDOT:PSS can reduce the energy barrier between the HOMO energy of the HTL and ITO and even form ohmic contact. Besides that, PEDOT:PSSS is a material with good film-forming property, high electrical conductivity and high transmittance in the visible spectrum.

Table 2.3 Comparison of ITO deposition methods(*Non reactive sputtering: all the atoms consisting of the film are present in the target. Reactive sputtering: partial of the atoms consisting of the film are gaseous.)

Method for ITO deposition	Advantage	Disadvantage	Groups reporting the method
Thermal evaporation of a metallic indium and tin alloy	Simple ,direct thermal evaporation	Indium has a higher vapor pressure than that of tin leading to inhomogeneous ITO composition	Ma et al.[58]
Thermal evaporation of pure Indium and Tin from two crucibles	Accurate composition control and low cost	Resistivity is high Film properties strongly depended on oxgen partial pressure ,film thickness, deposition rate, substrate	Yao et al.[59]

		temperature, and tin concentration	
*Non reactive sputtering	Necessitate hot pressed pure or mixed oxide target	The porosity of the target determines its susceptibility to contamination materials	Nadaud et al.[60]
Reactive sputtering	Bulk diffusion of the constitute is avoided	Optical and electrical properties are depend on oxgen flow	Wu and Chiou [61]

Low work function metal has been commonly employed as cathode. Low workfunction metal such as an alloy of Mg and Ag, Li, and Cs have been used for the cathode. To date, LiF and CsF, have been used with Aluminum and become most popular cathodes among worldwide OLED research groups. Common low work function metals are listed in Table 2.4.

Table 2.4 Low work function metals in OLED devices

Electrodes	Metal or Alloys	Work function
Cathode	Cs	2.14
Cathode	Ba	2.52
Cathode	Sr	2.59
Cathode	Yb	2.6
Cathode	Ca	2.87
Cathode	Li	2.90

2.7.3 Injection Materials

Designing efficient OLEDs requires improved charge injection from electrodes into the organic layers. For instance, the work function of ITO is around 4.8eV, which is 0.7-0.9eV lower than the HOMO of a general HTL layer. A HIL located in between the anode and the HTL can enhance the hole injection efficiency. On the opposite side of the OLED, the work function different between the cathode and the common ETL is 0.4-0.7eV .Inserting a EIL between the cathode and ETL will reduce the injection barrier and therefore increase device efficiency. Figure 2.15 shows the commonly used hole injection materials

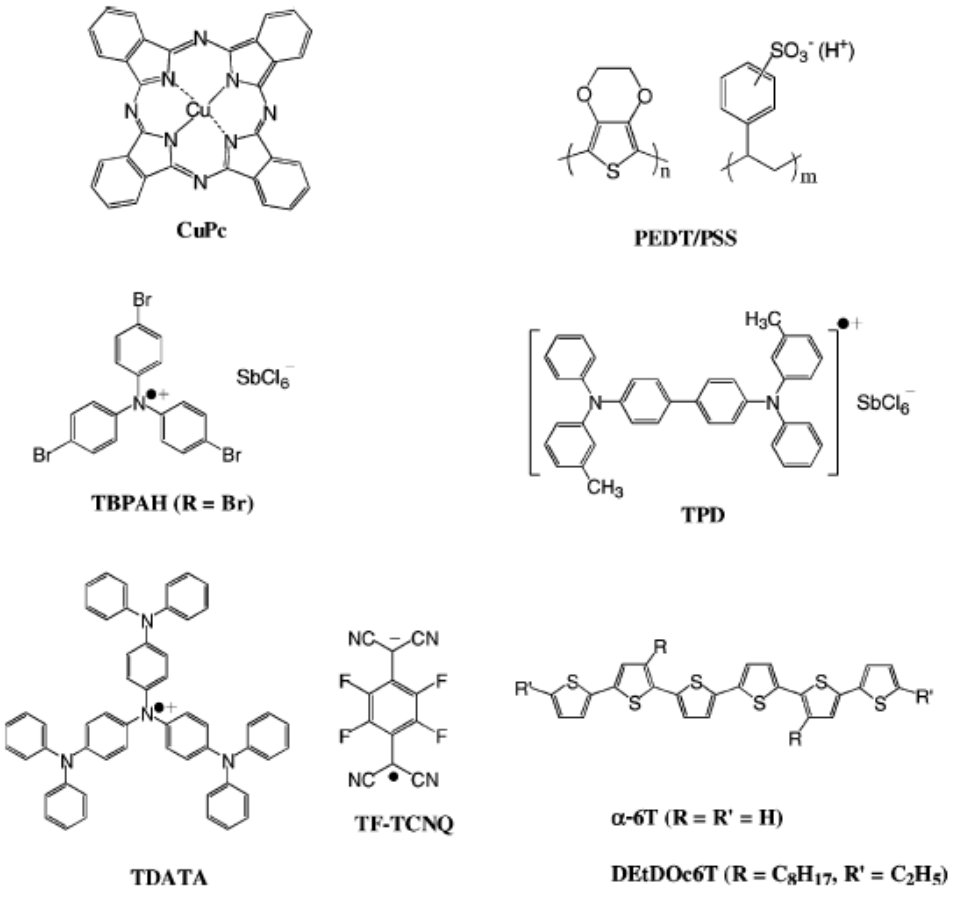

Figure 2.15 Hole-injection materials. Reproduced from reference [77]

Cleaning and oxidation of the ITO surface by O2 plasma, CF4/O2 plasma [67] or UV

treatment can remove the residual organic particles and increase the work function of ITO. The increase of work function result from vacuum level shift due to surface dipole field, surface states, and Fermi level shift which is believed to have its origin from the decrease of free carrier density. Phthalocyanine, Copper complex (CuPc), tetra(fluoro)-tetra(cyano)quinodimethane (TF-TCNQ), tris(4-bromophenyl)aminium hexachloroantimonate (TBAHA), 4,4′′ -tris-(3-methylphenylphenylamino)triphenylamine (Mtdata) have been reported as effective materials for hole injection. From Fig 2.16, it is seen that Mtdata has the largest energy barrier with ITO, the main reason for effective hole injection is due to its dense film structure and fine surface morphology[68].

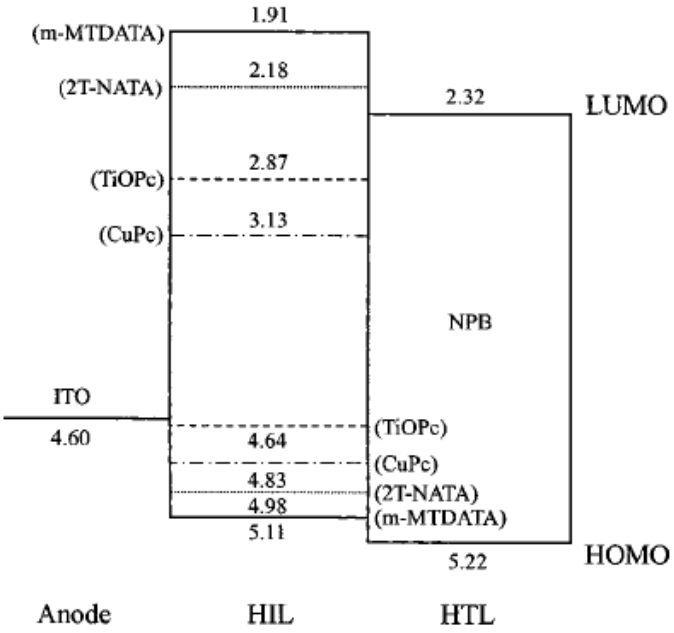

Figure 2.16 HOMO and LUMO of HIL materials. Reproduced from reference [68]

The most widely used material for electron injection is LiF. Devices with the structure ITO/TPD/Alq3/LiF/Al [69] has been studied thoroughly for the purpose of investigating LiF layer thickness effect on the device performance. The best result was

achieved with 0.1nm of LiF. Proposals which are attempt to explain the LiF function includes preventing chemical reaction between Al and Alq3, tunneling through a thin insulator layer, and lowering the work function of the aluminum.

2.7.4 Transporting Materials

2.7.4.1 Hole Transporting Materials

The hole transporting layer in multilayer OLEDs commonly functions in two ways: Firstly, because the ionization potential of hole transporting layer is generally chosen in between the hole-injection and emissive layer, hole transport from HIL to EML will be improved. Secondly, the HTL also plays the role of blocking electrons and confining them to the EML. Two important issues are essential for the application in OLEDs: increasing hole mobility and Tg (glass transition temperature). After the electrons and holes are successfully injected, they will transport before they meet each other and recombine in the EML. The mechanism of carrier transport is through hopping on the localized states. The hole mobility in thes HTL should be high in order to swiftly let the holes pass through.

The most popular HTL materials are N,N'-Bis(3-methylphenyl)-N, N'-diphenyl-[1,1'-biphenyl]-4,4'-diamine(TPD) and N,N'-di(1-naphthyl)-N,N'- diphenyl-[1,1'-biphenyl]-4,4'-diamine(α-NPD). Both of them possess high electrochemical stability. Their hole mobilities are in the range of between 10^{-4} and 10^{-3} cm $^{2}.V^{-1}.s^{-1}$ which was measured by using the TOF method [74]. Their glass transition temperatures Tg are low (Tg(TPD) = 63°C),which may lead to crystallization at high temperature and even shorten the device lifetimes. So further HTL material development and synthesis are focused on increasing the glass

transition temperature, improving hole mobility and lower ionization potential. Pinhole free thin film can form with high Tg hole transport materials. Three ways are proposed by Shirota et al.[75] to achieve amorphous molecular materials:(1) to increase the number of conformers together with non-planar molecular structure; (2) to introduce bulky and heavy substituents so as to enlarge the molecular size for attaining and maintaining the stability of the glassy state; (3) to increase Tg by the incorporation of a rigid moiety or an intermolecular hydrogen bonding site into non-planar molecules and by increasing the molecular weight.

Three groups of materials are designed to achieve high thermal and thin film morphological stabilities and on finding ways to control and optimize carrier injection and transport [5]. They are biphenyl diamine derivatives shown in Fig 2.17, starburst amorphous molecular glass shown in Fig 2.18 and spiro-linked biphenyl diamines shown in Fig 2.19. The thermal and solid PL properties comparison between NPB and spiro-HTMs was shown in Table 2.5.

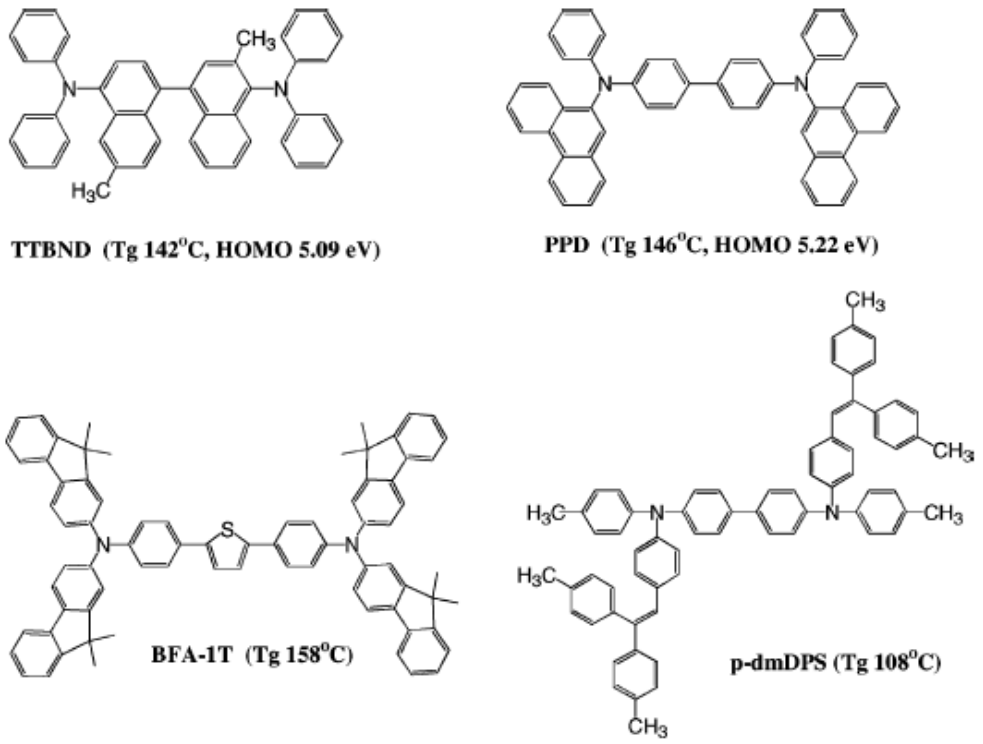

Figure 2.17 Biphenyl diamine derivatives. Reproduced from reference [5]

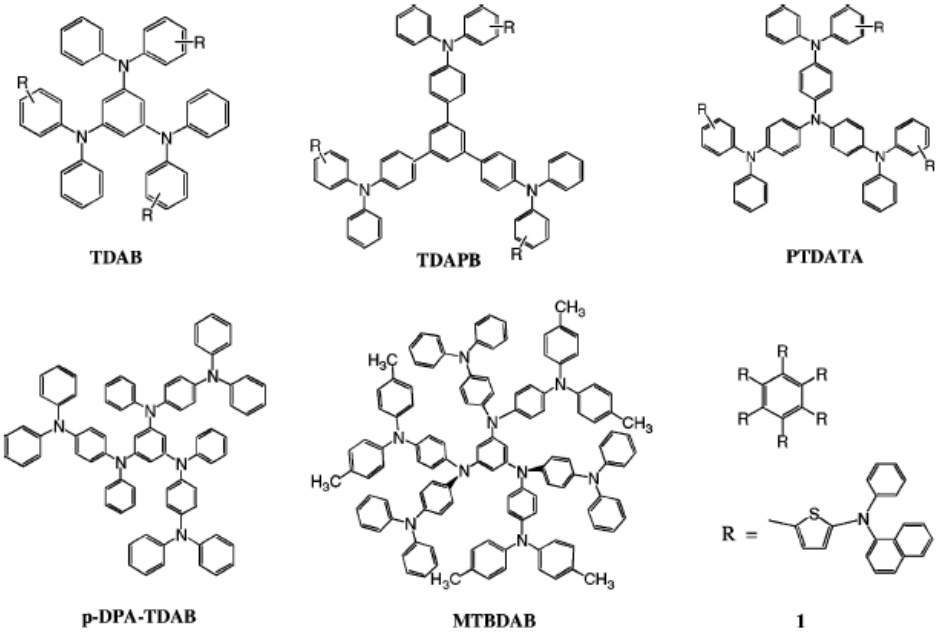

Figure 2.18 Starburst amorphous hole-transport materials. Reproduced from reference [5]

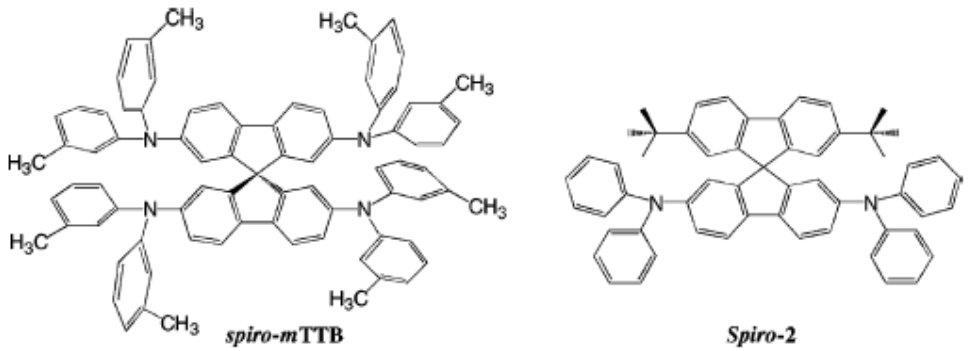

Figure 2.19 Example of spiro-linked hole-transport materials. Reproduced from reference [5]

Table2.5 Comparison of thermal and solid PL properties of spiro-HTMs with NPB.

Comparison of thermal and solid PL properties of *spiro*-HTMs with NPB

HTM	NPB	*Spiro*-NPB	*Spiro*-TAD
Molecular weight	588.8	1185.5	985.3
T_g (°C)	98	147	133
T_m (°C)	290	294	276
T_{sublim} (°C at 4×10^{-5} mbar)	310	430	355
λ_{max} (PL film)	440	450	405

Reproduced from reference [5]

Because the carrier transport occurs by hopping, the hole mobility can be improved by bringing the localized states nearer. This can be done, (1) by doping the organic material,(2) by attaching a carrier-transport moiety to the molecule, and (3) by a regular arrangement of the molecules [76].

2.7.4.2 Electron Transport Materials

In order to achieve a high efficiency electron transport material for OLEDs, several properties of ETM must be satisfied:(1) ETM should undergo reversible cathodic reduction to form stable anion radicals[77]. (2)High electron drift mobilities are desired because in that case the recombination point will be far away from cathode side and the exciton forming

efficiency will be improved. (3) The HOMO of the ETM ideally should be in between that of EIL and EML to facilitate electron injection.(4) They should have a wide optical bandgap to minimize optical loss due to light absorption in the ETL and deep HOMO which can confine holes to the EML[2]. 5) High Tg are expected in ETM for high temperature stability and pinhole free glassy films. Below are the examples of modified Alq3 molecules shown in Fig 2.20, fluorescent metal chelates shown in Fig 2.21 and novel electron transport materials shown in Fig 2.22 for ETM application.

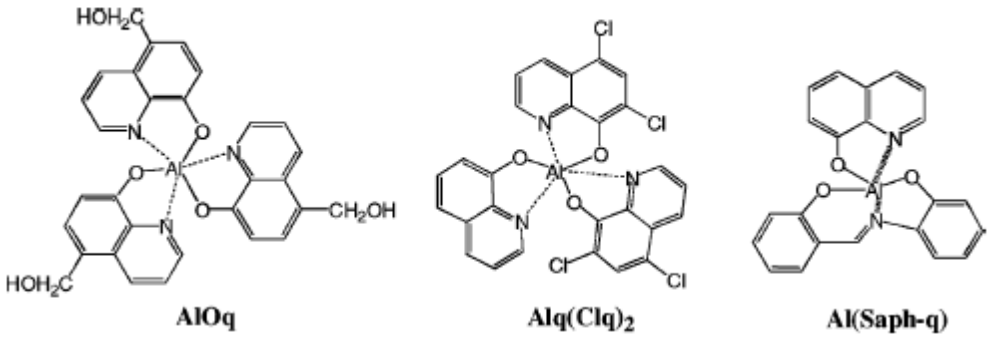

Figure 2.20 Modified Alq3 molecules. Reproduced from reference [5]

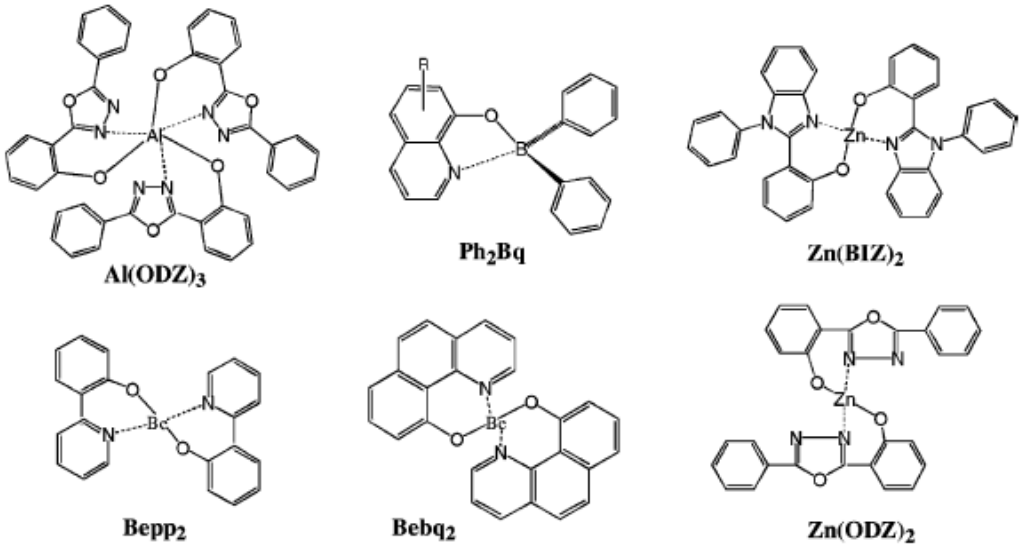

Figure 2.21 Fluorescent metal chelates. Reproduced from reference [5]

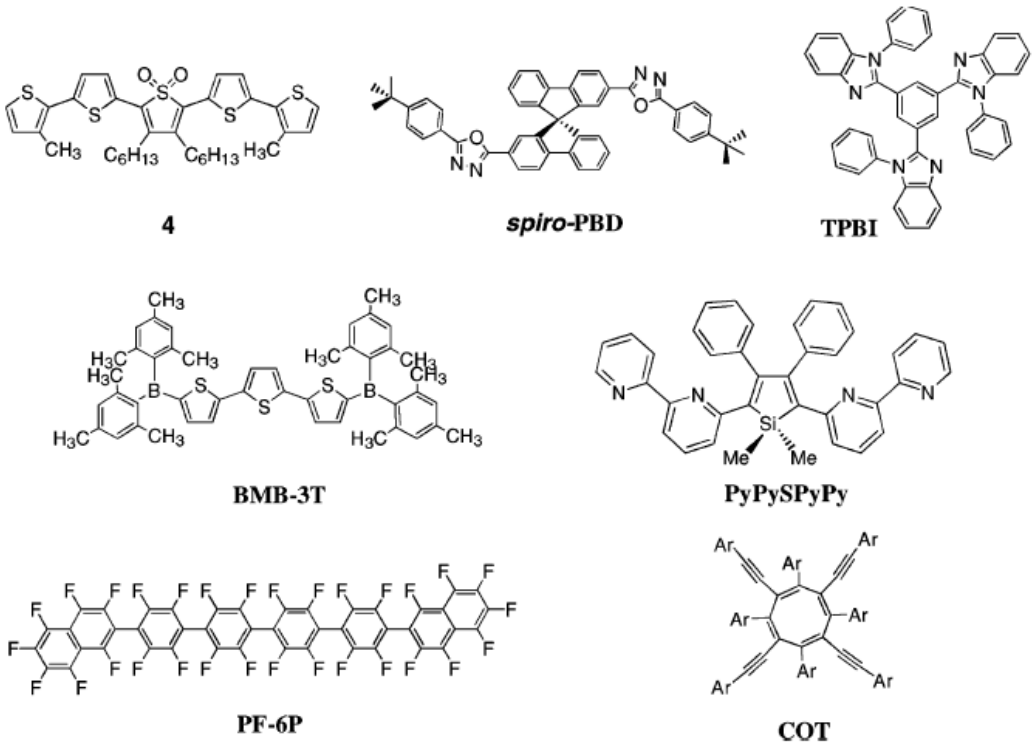

Figure 2.22 Novel electron transport materials. Reproduced from reference [5]

2.7.5 Blocking Materials

2.7.5.1 Hole/Exciton Blocking Materials

A hole blocking material is located between the electron transport layer and emissive layer to stop holes from escaping before recombining with electrons and also to transport electrons as shown in Fig 2.23.

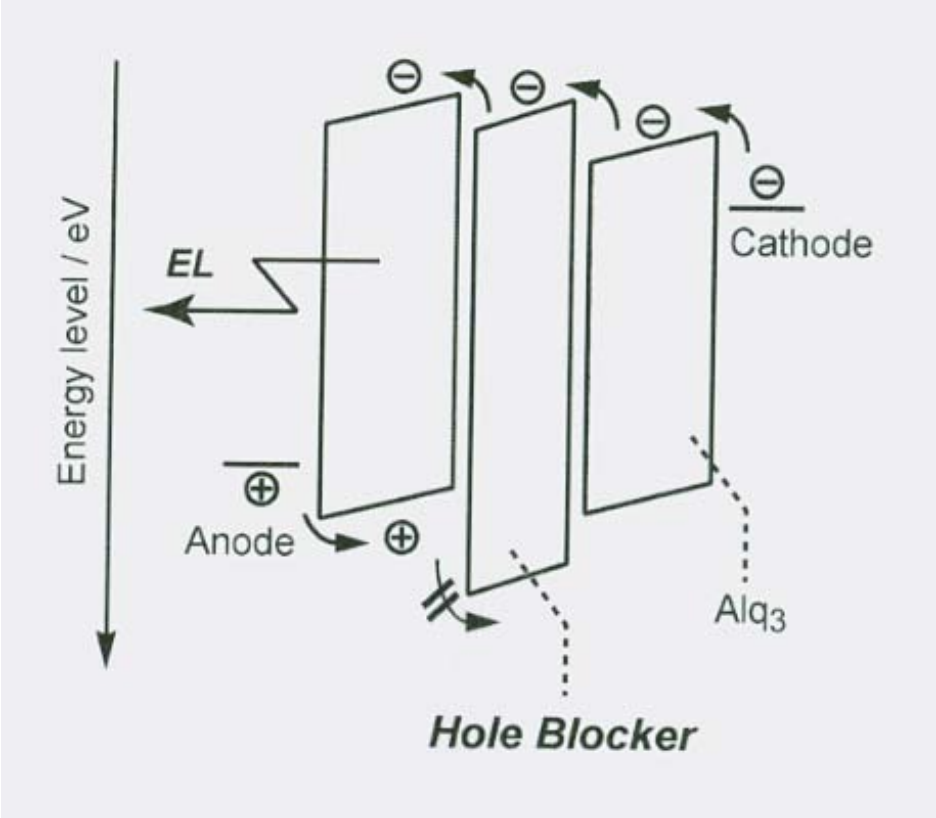

Figure 2.23 Roles of hole blocking material. Reproduced from reference [77]

Hole blocking materials in practice should fulfill two requirements:(1)The HOMO difference between the EML and HBL should be larger than their LOMO difference.(2) The cathodic reduction processes of hole blockers should be reversible to form stable anion radicals[77]. However, even though some materials can fulfill the above requirements, there are still other limitations. For example, BCP which is an efficient hole blocking layer will easily form exciplexes with host in the EML, e.g., TPD and m-MTDATA and emit in the longer wavelength region [78].

It is known that phosphorescent devices can achieve higher efficiency, but they are more complicated than fluorescent devices due to longer triplet lifetime. Specifically, triplet excitons can diffuse more than 100 nm, so they may easily diffuse into other layers, which

leads to color impurity and reduced luminous efficiency. In comparison, the singlet exciton diffusion length is much shorter and in the 10nm range. So the stack must be judiciously designed to confine triplets in the emissive layer. The most direct way to this end is to take advantage of the triplet energy differences between the HTL, ETL and phosphorescent dopant. In the structure proposed by O'Brien ITO / NPB / CBP-PtOEP/ BCP/Alq3/Mg-Ag [79], BCP was functioning as the hole blocker layer. The triplet energy for BCP, PtOEP and NPB are 2.5, 1.9 and 2.3eV respectively. The energy difference between BCP and PtOEP is 0.6eV, which is a large energy barrier to prevent excitons from diffusing into the Alq3 layer. Beyond that, the HOMO of BCP is 6.5eV.which can block holes from escaping the EML. This phenomenon can be observed from in the EL spectra in Fig2.24. Characteristic peaks for both Alq3 and PtOEP showed up in the structure without BCP layer and the characteristic peak for Alq3 disappeared after adding the BCP layer, which indicates that BCP functions as an efficient exciton and hole blocker in this situation.

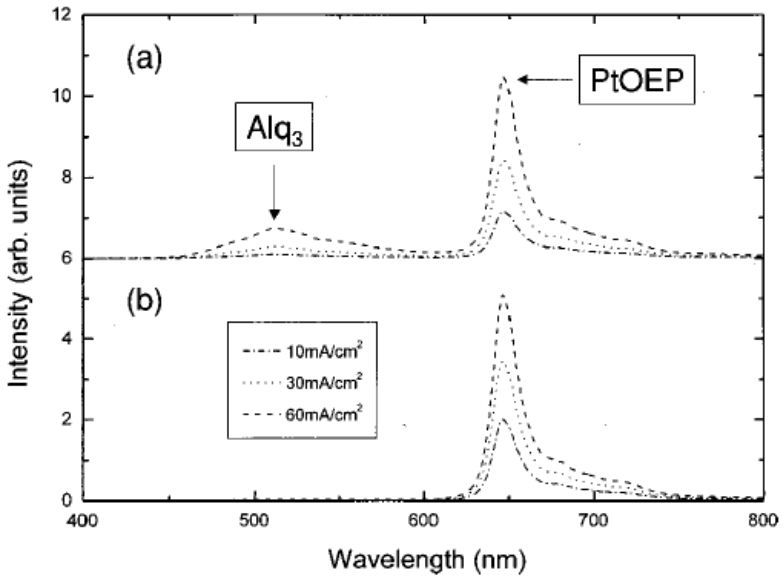

Figure 2.24 Emission spectra of CBP-based electroluminescent devices with and without a BCP exciton blocking layer. Reproduced from reference [79].

Families of triarylbenzenes and triarylboranes have been synthesized and developed as new generation of hole-blocking amorphous materials due to their high T_gs and appropriate electron-accepting properties for electron transporting.

2.7.5.2 Electron /Exciton Blocking Layer

Electron blocking layer are used for blocking electrons and simultaneously transporting holes. In the structure proposed by Vadim Adamovich, NPD (400 A)/Irppz (200 A)/mCP :Pt complex (16%, 300A)/ BCP (150 A)/Alq3 (200 A)/LiF (10 A)/Al (1000 A)[80], by using Irppz(LOMO:2.1eV;HOMO:5.5Ev) as an electron and exciton blocking layer, roughly a factor of 2 increase in quantum efficiency was reported. Also the spectral contribution from NPB was eliminated which indicates Irppz is also an effective exciton blocker. Other well known electron blocker is mCP [81].

2.7.6 Light-Emitting Host Materials

2.7.6.1 General Requirements

High efficiency OLED host materials require efficient electron injection which means the electron affinity should be high.

2.7.6.2 Fluorescent Host:

Most electron transport materials are effective light emitting host materials provided that they are not the luminescence quenchers[2]. For example, NPB which is a widely used hole transporting material can be doped with rubrene to emit yellow light, and Alq3 can be

doped with 6,13-diphenylpentacene (DPP) [82] or 7-(9-anthryl)dibenzo[a,o]perylene (PAAA) [83] to emit red, etc.

2.7.6.3 Phosphorescent Host:

Generally speaking, the bandgap of the host materials should be larger than dopant materials, so that energy transfer from host to guest should be irreversible. However, if the dopant is a phosphorescent dye, the efficiency can be quenched by energy transfer from the triplet excited state of the dopants to the triplet excited state of the host. It has been proved by Yang experimentally when they were trying to dope different phosphorescent dyes into poly-[9,9-bis(octyl)fluorene-2,7-diyl](PF)[84], that even though the HOMO and LUMO level of PF covers the bandgap of the phosphorescent material, energy transfer and device efficiency differs as the triplet energy of the phosphorescent material differs. If the triplet energy of the phosphorescent material is higher than the triplet energy of the PF, the device efficiency will quenched by energy transfer. To avoid this, the triplet energy of the host should be higher than that of the dye to confine the triplet exciton of the phosphorescent material in the emissive layer. Thompson and his colleagues did similar experiments to prove this efficiency quenching issue as well [85].

Nowadays, most phosphorescent host materials are based on carbazole, and carbazole derivatives can be good hole transporters [86]. CBP is one of the most well-known hosts, which is also reported as a bipolar transporter [87]. When CBP is used as a host for green, yellow and red phosphorescent emitters, device internal quantum efficiency can reach 60%-80% [88-93] and EQE can be higher than 10%. However, the triplet energy of CBP is only

2.56 eV. Thus, if CBP is doped with a blue phosphorescent material with a triplet energy higher than 2.56eV, the EQE of the device will drop to (5.7±0.3) % due to energy transferring back to CBP [94].

Several phosphorescent materials based on carbazole derivatives have since been developed as host materials, for example -4, 4'4''-tris (9-carbazolyl)triphenylamine (TCTA) [95]. By using the star-like hole transport material TCTA as a host material and star-like CF-X as hole and exciton blocker, devices doped with $Ir(ppy)_3$ driven by a voltage of 3.52V can produce EQE increases to 19.2%.

In order to increase the blue phosphorescent device efficiency, host materials with high triplet energy are needed. If mCP is doped with Iridium bis (4,6-di-fluorophenyl) – pyridinato - $N,C^{2'}$ -picolinate(FIrpic), EQE of the device can reach (7.8±0.8) %.

After that, 4,4'-bis(9-carbazolyl)-2,2-dimethyl-biphenyl (CDBP) , N-N'-dicarbazolyl-1,4-dimethene-benzene (DCB) have been developed as hosts for blue phosphorescent emitters [95]-[97].

Nowadays, the challenge for the host material design is always associated with host for deep blue emission. Due to the wide bandgap of the deep blue phosphorescent material, the host material must also have large bandgap in order to have efficient energy transfer. In the application of OLED devices, wide bandgap host materials always impedes electron and hole injection from adjacent supporting layers. In order to solve this problem, Thompson and his colleagues proposed that electron and hole can be injected into the phosphorescent material, form excitons and emit light from the phosphorescent material directly. In this case, even though the host material is not excited, the triplet energy level in the host material needs

to be maintained high enough to avoid energy triplet energy transferring back to the host.

1,3-bis(triphenylsilyl)-benzene (UGHx) has been developed to achieve high triplet energy level. In the chemical structure of UGHx, two benzene rings are separated by one silicon atom. However, in UGHx devices, mCP has to be inserted between the hole transport layer and emissive layer to facilitate hole injection and prevent electrons from escaping emissive layer. Devices made of UGH2 doped with bis(4′,6′-difluorophenylpyridinato)tetrakis(1-pyrazolyl)borate (Fir6) can reach an EQE of (11.6±1.2)% and power efficiency of (13.9±1.4) lm/W, with CIEx,y of (0.16,0.26).

2.7.6.4 Fluorescent Dopants and Phosphorescent Dopants

Radiative relaxation in the organic molecules occurs from two kinds of excited states: singlet and triplet. Electrons of anti-symmetric spin in the excited state will form singlet excited states and decay to ground state in the form of fluorescence. Electron of symmetric spin in the excited state will form triplet excited states and decay to ground state in the form of phosphorescence. From the theory of quantum mechanical selection rules, electron decay from singlet excited state to ground state is allowed, so the time electrons dwells in the singlet state is very short, around1~10ns and fluorescence will be observed. However, when the electron decay from triplet excited state to the ground state, the two electrons in the ground state will have the same spin and Pauli exclusion principle is violated, which leads to longer dwelling time of electron in the triplet excited state, around several ms. Alternative mechanisms must be found to take advantage of phosphorescence and make it more efficient. In 1998, Prof. Baldo and Forrest found that phosphorescent material containing heavy metal

(Ir, Pt, Pd, Eu, etc) showed very strong spin-orbital interaction between heavy metal and its ligands. Mixing of singlet excited states and triplet excited states lead to 100% internal quantum efficiency. Below in Fig 2.25 are the commercialized fluorescent green, red and blue dopants from a Taiwan OLED company Lumtec. Among them the green fluorescent dopants are the earliest commercialized products, which have the highest fluorescent efficiencies. One of the best green fluorescent materials is 10- (2-benzothiazolyl)-1,1,7,7-tetramethyl - 2,3,6,7 - tetrahydro-1H,5H,11H-[l]-benzopyrano [6,7,8-ij]quinolizin-1-one , known as C-545T [98]-[100], which is categorized as highly fluorescent class of coumarin laser dyes. By virtue of its structural co-planarity, the julolidine donor situated at carbon#7 aligns its p-orbital of nitrogen to overlap with π-orbitals of the phenyl ring for more effective conjugation which results in increasing its relative PL quantum yield(η)to 90%[5]. N,N-dimethylquinacridone(DMQA) [101]was firstly synthesized by Kodak company. Some of other fluorescent molecules are also listed in Fig 2.25below.

Green-Fluorescent Dopants

Dopants	Emission Wavelength(nm) In THF
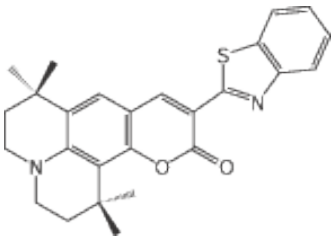 C545T	506

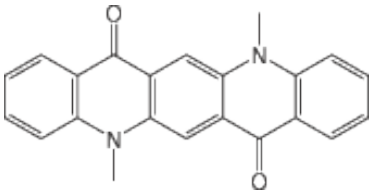

523

DMQA

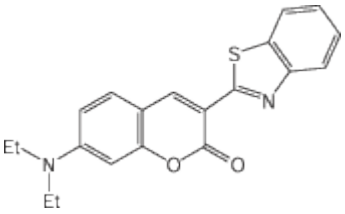

494

Coumarin 6

Red-Fluorescent Dopants

Dopants

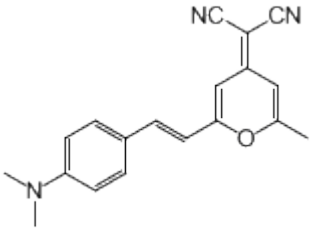

577

DCM[102]

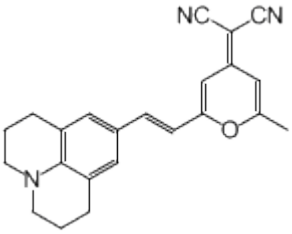

605

DCM2[103]

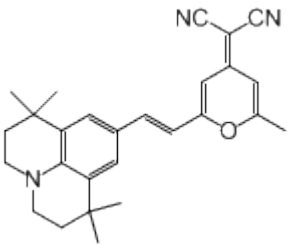

604

DCJT

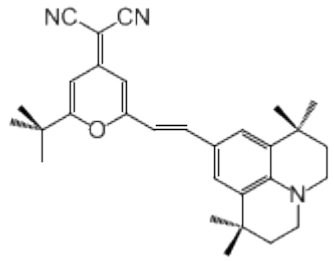

602

DCJTB[104]

Blue-Fluorescent Dopants

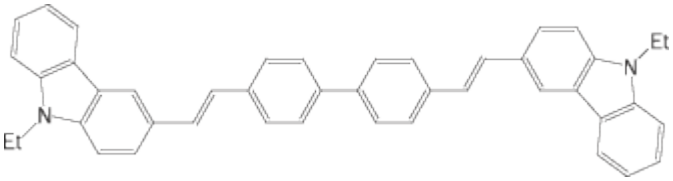

438, 459

Bczvbi

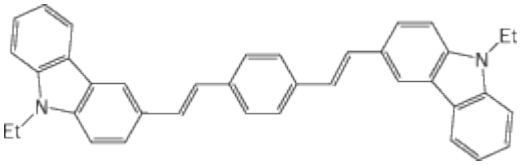

438, 459

BCzVB

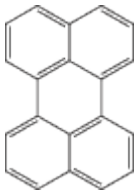

447,471

Perylene

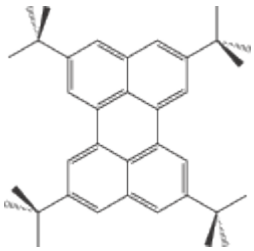

459, 487

TBPe

Figure 2.25 Fluorescent dopants and emission wavelengths. Reproduced from reference [77]

In phosphorescent emitters, a central rare-earth or transition metal such as ruthenium, iridium, or platinum is always surrounded by an array of ligands. In theory, 100% IQE can be achieved by phosphorescent emitters since both singlet (25%) and triplet (75%) exciton can be harvested.

However, most of them emit phosphorescence at extremely low temperature, and only a few classes of transition metal complexes show high efficiency quantum yield at, or above room temperature. In 1999, Forrest's group first reported 2,3,7,8,12,13,17,18-octa(ethyl)-12H,23H-porhine platinum(II)(PtOEP) [105] in OLED devices and EQE of 5.6% with CIEx,y (0.7,0.3) was achieved. Iridium complexes have appeared over the years. By changing the ligand of iridium phosphorescent emitters, the whole visible range of the electromagnetic spectrum can be covered [106-108]. Below in Fig 2.26 are some widely used commercially available phosphorescent materials emitting green, red and blue from lumtec.

Green phosphorescent dopants

Dopants	Emission wavelength (nm) In THF
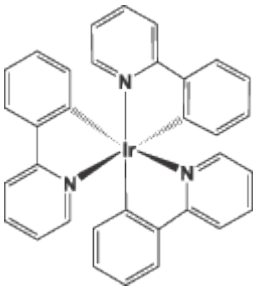	513
Ir(ppy)3	
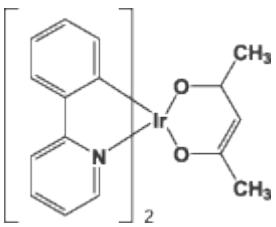	378, 524

$Ir(ppy)_2(acac)$

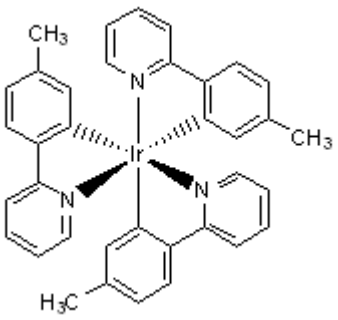

514

$Ir(mppy)_3$

Red phosphorescent dopants

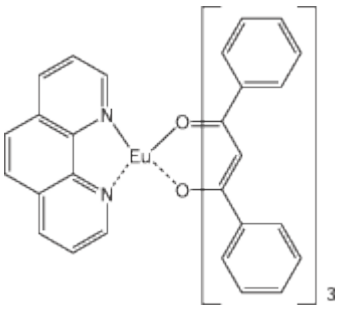

615

$Eu(dbm)_3(phen)$

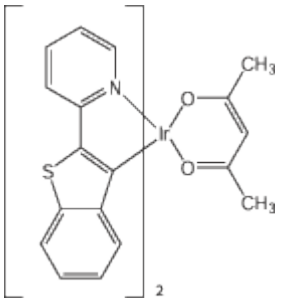

615

$Ir(btp)_2(acac)$

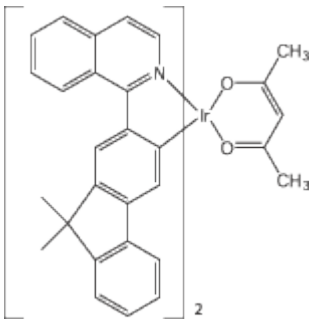

653

$Ir(fliq)_2(acac)$

Blue phosphorescent material

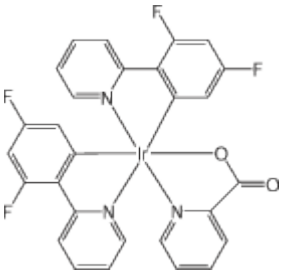

472

FIrpic

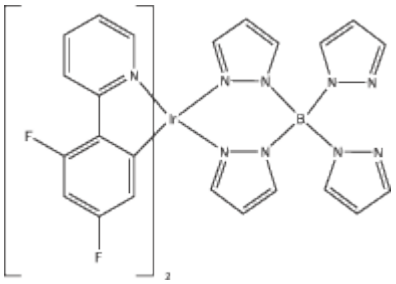

461, 490nm

Fir6

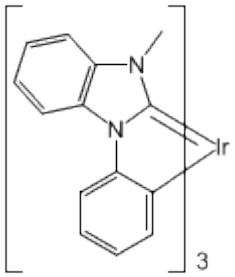

389,405nm

fac-$Ir(Pmb)_3$

Figure 2.26 Phosphorescent dopants and emission wavelength. Reproduced from reference [77]

2.8 Physical Process in Organic Electrophosphorescent Devices

2.8.1 Organic Electroluminescence Principle

Organic electroluminescence principles can be simply explained in three steps. In Fig 2.27, in the first step, when forward bias is applied, holes are injected from anode side to the HOMO of the hole transport material and electrons are injected from cathode side to the LUMO of the electron transport material. In the second step, electrons and holes will pile up at the interfaces between ETL (HTL) and EML. In the last step, excitons will form in the EML and then decay back to the ground state radiatively.

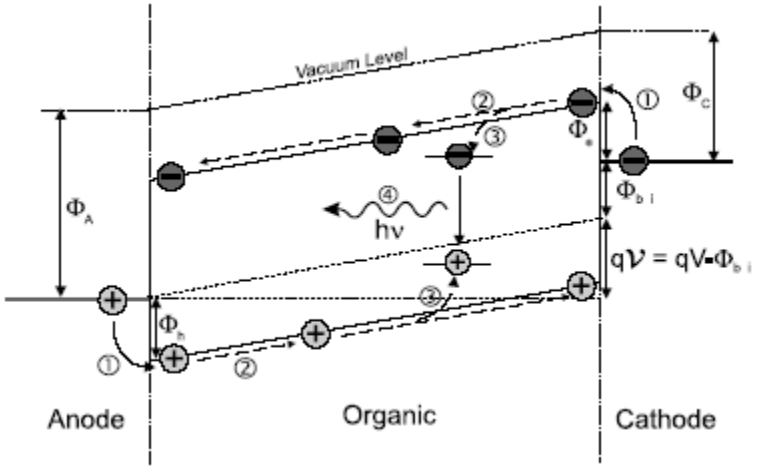

Figure 2.27 Basic steps of electroluminescence in OLEDs. Reproduced from reference [109]

2.8.2 Charge Injection and Transport

When a current passes through an OLED, two things will happen in a sequence. Firstly, carriers are injected to organic layers from the electrodes, then charge through the organic layers must occur. The current that flows through the semiconductor device can be determined either by the semiconductor bulk or by its contact with an electrode. When the energy barrier between the organic layer and charge injection contacts is very small (their

workfunctions are essentially equal), ohmic contacts are obtained,which makes injection of as much current as the semiconductor bulk requires possible. This is called the space charge limited current (SCLC) which means the current is limited by intrinsic transport properties of the semiconductor. On the other hand, when the barrier for carrier injection from the electrode into the organic is large, current injection will be much less than the SCL, the electron current will be strongly determined by the interface barrier height and the presence of the traps, due to metal-organic interactions.

2.8.2.1 Current Injection from Electrodes

In the OLEDs research, two injection models from inorganic semiconductor devices are used: Fowler-Nordheim tunneling and the Richardson-Schottky emission model.

According to Richardson-Schottky emission theory, electrons (or holes) must have enough energy, usually due to thermal agitation to overcome the energy barrier at the metal-organic interface. The injected current density J_{RS} is temperature sensitive, and changes according to:

$$J_{RS} = AT^2 \exp(-\frac{\Delta - \beta_{RS}\sqrt{E}}{kT})$$

Where T is temperature, E is the electric field strength, k is Boltzmann constant, A is Richardson constant, Δ is the metal-organic interface barrier when the electrical field is zero, $\beta_{RS} = (e^3 / 4\pi\varepsilon\varepsilon_0)^{1/2}$, ε is relative dielectric constant of organic material and ε_0 is the permittivity of vacuum. As the equation shows, the injected current exponentially increases with temperature.

In the Fowler-Nordheim tunneling theory, the injected current is independent of temperature and exponentially dependent on the applied field. When the applied voltage is big enough, the band bending on the organic side of the interface increases, the depletion region becomes thinner, and due to quantum mechanical tunneling charge is Fermi level of the electrode into the LOMO (or HUMO) of the organic layer. The current density is described by the equation given below:

$$J_{FN} = \frac{Ae^2E^2}{\alpha^2 k^2 \Delta}\exp(-\frac{2\alpha\Delta^{3/2}}{3eE})$$

Where E is the electric field strength, k is Boltzmann constant, A is Richardson constant, Δ is the metal-organic interface barrier when the electrical field is zero, $\alpha = (4\pi/h)(2m_0)^{1/2}$,e is electron charge.

2.8.2.2 SCL Current

Space charge limited (SCL) current occurs when injected free carriers are more than can be accommodated by the organic material. This event is usually the case in material with low charge mobilities, where injected charge tends to buildup in the organic layer. The current density is related to the thickness of the organic layer and in the trap free organic material whose carrier mobility is a constant, the current density and thickness(d) obey the Mott-Gurney equation[110]:

$$J=\frac{j(E)}{d} = (\frac{9}{8})(\frac{\varepsilon\varepsilon_0\mu V^2}{d^3})$$

ε is relative dielectric constant of organic material and ε_0 is the permittivity of vacuum.μ is the charge mobility and V is electrical field.

2.8.2.3 Carrier Mobility

From the optimum efficiency standpoint of OLEDs, a balanced charge state must be maintained between injected electrons and holes. This implies that if the hole and electron mobility can be measured in the organic material, the charge transport range and recombination zone will be successfully estimated. The drift current density may be written as $J = e(\mu_n n + \mu_p p)F = \sigma F$

And e is the electron charge, μ_n and μ_p are the mobility of electrons and holes and p are electron and hole concentrations, respectively.

The total velocity is the sum of thermal velocity and the drift velocity. The carrier drift mobilities are typically in the order of 10^{-4} and 10^{-6} cm²/Vs for holes and electrons for organic molecules. In some very high quality organic semiconductors, electron as well as hole mobilities exceeding 10³cm²/Vs can be observed [111]. However, in the case of thin film devices, carrier drift mobility may be increased to due to enhanced electrical field. Pai[112] proposed the following expression to describe field dependent mobility in organic semiconductors:

$\mu(E)=\mu(0)\exp(\gamma\sqrt{F})$

Where, μ(0)is the mobility at zero field and γ is an electric field coefficient dependent on the temperature. Carrier mobility can be measured by several techniques. The Hall Effect measurement can measure the mobility from the conductivity of the organic thin film, and, the concentration of the electrons if it is n-type and that of the holes if it is p-type. Field effect transistors are also used to measure effective mobilities in the accumulation mode of

the organic semiconductors [113][114]. Time of flight (TOF) is another common way of measuring charge carrier mobility in the semiconductor bulk [115]-[117]. In the TOF method a sheet charge is generated by the absorption of the incident light and it moves under the effect of the external applied electric field. Once the transit time τ_t of the photo-generated charge sheet is measured for a non-dispersive transport, one can calculate the charge carrier mobility μ using the relation [113]

$$\mu = \frac{L^2}{\tau_t V},$$

where L is the sample thickness and V is the applied voltage. Transient EL measurements is another way of measuring charge carrier especially field dependent charge carrier mobility in OLEDs. The pulse profile of the EL after applying a voltage to the OLED provides information of carrier kinetics and mobility properties[113].

2.8.3 Electron and Hole Recombination and Decay

The invention of host-guest system in the EML implies that the host material can be used together with a variety of highly fluorescent or phosphorescent guest dopants leading to a gamut of electroluminescence wavelengths (colors) with high efficiencies. Another advantage of the doped emitter system in OLEDs is the transfer of electrogenerated excitons from the host to highly emissive and stable dopants which reduces the possibility of non-radiative decay [29]. Excitons are formed with the spin states statistically distributed between the triplet and singlet configurations; three times as many triplet excitons are formed compared to the singlet excitons [8]. All early OLED devices were fluorescent and therefore restricted to a maximum internal quantum efficiency of 25%. By harvesting both triplet and

singlet exciton, phosphorescent material can achieve nearly 100% internal EL efficiency [30][31].

2.9 Photochemistry Theory

2.9.1 Photoluminescence and Photoluminescence Excitation Theory

Photoluminescence is observed when photons cause electronic excitation events in a a material, which in turn re-emits light, typically of a lower energy [118]. Photoluminescence has the advantage of very high sensitivity to determine doping densities. It can also be used to detect defects in both the bulk and surface of the materials [119].

In the direct bandgap semiconductor materials, if the excitation energy is larger than the bandgap energy, electrons will be excited from valence band to conduction band and leave a hole behind. Thus an electron-hole pair is than formed. If this electron-hole pair recombines radiatively, a photon will be emitted. However, there are chances that the electrons and holes may recombine in the form of heat.

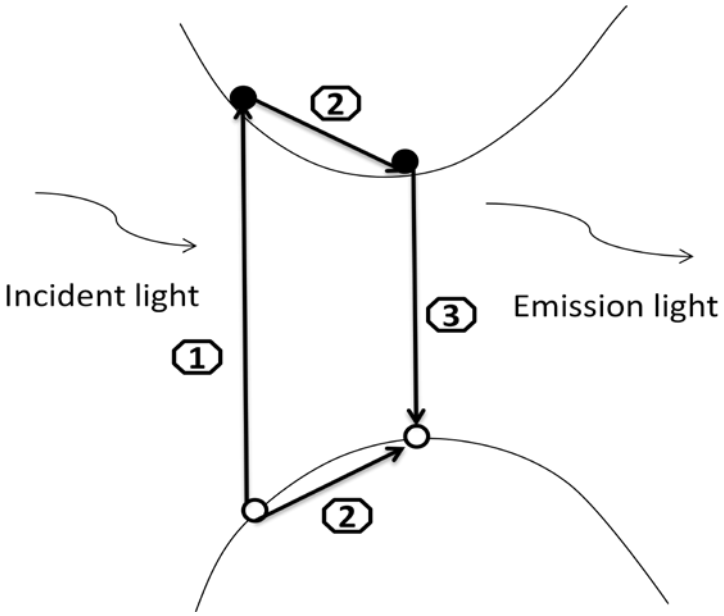

Figure 2.28 PL in a direct bandgap semiconductor

The three steps that contribute to the photoluminescence process shown in Fig 2.28 are:

1. Excitation
2. Excited state relaxation
3. Recombination

Under the incident light, electrons will be excited from valence band to the conduction band, after which electrons (holes) in the higher energy levels of the conduction (valence) band will relax to the lowest energy levels(the highest energy levels) within the conduction (valence) band by releasing phonons or other physical processes. Light is then generated by the recombination of electrons and holes.

The emitted photon energy depends on the radiative recombination Illustrated in Fig 2.29, are five commonly observed PL transitions which include: (a) Band-to-band recombination,(b) a free exciton recombination,(c) a free hole that can combine with a neutral donor, (d) a free electron that can combine with a hole on a neutral acceptor,(e)an electron on a neutral donor can recombine with a hole on a neutral acceptor.

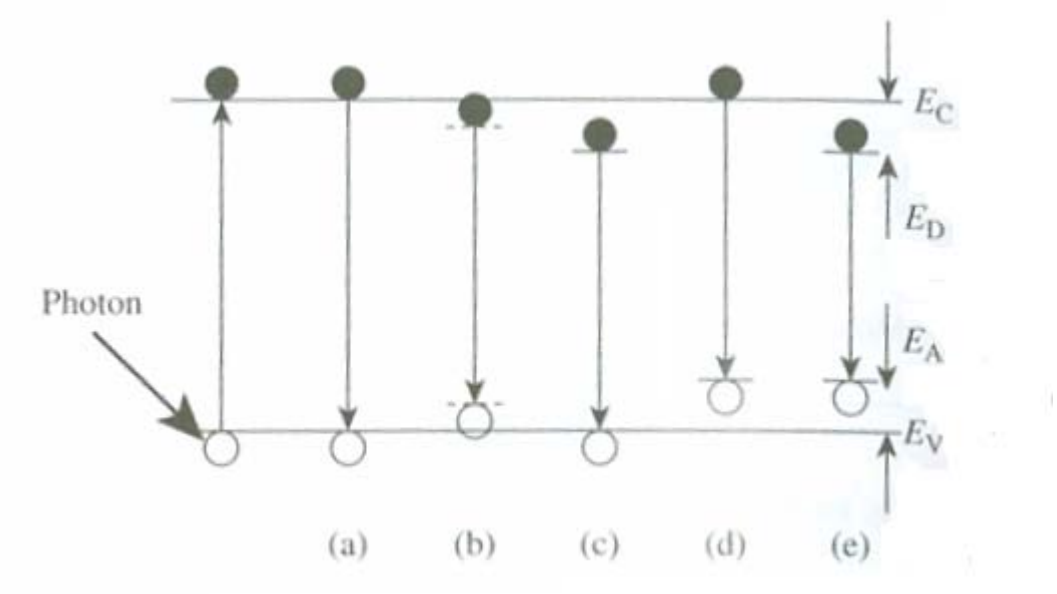

Figure 2.29 Radiative transitions observed with photoluminescence. Reproduced from reference [120]

Photoluminescence excitation is measured by keeping the monitored wavelength constant and changing the excitation wavelength. The best excitation for the emission being monitored is thus determined.

2.9.2 Thin Film Lifetime Theory

For singlet excitons, nonradiative decay modes can be (i) an intercrossing of singlets to a lower triplet state with emission of phonons:$S_1 \rightarrow T_1$+phonons; or (ii) a direct decay to ground state with emission of phonons: $S_1 \rightarrow S_0$+phonons . On the other hand, fission of singlets can also occur leading to the formation of (i) two triplets when the lowest level of the triplet is less than half that of a singlet exciton: $S_1 \rightarrow T_1 + T_1$+phonons; or(ii) two polarons,\ when the polaron levels are close to that of a singlet exciton: $S_1 \rightarrow P^+ + P^-$ + phonons. Finally, interactions of singlet excitons with polarons which is a quasiparticle composed of a charge and its accompanying polarization field are also the cause of nonradiative decays: $S_1 + P^+ \rightarrow P$

$^{-}$ + phonons; $S_1 + P^- \rightarrow P^+ +$ phonons. For the triplets, the nonradiative decay modes can be (i) a direct way to ground state with emission of phonons: $T_1 \rightarrow S_0 +$phonons; or(ii) interactions of triplet excitons with polarons:$T_1 + P^+ \rightarrow P^- +$ phonons; $T_1 + P^- \rightarrow P^+ +$ phonons. Comparatively, the radiative decay modes are much less numerous. From singlet excitons, emission of a photon is obtained by a direct decay of excitons to the ground state:$S_1^* \rightarrow S_0$ +hν+phonons. From triplet excitons, radiative decay is indirect and is obtained through the collision of two triplets forming a singlet that radiatively decays to the ground state: $T_1 + T_1 \rightarrow S_1^* \rightarrow S_0 +$hν+phonons

Theoretically, only 25% of the excitons can lead to radiative decay in a material without traps [120]. However, the efficiency of devices is much less than this value because of the different nonradiative decay modes that are in competition. If *b* is the fraction of absorbed photons generating the emission ($0 \leq b \leq 1$), the quantum yield is $\varphi = \frac{b\tau}{\tau_r}$,with $\frac{1}{\tau} = \frac{1}{\tau_r} + \frac{1}{\tau_{nr}}$,where τ_r is the natural radiative lifetime, and τ_{nr} is the nonradiative decay.

2.9.3 Quantum Yield Theory

The fluorescence lifetimes and quantum yields of fluorescent substances are frequently measured. The meanings of these parameters are best illustrated by reference to a modified Joblonski diagram (Figure 2.30). In this diagram we did not explicitly illustrate the individual relaxation processes leading to the relaxed S1 state. Instead, we direct attention to those processes responsible for return to the ground state. In particular ,we are interested in the emissive rate of the fluorophore (Γ) and its rate of non-radiative decay to S_0(k).

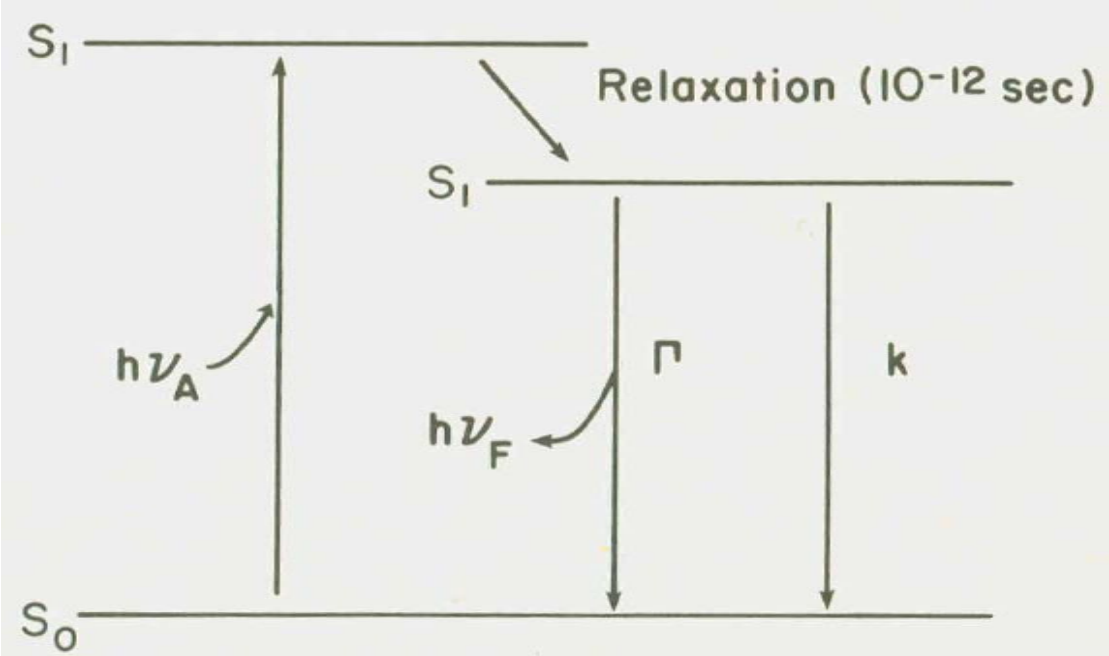

Figure 2.30 Modified Jablonski diagram. Reproduced from reference [120].

The fluorescence quantum yield is the ratio of the number of photons emitted to the number absorbed. The rate constants Γ and k both depopulate the excited state. The fraction of fluorophores which decay through emission, and hence contribute to quantum yield is given by $Q = \frac{\Gamma}{\Gamma + k}$

2.10 Limitation of OLED Technologies

Before commercialization of the OLEDs, several problems have to be resolved., OLED lifetime, efficiency and color stability in particular must be addressed. Researchers at Kodak proposed an equation to calculate device lifetime; $L_0 \times t_{1/2}$=constant (L_0 is the initial brightness, $t_{1/2}$ is the time the device takes to decay from the initial brightness to half of the initial brightness). This equation indicates the higher the device operating brightness, the shorter the device takes to decay from the initial brightness to half the initial brightness.

Device degradation can be caused by many reasons and more research has to be done to further clarify this issue. Intrinsic and extrinsic properties of OLEDs govern the two main degradation mechanisms, and both of them have to be thoroughly investigated before achieving the goal of 50,000-70,000 hours OLED lifetime.

2.10.1 Extrinsic Property

Generally speaking, degradation mechanism which is not caused by OLED material and structure properties will be categorized as extrinsic property, the main characteristic of which is the occurrence of dark spots. The gradual increase of non-emitting area eventually shortens device lifetime. Most OLED materials are extremely sensitive to water and oxygen. If the encapsulation of the OLED is not well done, black spots will be easily observed in the pixel and as time goes, black spots will swell. Black spot is the key factor that can influence device lifetime which are caused by the rough and uneven features of the ITO substrate[121], small particulate contamination on the ITO substrate, separation between organic layer and electrodes[122], and pinholes on the cathode electrode [123]-[124].

2.10.2 Intrinsic Property

The way to measure lifetime of the OLED device can be under DC or AC drive conditions. In general, ac measurements produce longer life time result than dc lifetime measurements. Even though dark spots may not appear in certain devices after certain control conditions, degradation of brightness still can be observed in these lifetime measurement. Intrinsic degradation can be generally categorized into six groups:(1) stability of organic

layer and (2) the interface between anode and organic layer (3) stability of excited states (4) diffusion of indium into organic layers (5) mobile ionic contaminations (6) accumulation of positive charge mechanism.

2.10.3 Efficiency Stability for Application of Phosphorescent OLEDs(PHOLEDs)

Numerous studies have investigated the reasons for efficiency roll-off in PHOLEDs. The main mechanisms responsible for the decrease in efficiency at high current density can be sorted as: triplet-triplet quenching [125], triplet polaron quenching [125], and dissociation of excitons into free carriers [126]. A lot of research has been done to achieve a significant reduction in roll-off. For instance, PHOLEDs with a broad exciton formation zone are needed [127], and efficiency can be stabilized by inserting an exciton blocker, or, by controlling the charge transport properties of interlayers and the triplet host materials[128]. However, before PHOLEDs can be efficient enough for application in larger applications more research has to be done.

2.10.4 Color Stability for PHOLED Application

The issues that may cause color instability in PHOLEDs have been discussed in chapter 2.6.2. Strategies such as fine-tuning the thickness of individual emitting layers, adjusting interlayer structure, rearranging stacking sequence and varying doping concentration are important to improve color stability. More research also needs to be done to improve color stability before OLED devices will find more widespread applications.

2.11 Reference:

[1]Y. A. Ono, *Electroluminescent displays*, 2nd edition, (WSP, Singapore, 2000), chapter 3.

[2]Sam-Shajing Sun, Larry R. Dalton, Introduction to Organic Electronic and Optoelectronic Materials and devices, 2nd edition, (CRC press, Maryland, 2008) chapter 12.

[3]A. N. Krasnov, Displays, **24**, 73 (2003)

[4] D. Carkner, Inf. Display **13**, 10 (1997).

[5] L.S. Hung, C.H. Chen, Materials Science and Engineering R **39**, 143 (2002).

[6] R. Friend, J. Burroughes, D. Bradley, WO Patent 90/13148 (1990).

[7] R. Friend, J. Burroughes, D. Bradley, US Patent 5247190 (1993).

[8] Hari Singh Nalwa, and Lauren Shea Rohwer (Eds.), *Handbook of Luminescence, Display Materials and Devices*, (ASP Press, California, 2003) vol. 1.

[9]David Mitzi, *Solution Processing of Inorganic Materials*. (JW&S, New Jersey, 2009). Chapter 2.

[10] http://www.ledtronics.com/html/ColorChart.htm

[11] Pope, H. Kallmann, P. Magnante, J. Chem. Phys **38**, 2042 (1963)

[12] W. Heilfrich and W.G. Schneider, Phys. Rev. Lett **14**, 229 (1965)

[13] C.W. Tang, S.A. VanSlyke, Appl. Phys. Lett **51**, 913 (1987).

[14] M. Gross, D. Mu¨ ller, C. Bra¨uchle, K. Meerholz, Synth.Met, **102**, 1147(1999).

[15] K. Sugiyama, H. Ishii, Y. Ouchi, K. Seki, J. Appl. Phys **87**, 295(2000)

[16]J.S. Kim, M. Granstro¨m, R.H. Friend, N. Johansson, W.R. Salaneck,R. Daik, W.J. Feast, F. Cacialli, J. Appl. Phys **84**, 6859(1998).

[17] Y. Shen, D.B. Jacobs, G.G. Malliaras, G. Koley, M.G. Spencer,A. Ioannidis, Adv. Mater

13, 1234 (2001).

[18] C. Qiu, Z. Xie, H. Chen, M. Wong, H.S. Kwok, J. Appl. Phys **93**, 3253 (2003).

[19] Y. Kurosaka, N. Tada, Y. Ohmori, K. Yoshino, Electr. Eng. Jpn **132**, 14 (2000).

[20] W. Hu, K. Manabe, T. Furukawa, M. Matsumura, Appl. Phys. Lett. **80**, 2640 (2002).

[21] C. Qiu, Z. Xie, H. Chen, M. Wong, H.S. Kwok, J. Appl. Phys. **93**, 3253 (2003).

[22] L.S. Hung, C.W. Tang, M.G. Mason, Appl. Phys. Lett. **70,** 152 (1997).

[23] G.E. Jabbour, B. Kippelen, N.R. Armstrong, N. Peyghambarian, Appl.Phys. Lett. **73,** 1185 (1998).

[24] J. Lee, Y. Park, D.Y. Kim, H.Y. Chu, H. Lee, L.M. Do, Appl. Phys.Lett. **82,** 173(2003).

[25] Q. Xu, J. Ouyang, Y. Yang, T. Ito, J. Kido, Appl. Phys. Lett. **83**, 4695(2003).

[26] Y.E. Kim, H. Park, J.J. Kim, Appl. Phys. Lett. **69**, 599(1996).

[27]Hartmut Yersin, *Highly efficient OLEDs with phosphorescent materials*.(WILEY-VCH,New York, 2008).

[28]C.W.Tang, S.A.VanSlyke, C.H.Chen, J.Appl.Phys.**65**, 3610 (1989).

[29]J.Shi, C.W.Tang, Appl phys lett **70**, 1665 (1997)

[30] H. Yersin, Top. Curr. Chem. **241**, 1 (2004)

[31](a) M.A.Baldo and D.F.O'Brien ,Physical review B, **60**, 20 (1999)

(b) M.A.Baldo, M.E Thompson, S.R Forrest, Nature **403**, 750 (2000).

[32]G. Gu, D. Z. Garbuzov, P. E. Burrows, S.Vendakesh, S. R. Forrest, and M. E. Thompson,Opt. Lett, **22**, 396 (1997).

[33] S. Moller and S. R. Forrest,J. Appl.Phys. **91**, 3324(2002).

[34] M. Fujita, T. Ueno, S. Noda, H. Ohhata, T. Tsuji, H. Nakada, and N. Shimoji, Organic

Electronics Lett. **39**, 24 (2003).

[35] S.T. Zhang, X.M. Ding, J.M. Zhao, H.Z. Shi, J. He, Z.H. Xiong,H.J. Ding, E.G. Obbard, Y.Q. Zhan, W. Huang, X.Y. Hou, Appl. Phys.Lett. **84,** 425 (2004).

[36]R.Schlaf, B.A.Parkinson, P.A.Lee, K.W.Nebesny, G.Jabbour, B.Kippelen, N.Peyghambarian, N.A.Armstrong, J.Appl.Phys **84**, 6729 (1998).

[37]Y.-H.Niu, M.S .Liu, J.-W.Ka,A K.-Y. Jen, Appl. Phys .Lett . **88**, 93505(2006).

[38]X.Ren,J.Li,R.J.Holmes,P.I.Djurovich,S.R.Forrest,M.E.Thompson,Chem.Mater.**16**, 4743(2004).

[39]M.E. Thompson, (private communication).

[40] J. X. Sun, X. L. Zhu, Z. G. Meng, X. M. Yu, M. Wong and H. S. Kwok SID 06 DIGEST p1193(2006)

[41]Xiangfei Qi, Michael Slootsky,and Stephen Forrest,Appl. Phys. Lett. **93**, 193306(2008)

[42] V.Adamovich, J. Brooks, A. Tamayo, A. M. Alexander, P. I. Djurovich,B. W. D'Andrade, C. Adachi, S. R. Forrest, M. E. Thompson,New J. Chem. **26**, 1171(2002).

[43] B. W. D'Andrade, J. Brooks, V. Adamovich, M. E. Thompson, S. R. Forrest, Adv. Mater. **14**, 1032 (2002).

[44] S. Tasch, E. J. W. List, O. Ekstrom, W. Graupner, G. Leising, P. Schlichting, U. Rohr, Y. Geerts, U. Scherf, K. Mullen, Appl. Phys. Lett. **71**, 2883 (1997).

[45] P.-I. Shih, C.-F. Shu, Y.-L. Tung, Y. Chi, Appl. Phys. Lett. **88**: 251110(2006).

[46] S. Tasch, E. J. W. List, O. Ekstrom, W. Graupner, G. Leising, P. Schlichting, U. Rohr, Y. Geerts, U. Scherf, K. Mullen, Appl. Phys. Lett. **71**, 2883 (1997).

[47] P.-I. Shih, C.-F. Shu, Y.-L. Tung, Y. Chi, Appl. Phys. Lett. **88**, 251110 (2006).

[48] B. W. D'Andrade, R. J. Holmes, S. R. Forrest, Adv. Mater. **16**, 624 (2004)..

[49] J. Kido, H. Shionoya, K. Nagai, Appl. Phys. Lett. **67**, 2281 (1995)..

[50] M. Granström, O. Inganäs, Appl. Phys. Lett. **68**, 147 (1995).

[51] J.-H. Jou, M.-C. Sun, H.-H. Chou, C.-H. Li, Appl. Phys. Lett. **87,** 43508 (2005).

[52] Jan Kalinowski, Massimo Cocchi, Dalia Virgili, Valeria Fattori, and J. A. Gareth Williams Adv. Mater **19**, 4000 (2007).

[53] Evan L. Williams, Kirsi Haavisto, Jian Li, and Ghassan E. Jabbour Adv. Mater.**19**, 197 (2007).

[54] Brian W. D'Andrade, Mark E. Thompson, and Stephen R. Forrest Adv. Mater. **14**, 147(2002)

[55] Yuichiro Kawamura, Shozo Yanagida, J. Appl. Phys., **92**, 87 (2002).

[56]Brian W.D'Andrade, Jason Brooks,Vadim Adamovich, Adv. Mater, **14**, 1032 (2002).

[57]Edited by Hartmut Yersin, *Highly Efficient OLEDs with phosphorescent Materials,* (Wiley-VCH, Regensburg, German, 2008)

[58]H.L.Ma,D.H.Zhang,P.Ma,S.Z.Win,and S.Y.Li,Thin Solid Films **263**, 105(1995)

[59]J.LYao,S.Hao ,and J.S.Wilkinson,Thin Solid Films **189**, 227(1990)

[60]N.Nadaud ,D.Y.Kim ,and P.Boch,J .Am .Ceram.Soc **80**, 1208(1997)

[61]W.F.Wu and F.S.Chiou,Semicond.Sci .Technol.**11**, 196(1996)

[62]T.Maruyama and K.Fukui ,J.Appl.Phys,**70**, 3848(1991)

[63] T.Maruyama and K.Fukui,Thin Films **203**, 297(1991)

[64]H.Kim ,A .Pique,J.S.Horwitz,H.Mattoussi,H.Murata,Z.H.Kafafi,and D.B Chrisey,Appl.Phys lett.**74**, 3444(1999).

[65]S.Ashok ,P.P.Sharma,and S.J.Fonash,IEEE Trans.Electron Devices ED-27(4),725(1980).

[66]T.Furusaki,J.Takahashi and K.Kodaira,J.Ceram,Soc ,Jpn,**102**, 200 (1994)

[67] I.-M. Chan, W.-C. Cheng, F.C. Hong, Asia Display/IDW'01, p1483 (2001).

[68]Shih-Fang Chen,Ching-Wu Wang, Appl. Phys. Lett., **85**, 765 (2004).

[69] M.Matsumura, K.Furukawa, and Y.Jinde,Thin Soild films **331**, 96 (1998).

[70] Alex Ryer, *Light measurement handbook, (*International Light Inc, Gilbert, 1998).

[71]Greenham,N.C. and Friend,R.H. Solid State Phys.**49**, 1(1995).

[72] Chihaya Adachi, Marc A. Baldo, Mark E. Thompson, and Stephen R. Forrest, Journal of applied physics volume **90**, 5048(2001).

[73] CIE (1932). Commission internationale de l'Eclairage proceedings, 1931. Cambridge University Press, Cambridge.

[74]S.Naka,H,Okada,H.Onnagawa,Y.Yamaguchi,and T.Tsutsui,Synth.Met. **331**, 111(2000).

[75] Y. Shirota, K. Okumoto, H. Inada, Synth. Met. **111**, 387(2000).

[76]Thien Phap Nguyen and Pierre Destruel, *Handbook of Luminescence, Display Materials, and Devices*(ASP, Valencia, 2003).

[77]Edited by Klaus Mullen and Ullrich Scherf ,*Organic Light-Emitting Devices Synthesis,Properties,and Applications* (Wiley-VCH, Weinheim, German, 2006).

[78]Y.Shirota,M.Kinoshita,K,Okumoto,Proc.SPIE-Int.Soc.Opt.Eng. **4464**, 203 (2002).

[79]D.F.O'Brien,M.A.Baldo,M.E.Thompson,S.R.Forrest,Appl.Phys.Lett.,**74**, 442 (1999).

[80] Vadim Adamovich, Jason Brooks, New J. Chem., **26**, 1171 (2002)

[81]Biwu Ma,Peter I.Djurovich,Simona Garon,etc.,Adv.Func.Mater. **16**, 2438 (2006).

[82]L.C.Picciolo,H.Murata and Z.H.Kafafi,Appl.Phys.Lett.,**78**, 2378 (2001)

[83]B.X.Mi,Z.Q.Gao,M.W.Liu,K.Y.Chan,H.L.Kwong,N.B.Wong,C.S.Leee,L.S.Hung and S.T.Lee,J.Mater.Chem.,**12**, 1307(2002).

[84]F.-C.Chen,G.He,Y.Yang,Appl.Phys.Lett.,**82**, 1006(2003).

[85]M.Sudhakar,P.I.Djurovich,T.E.HogenEsch,M.E.Thompson,J.Am.Chem.Soc.,**125**, 7796(2003).

[86]D.M.Pai,J.F.Yanus,M.Stolka,J.Phys.Chem.,**88**, 4714(1984).

[87]H,Kanai,S.Ichinosawa,Y.Sato,Synth.Met.,**91**, 195(1997).

[88]S.Lamansky,P.Djurovich,D.Murphy,F.AbdelRazzaq,H.E.Lee,C.Adachi,P.E.Burrows,S.R. Forrest,M.E.Thompson,J.Am.Chem.Soc.,**123**, 4304(2001).

[89]T.Tsuisui,M.J.Yang,M.Yahiro,K.Nakamura,T.Watanabe,T.Tsuji,M.Fukuda,T.Wakimoto, S.Miyaguchi,Jpn.J.Appl.Phys. **38**, 1502(1999).

[90]C.Adachi,R.C.Kwong ,S.R.Forrest,Org.Electron.**2**, 37(2001).

[91]M.A.Baldo,M.E.Thompson,S.R.Forrest,Nature(London),**403**, 750(2000).

[92]B.W.D'Andrade,M.A.Baldo,C.Adachi,J.Brooks,M.E.Thompson,S.R.Forrest,Appl.Phys.L ett.,**79**, 1045(2001).

[93]T.Watanabe,K.Nakamura,S.Kawami,Y.Fukuda,T.Tsuji,T.Wakimoto,S.Miyaguchi,M.Yah iro,M.J.Yang,T.Tsutsui.Synth.Met.,**122**, 203(2001).

[94]C.Adachi,R.C.Kwong,P.Djurovich,V.Adamovich,M.A.Baldo,M.E.Thompson,S.R.Forrest ,Appl.Phys.Lett.,**79**, 2082(2001).

[95]R.J.Holmes,S.R.Forrest,Y.J.Tung,R,C.Kwong,J.J.Brown,S.Garon,M.E.Thompson,Appl.P hys.Lett. **82**, 2422 (2003).

[96]S.Tokito,T.Iijima,Y,Suzuri,H.Kita,T.Tsuzuki,F.Sato,Appl.Phys.Lett.,**83**, 569 (2003).

[97]I.Tanaka,Y.Tabata,S.Tokito,Chem.Phys.Lett.,**400**, 86 (2004).

[98]J.L.Fox and C.H.Chen,US4,736,032(1988)

[99]T.Inoe and K.Nakatani,JP6,009,952(1994)

[100]J.Ito,JP7,**166**,160(1995).

[101]A.B.Tamayo,B.D.Alleyne,P.I.Djurovich,S.Lamansky,I.Tsyba,N.N.Ho,R.Bau,M.E.Tho mpson,J.Am.Chem.Soc.**125**, 7377(2003).

[102] Brian W. D'Andrade, Marc A. Baldo, Chihaya Adachi, Jason Brooks,Mark E. Thompson,and Stephen R. Forrest,Appl. Phys. Lett. **79**, 1045 (2001).

[103] V. Bulovic´, A. Shoustikov , M.A. Baldo, E. Bose , V.G. Kozlov, M.E. Thompson , S.R. Forrest, Chem. Phys. Lett. **287**, 455 (1998).

[104]C.H.Chen,J.Shi,K.P.Klubek,US Patent 5,908,581(1999).

[105]M.A.Baldo,D.F.O'Brien ,Y.You,A.Shoustikov,S.Sibley,M.E.Thompson,S.R.Forrest,Nat ure,**395**, 151(1998).

[106]S.Lamansky,P.Djurovich,C.E.Murphy,F.AbdelRazzaq,R.C.Kwong,I.Tsyba,M.Bortz,B. Mui,R.Bau,M.E.Thompson,Inorg.Chem. **40**, 1704 (2001).

[107]S.Lamansky,P.Djurovich,D.Murphy,F.AbdelRazzaq,H.E.Lee,C.Adachi,P.E.Burrows,S. R.Forrest,M.E.Thompson,J.Am.Chem.Soc. **123**, 4304 (2001).

[108]A .Tsuboyama,H.Iwawaki,M.Furugori,T.Mukaide,J.Kamatani,S.Igawa,T.Moriyama,S. Miura,T.Takiguchi,J.Am.Chem.Soc. **125**, 12971 (2003).

[109] Wolfgang Brutting, Stefan Berleb, Anton G. Muckl, Organic Electronics **2,** 1(2000)

[110]M.A.Lambert and P.Mark,*Current injection in Solids*,(Academic Press, New York,1970)

[111]J.H.Schön,Synth.Met.**122**, 157(2001).

[112]D.M.Pai ,J.Chem.Phys,**52**, 2285(1970).

[113] Pankaj Kumar, S C Jain, Vikram Kumar, Suresh Chand, M N Kamalasanan and R P Tandon, J. Phys. D: Appl. Phys. **40**, 7313 (2007).

[114] Raja M, Lloyd G C R, Sedghi N, Eccleston W, Lucrezia R D and Higgins S J J. Appl. Phys. **92,** 1441(2002)

[115] Poplavsky D, Nelson J and Bradley D D C Appl. Phys.Lett. **83**, 707(2003)

[116] Fong.H .H, Lun. K C and So. S K,Chem. Phys. Lett. **353,** 407(2002)

[117] Pai.D.M, J. Chem. Phys. **52,** 2285(1970)

[118]Dieter K. Schroder*: Semiconductor material and device characterization*(John Wiley& Sons, Inc, Canada, 1998)

[119] J. Brooks, Y. Babayan, S. Lamansky, P.I. Djurovich, I. Tsyba, R. Bau, M.E. Thompson, Inorg. Chem. **41,** 3055 (2002).

[120] Thien Phap Nguyen and Pierre Destruel, *Handbook of Luminescence, Display Materials, and Devices*(ASP, Valencia, 2003).

[121]P.N.M.dos Anjos,H.Aziz,H.-X.Hu,Z.D.Popovic,Organic Electronics,**3**, 9(2002).

[122]H.Aziz,Z.D.Popovic,C.P.Tripp,N.Hu,A.Hor,G.Xu,Appl.Phys.Lett.,**72**, 2642(1998).

[123]S.F.Lim,L.Ke,W.Wang,S.J.Chua,Appl.Phys.Lett.,**78**, 2116(2001).

[124] S.F.Lim, W.Wang, S.J.Chua,Mater.Sci.Eng.,B**85**, 154(2001).

[125] M. A. Baldo, C. Adachi, and S. R. Forrest, Phy. Rev. B **62**, 10967,(2000).

[126] J. Kalinowski, W. Stampor, J. Mezyk, M. Cocchi, D. Virgili, V. Fattori, and P. Di Marco, Quenching effects in organic electrophosphorescence, Phy. Rev. B **66,** 235321(2002).

[127]D. Zhang,W. Li, B. Chu, J. Zhu, T. Li, L. Han, D. Bi, X. Li, D. Yang, F. Yan, H. Liu, D.

Wang, and T. Tsuboi , Appl. Phy. Lett. **91**, 183516 (2007).

[128] K.S. Yook et al. Journal of Industrial and Engineering Chemistry **15**, 420 (2009)

CHAPTER 3

STRUCTURE, CHEMICAL AND PHOTOLUMINESCENCE OF BIS[3,5-BIS(2-PYRIDYL)-1,2,4-TRIAZOLATO]PLANTINUM(II)-BASED THIN FILMS

3.1 Introduction

As mentioned in the previous Chapter, electrophosphorescent materials can potentially harvest both triplet and singlet exciton and improve the internal quantum efficiency of devices to 100%. Iridium (III) cyclometalated complexes and platinum(II) complexes both have unique photo-physical properties and their application in OLEDs have been widely reported. Up to 19% external quantum efficiency has been achieved by many research groups using neutral iridium complexes [1-4]. Daisaku Tanaka, Hisahiro Sasabe et al have fabricated the structure ITO/TPDPES: TBPAH10wt% (20 nm)/TAPC (30nm)/CBP: Ir(ppy)3 8wt%(10nm)/ B3PYMPM (50 nm)/LiF(0.5nm)/Al(100nm) and report a high power efficiency (PE) of 133 lm/W and external quantum efficiency (EQE) of 29% from this structure [5]. For white OLEDs using Ir(ppy)3, 53 lm/W PE and 25 % EQE at a brightness of 100 cd/m^2 were achieved [6]. More recently platinum (II) has attracted attention due to their high variety of energy transfer mechanisms and emissive excited states[7-21] which include [6]: (i) intraligand (IL) π-π^* energy transfer, (ii) intraligand transfer of the "excimer" type[$\sigma^*(\pi)\rightarrow\sigma(\pi^*)$], (iii) metal-to-ligand(MLCT) [Pt(5d)$\rightarrow\pi^*$ (ligand)] transfer,(iv) oligomeric metal-metal-to-ligand charge transfer [$d\sigma^*(dz^2)\rightarrow\sigma(\pi^*)$](MMLCT), and(v)monomer ligand –field (LF) processes.

In order to maximize the luminescence efficiencies of simple square-planar platinum(II) complexes in solution, chemists have introduced high field co-ligands to di- and

tri-imine complexes, exploited intraligand charge transfer in excited states, and used cyclometallation [22]. Among the platinum (II) compounds that have potential use in practical OLED applications, there are several prominent, efficient ones. The oldest is octaethylporphyrin (PtOEP) which belongs to platinum prophyrins and emits in the red with a peak at λ_{max} = 641 nm, excited state lifetime τ =65μs, and relatively high quantum yield, ϕ_{lum} = 0.6 [23]. However, saturation of the emission signals and a rapid drop in device efficiency at high driving currents (see Fig3.1 b) are observed due to the planar geometry which easily induces the formation of aggregates [24] or excimers [25] via efficient π-π stacking at the vacant coordination sites on the Pt(II) atom [26].

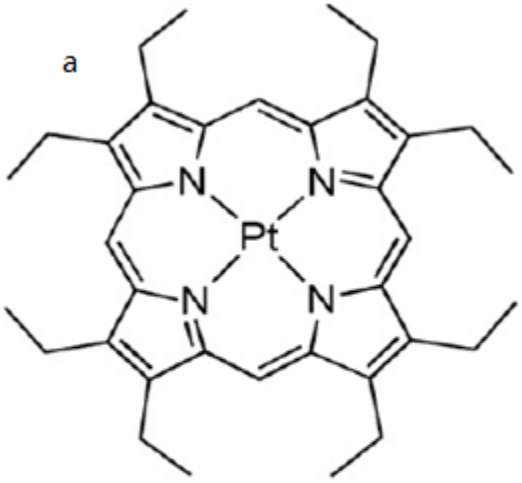

PtOEP

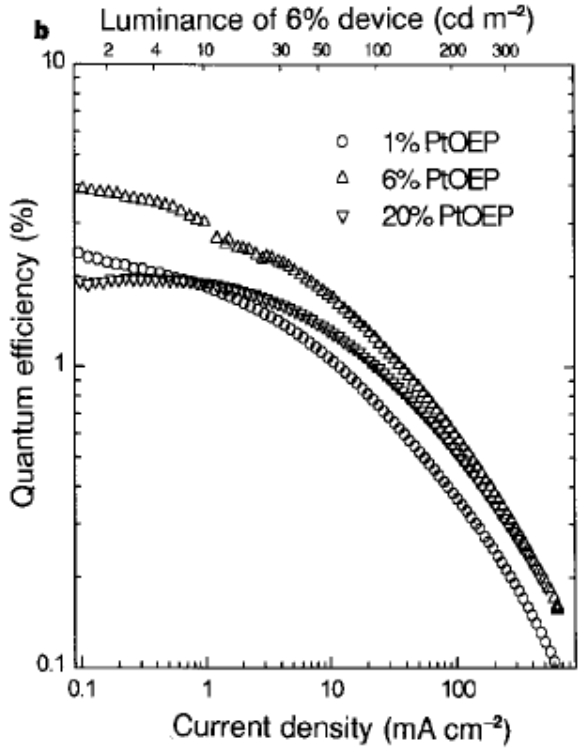

Figure 3.1 Pt(OEP) molecular structure and quantum efficiency of Pt(OEP) emission as a function of doping concentrations for Alq3:Pt(OEP) devices. Reproduced from reference [28].

D. F. O'Brien and M. A. Baldo have reported external quantum efficiencies of up to 5.6±0.1% at low brightness and 2.2±0.1% at 100 cd/m^2 by doping PtOEP into 4,4'-*N*,*N*'-dicarbazole-biphenyl (CBP) host in the structure ITO/NPD/CBP:PtOEP(6%)/BCP/Alq3 /Mg:Ag [28]. In general, sterically unencumbered platinum (II) complexes are frequently prone to self-quenching at elevated concentrations. Pt (OEP) will form excimers at higher concentrations which are emissive at longer wavelengths than the isolated monomers [22][29]. Pt(OEP) doped at 6% into Alq3 devices exhibit 4% EQE, whereas 20% Pt(OEP) doped devices exhibit only 2% EQE as is shown in Fig 3.1.

In the solid state, excimer-like emission is mainly achieved from either the close packing of molecules or aggregation of the molecules in the ground state. Efficient excimer

emission from several (C^N)Pt(O^O) dopants have been described in Thompson's papers [30][31]. From the point of view of OLEDs, the combination of broad monomer and excimer emission from a single metal complex is potentially and effective way forward in the development of white light emitting devices (WOLEDs)[22]. The four compounds in Fig 3.2 a are all (C^N)Pt(O^O) dopants, but in contrast to compound1, compounds 2-4 have greater steric bulk. Due to the more sterically encumbered arrangement, the tendency to form aggregates is reduced. In other words, higher doping concentrations are needed for compounds 2-4 to produce balanced monomer/excimer emission as the comparison in Fig 2b shows..

a

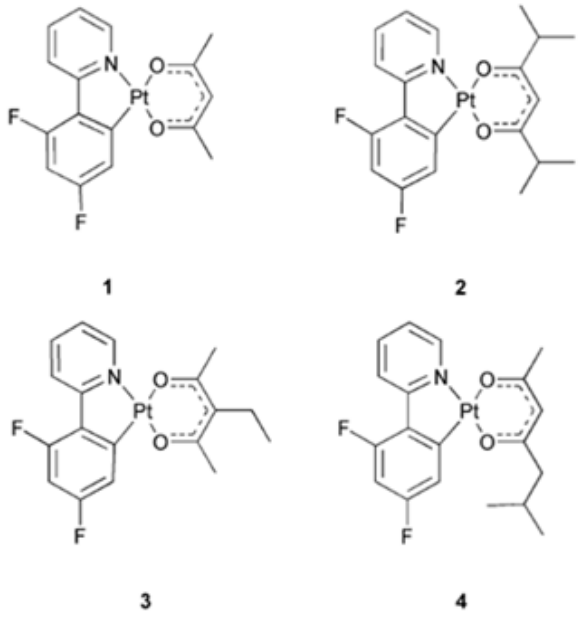

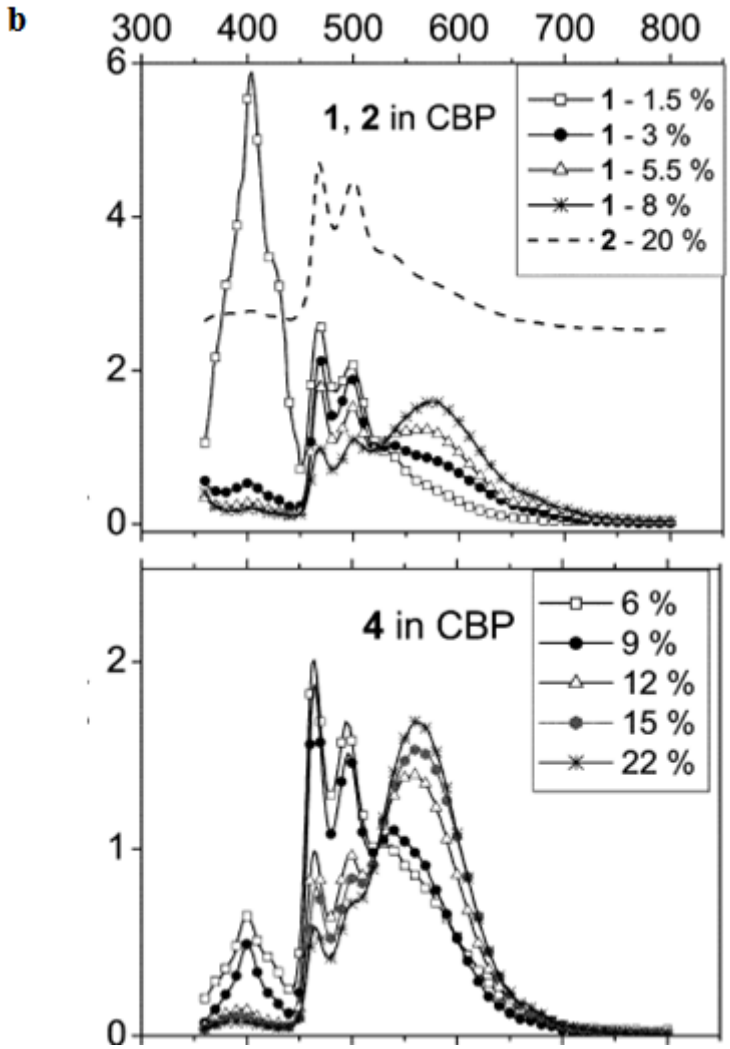

Figure 3.2 The structures of 4 kinds of (C^N)Pt(O^O) dopants and photoluminescence of different doping concentrations of these Pt phosphors in the CBP host. Reproduced from reference [32].

It was reported by Forrest's group that by combining monomer and excimer emission from platinum(II) (2-(4',6'-difluoro-phenyl) pyridinato -N,$C^{2'}$) (2,4-pentanedionate) (FPt1) with the blue emission from a fluorescent dopant (FIrpic) , broad emission, a peak external quantum efficiency of 4.0±0.4%, and peak power efficiency of 4.4±0.4lm/W could be obtained from OLEDs featuring this combination [33].

Exciplexes can be another method of achieving broad-band emission from a single dopant. An exciplex is an excited complex of an electron donor D and an electron acceptor A,

|DA|*, that is dissociative in the ground state, just like an excimer [22]. As a matter of fact, excimers are basically a special case of an exciplex, in which the two constituent entities are identical [22]. Excimers are formed in the excited state and is due to the overlap of the wavefunctions of two adjacent, similar molecules. The ground states of exciplexes and excimers are not bound, so energy can be transferred from the host to the luminescent center efficiently [33].

PtL2Cl complexes coordinated with N^C^N terdentate ligands based on 1,3-dipyridylbenzene, have been synthesized and reported by Williams, Cocchi, Kalinowski and co-workers. By forming triplexes which yield efficient phosphorescence with an electron donor D and an electron acceptor A, a broad emission band which may be suitable for WOLED applications was demonstrated A color rendering index of 90 with an external quantum efficiency of 6.5% have been reported [34] using MTdata: 4,4',4 -tris(*N*-(3-methylphenyl)-*N*-phenylamino)triphenylamine as an electron donor.

Other notable research on electrophosphorescence from Pt(II) complexes has been reported by Chang *et al.* utilizing pyridyl azolate-based chelates, which attained maximum external quantum and power efficiencies of 5.9% and 6.4 lm/W respectively. [35]. The luminescence in this work [35] has been assigned to metal-metal-to- ligand charge transfer in excimers and oligomers.

A new phosphorescent platinum(II)-pyridyltriazolate complex, bis[3,5-bis(2-pyridyl)-1,2,4-triazolato] platinum(II), $Pt(ptp)_2$, was synthesized and characterized by Wei-Hsuan Chen from the Omary's group at the Chemistry department of University of North Texas, and a major focus of the present work.

Single crystal X-ray diffraction indicates the short Pt-Pt separation of 3.442A, which can explain the high tendency of forming aggregation[7]. Similar to the two previously discussed platinum(II) compounds, single crystal X-ray diffraction shows that $Pt(ptp)_2$ forms planar stacks stabilized *via* strong intermolecular Pt(II)···Pt(II) interactions (3.289 Å), making it amenable to forming excimers. Fig 3.3 is the molecular structure of $Pt(ptp)_2$ obtained by X-ray crystallography. Although the X-ray diffraction data show significant disorder in the non-coordinated pyridine ring of each ptp ligand, the PtN4 coordination geometry is determined accurately showing a bidentate l2–N,N'– coordination mode from the nitrogen atom of the other pyridine ring and the nitrogen atom in the 1–position of the triazolate moiety to the platinum(II) center. The Pt(II) pyridyltriazolate square-planar units stack into infinite chains with relatively strong Pt(II)…Pt(II) intermolecular interactions extended in columnar one-dimensional chains. These intermolecular forces belong to the general category of closed-shell ‘‘metallophilic interactions" known for multiple classes of molecular materials, including d^8 and d^{10} complexes, which have been ascribed to correlation effects that are strengthened by relativistic effects [36]. Overall, the X-ray structure confirms that $Pt(ptp)_2$ is a non-organometallic/ non-cyclometalated square-planar complex with no C–Pt bonds, and that it exhibits intermolecular interactions that warrant formation of fully-overlapped excimer units. The desired advantages of the design include the symmetry of the coordination sphere, which facilitates formation of fully-overlapped excimers, and the extended p system (six aromatic rings total), which renders the molecule an excellent antenna with visible absorptions. The homoleptic nature of the Pt(N^N)2 coordination sphere in $Pt(ptp)_2$ is distinctly different from the heterolyptic Pt(C^N)(O^O) or Pt(N^C^N)Cl

coordination spheres in the aforementioned most efficient Pt(II) complexes used in the OLED literature thus far. None of these literature precedents have exhibited the symmetric overlap of adjacent square planar complexes in dimeric units or stacked chains as that seen in the structure of $Pt(ptp)_2$ [37].

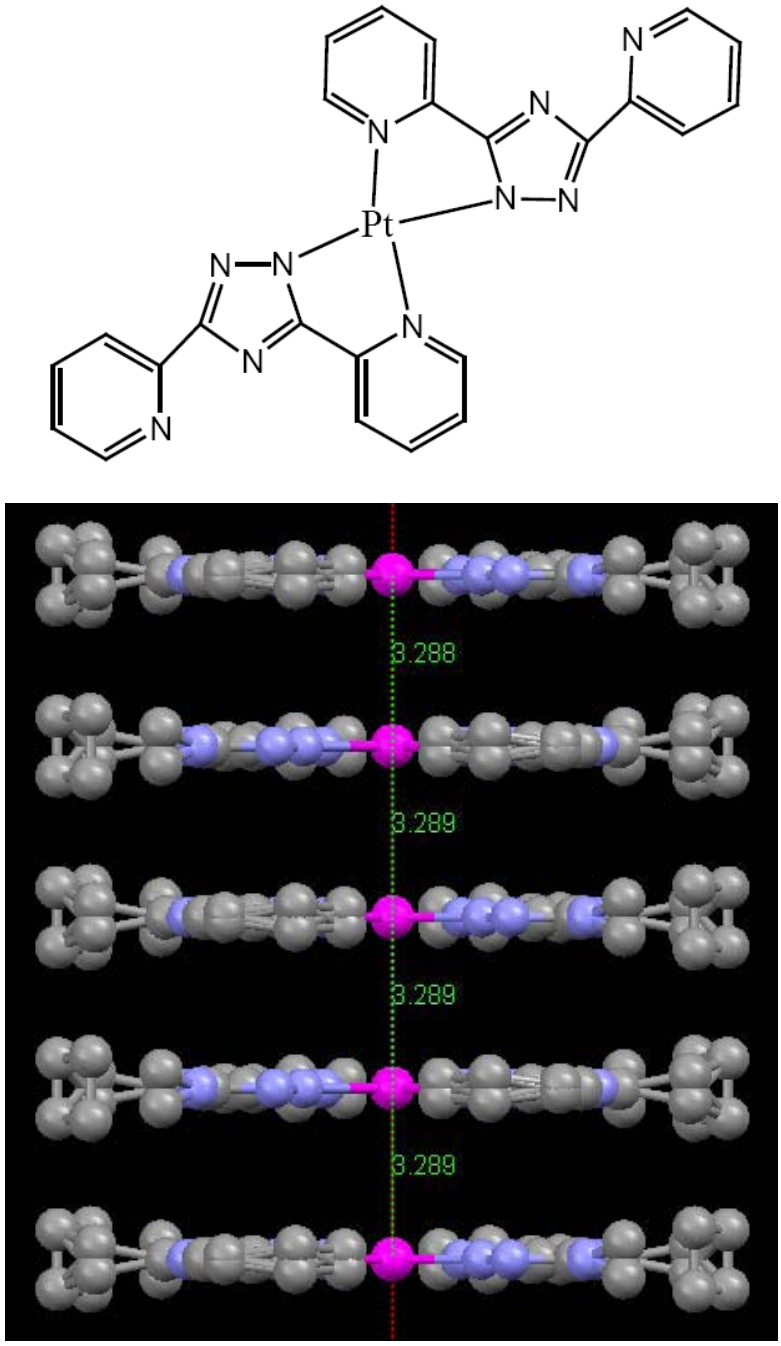

Figure 3.3 Molecular structure (top) and packing diagram (bottom) of $Pt(ptp)_2$ as determined by single crystal X-ray diffraction. Reproduced from reference [37]

In the following, the photoluminescence, photoluminescence excitation, lifetime, quantum yields, refractive index and thickness determination of Pt (ptp)2 is reported, and the experimental methods that were used are described.

3.2 Thin Film Photoluminescence and Photoluminescence Excitation

3.2.1 Instrument Description

Photoluminescence (PL) is a non-destructive technique for determination of the optical properties of luminescent materials [38]. It is used to identify material bandgap, emitting wavelength as well as dopant/impurity concentrations. Photoluminescence excitation (PLE) on the other hand identifies the optimal excitation of a given emission. With regard to OLEDs, PL and PLE allows the overlap between the emission of a potential host and the excitation of the dopant to be identified, which is ***critical*** for selecting host-dopant combinations that have a high probability of producing working devices. A typical PL,PLE set-up is illustrated in Fig 3.4.

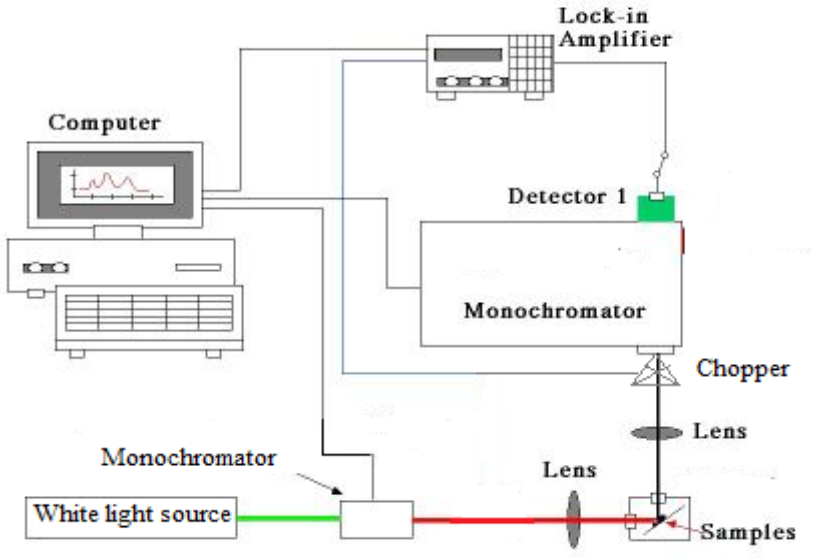

Figure 3.4 Schematic photoluminescence and photoluminescence excitation arrangement

Monochromator 1 is used to select excitation wavelength from the white light source (typically a tungsten lamp) for a subsequent photoluminescence spectral scan. The sample is excited with the selected light, typically with energy $h\nu > E_g$ (bandgap energy), which generates electron-hole pairs. When these recombine radiatively, the emitted light is focused into monochromator 2, where its spectral features are detected and measured.. For a PLE measurement, the monitored PL wavelength is fixed by the monochromator 2, and the excitation wavelength is changed by scanning monochromator 1. The light emitted from the sample is chopped by an optical chopper and lock-in detection is used to minimize noise. A low pass filter is used to ensure the excitation light source is removed from the measured signal. Both monochromators operate 200nm to 1000nmm and the signal being measured is detected by a photomultiplier tube (PMT). The details of monochromators, gratings and PMT are given below.

The monochromator, illustrated in Fig 3.5, selects a narrow band of wavelength, $\Delta\lambda$ from a source of radiation. Light enters the monochromator through a narrow entrance slit. Light falling on the prism or grating is dispersed, breaking the light into its spectral components, by virtue of having a wavelength-dependent refractive index. The dispersed light passes through a narrow exit slit that largely controls the spectal resolution; the narrower the slit, the narrower the wavelength range that reaches the detector [38].

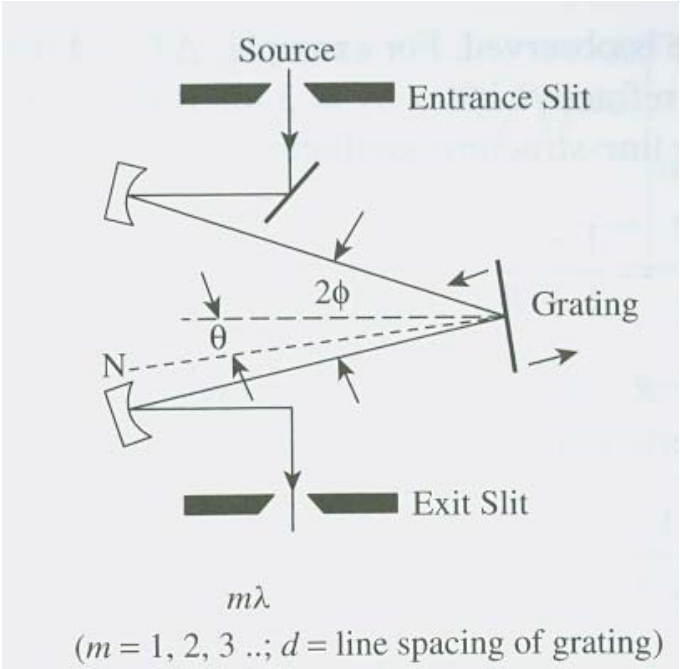

Figure 3.5 Monochromator. Reproduced from reference [38]

Below in Fig 3.6 is the efficiency curve of a 1200g/mm plane Ruled grating. Careful selection of gratings for targeted wavelength ranged is critical for at optimal signal detection.

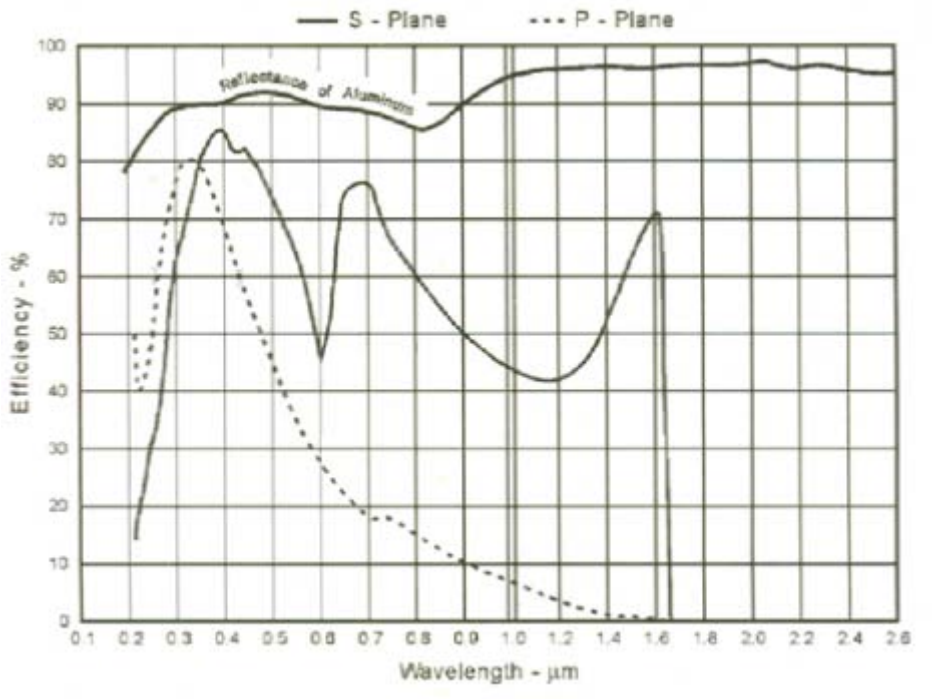

Figure 3.6 1200g/mm plane ruled grating efficiency vs wavelength. Reproduced from reference [39]

PMTs (Fig 3.7) consist of a photocathode and a series of dynodes in an evacuated glass enclosure. Photons which strike the photoemissive cathode cause electrons to be emitted due to the photoelectric effect. These few electrons are accelerated towards a series of additional electrodes called dynodes which are maintained at a positive potential, and more electrons are generated at each dynode. This cascading effect creates 10^5 to 10^7 electrons for each photon hitting the first cathode depending on the number of dynodes and the accelerating voltage. This amplified signal is finally collected at the anode where it can be measured.

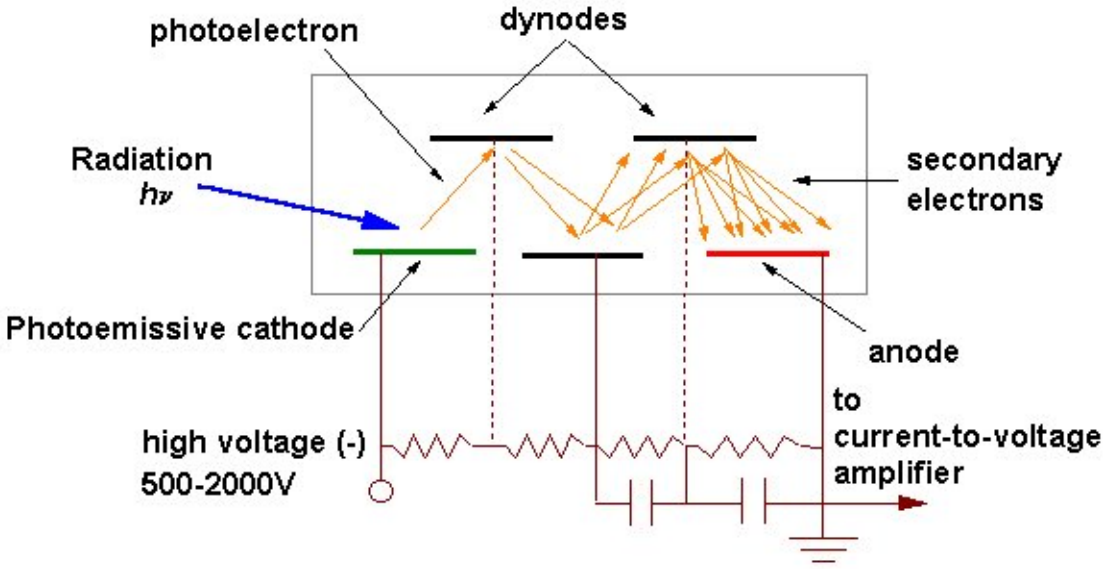

Figure 3.7 Schematic of a PMT. Reproduced from reference [40].

3.2.2 $Pt(ptp)_2$ Thin Film Photoluminescence and Photoluminescence Excitation[37]

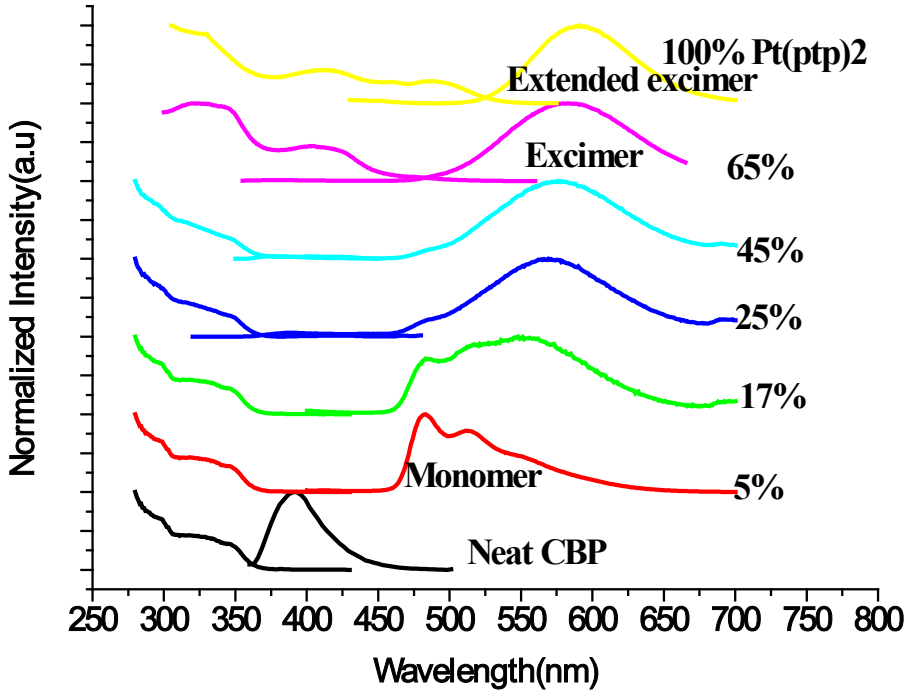

Figure 3.8 PL and PLE doped and undoped CBP:Pt thin film

Photoluminescence and photoluminescence excitation of a neat CBP film, CBP films doped with different concentrations of $Pt(ptp)_2$ and of a neat $Pt(ptp)_2$ film are plotted in Fig 3.8. The 4.4'-N,N'-dicarbazole-biphe-nyl(CBP) PL spectrum with a peak at 390nm is shown in Film 1, as well as and the corresponding PLE in the range of 280nm-400nm . The PLE of the CBP has a characteristic peak at 350nm and a shoulder at 300nm. These two CBP features appear in all of the doped films indicating that excitons are first formed in the CBP and later transfer energy to the dopants by Forster and Dexter mechanism. Since CBP is the dominant absorbing species for dopant concentrations from 0% to 45%, efficient energy transfer between host and guest must take place for the $Pt(ptp)_2$ emission to occur. The PL of

the CBP is overlapped with the PLE of the $Pt(ptp)_2$ which result in an excellent energy transfer between them. The PL spectrum of Film 2 shows three characteristic monomer peaks at 480nm and 520nm and 550nm.There is no CBP peak around 390nm observed in the PL spectrum of Film 2 indicating complete energy transfer having taking place. We can also note that the absence of a broad, long wavelength peak at Film 2 suggests that there are no exciplexes forming between CBP and $Pt(ptp)_2$. It is discussed by Forrest paper that if exciplexes form between CBP and Pt dopant, it will be observed even in the most lightly doped thin films [33]. As the doping concentration increases to 17% as shown in Film 3, the monomer peak at 550nm begins to dominate but the monomer emissions 480nm and 520nm still exist. For Film 4, strong excimer emission with an orange-red peak at 570nm and characteristic monomer emission at 485nm was observed. In Film 5, the excimer emission further red shifted to 575nm. In Film 5, both host-guest energy transfer and direct excitation of the dopant can be observed in the PLE spectrum. The peak at 350nm corresponds to the host-guest energy transfer mechanism, and the shoulder at 410nm is identical with the PLE characteristic peak of the neat $Pt(ptp)_2$ thin film. This result is consistent with an increase in the number of pairs of $Pt(ptp)_2$ molecules with the separation required for excimer formation as the dopant concentration increases. The neat film exhibits a PL maximum that is further red-shifted from the excimer band in doped films, which we assign to the formation of extended excimers in the neat material but localized excimers in the doped films. A careful inspection of the PL data in Figure 2 suggests a red shift in the excimer band at high concentration levels. While it is difficult to ascertain the crystal structure of aggregates in doped films, it is known from the published literature for molecular excimers (best-

established for pyrene) that a greater overlap between the two planar monomer units results in a red shift in the excimer emission band [41], suggesting increased overlap of the planar monomer units that constitute the excimeric luminophore upon increasing the doping concentration [37].

3.3 Thin Film Lifetime and Quantum Yields

3.3.1 Thin Film Lifetime Theory and Instrument Illustration

The lifetime of the excited state is defined by the average time the molecule spends in the excited state prior to return to the ground state. In contrast with electroluminescence, in the absence of significant intersystem crossing for photoluminescence, only the excited singlet (S1) state is populated [22]. There are two widely used methods for the measurement of fluorescence lifetimes. These are the "pulsed method" and the "harmonic or phase-modulation" method.

In the pulsed method the sample is excited with a brief pulse of light and the time-dependent decay of fluorescence intensity is measured. The principle of the measurements is shown schematically in Fig 3.9. All the equipment are commercially available from PTI First, films were excited with a laser pulse, after the pulse is turned off, the luminescence intensity decrease from the singlet states is measured by the detector (PMT). A monochromator is used here for wavelength selection . Depending on how fast the decay time is, phosphorescence detection (>1μs) and fluorescence detection (<1μs) can be chosen from corresponding PTI software .

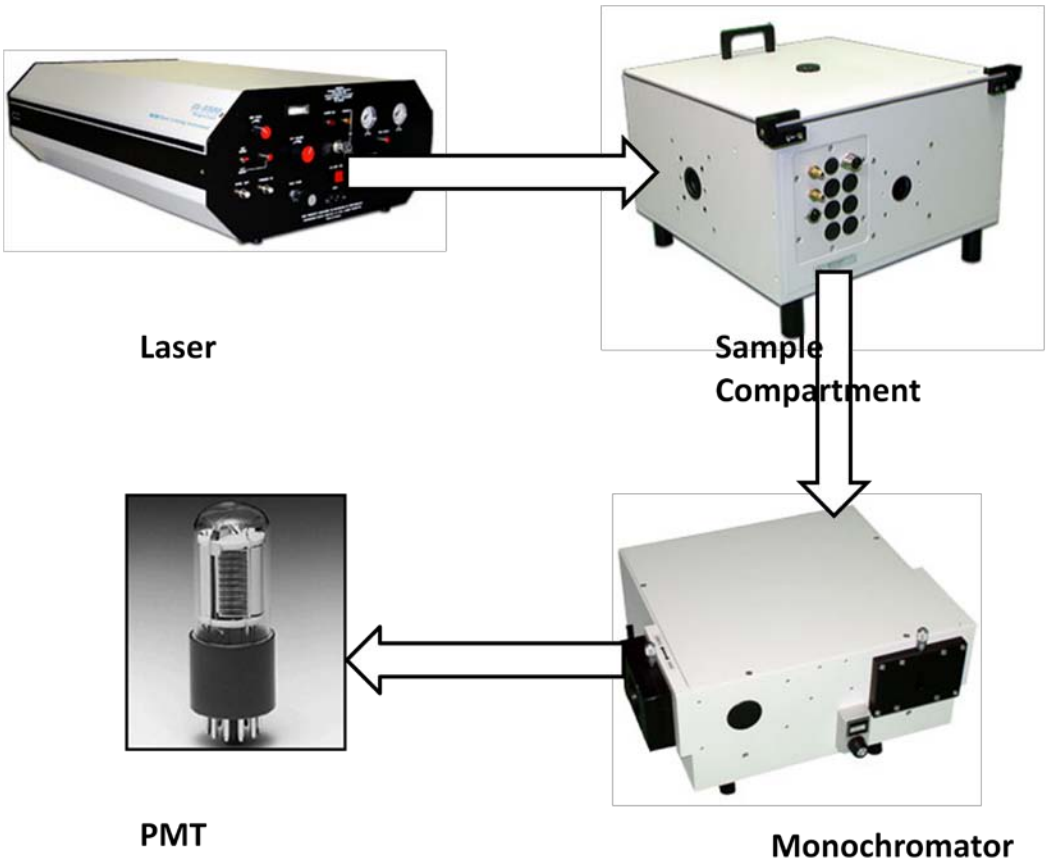

Figure 3.9 PL lifetime measurement set-up

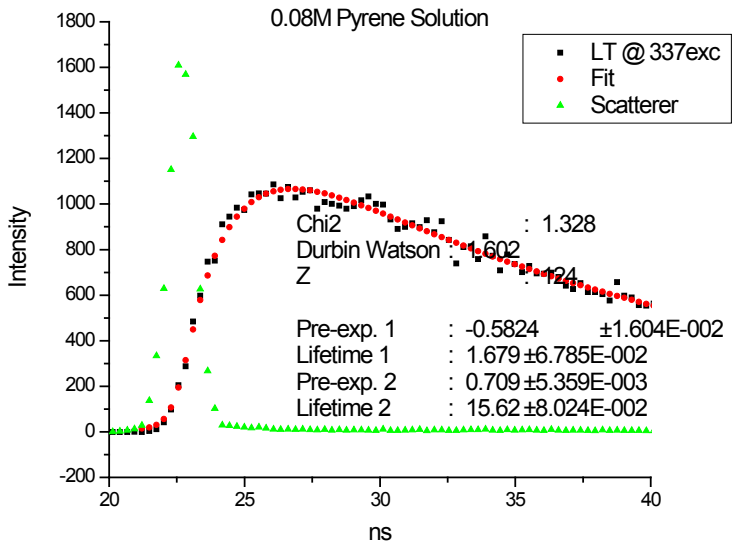

Figure 3.10 An example of lifetime measurement of Pyrene in solution (attributed to Omary's group)

Fig 3.10 is an example of a lifetime measurement of Pyrene in solution. The pulsed method is the technique used for this dissertation work. The other is the harmonic method; the sample is excited with sinusoidally modulated light. The phase shift and demodulation of the emission, relative to the incident light, is used to calculate the lifetime [42].

3.3.2 Thin Film Lifetime Measurement of $Pt(ptp)_2$ at Different Doping Concentrations

The lifetime of a 40nm thick films of 5% $Pt(ptp)_2$ doped CBP was measured with 500-ps pulses from a nitrogen laser at a wavelength of 337nm. CBP: $Pt(ptp)_2$ film was excited by the pulsed N2 laser, and singlet excitons on both the CBP and $Pt(ptp)_2$ molecules are generated. Singlets that transferred from CBP will intersystem cross to $Pt(ptp)_2$ triplet state. The measured lifetime is radiative lifetime from triplet of $Pt(ptp)_2$. For the low doped film (5%), the measured lifetime of 17.71μs at 485nm, 17.27μs at 515nm and17.35μs at 550nm are shown in Fig3.11.

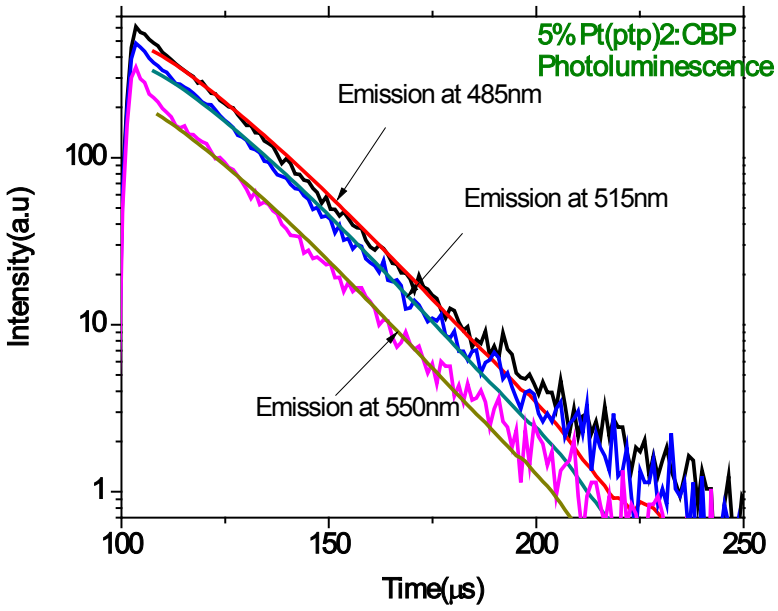

Figure 3.11 5% $Pt(ptp)_2$:CBP thin film lifetime measurement

For the highly doped films (68%), the measured lifetime decreases to 642ns at 582nm and an unusually low lifetime of 114ns is measured at 595nm for the neat $Pt(ptp)_2$ thin films shown in Fig 3.12. The brightness emission and the shortest radiative lifetime is from the orange form, corresponding to the neat thin film. For the low dopant film, there is only host-guest energy transfer taking place. As the concerntration goes up to 65%, both host-guest energy transfer and direct excitation of $Pt(ptp)_2$ are responsible for the exciton generation. A possible explanation for the reducing of lifetime is that as the direct excitation of $Pt(ptp)_2$begins to dominate in the exciton generation process when the concentration goes up, the host-guest energy transfer time which is the delay part in the lower dopant (5%) energy transfer process has been reduced.

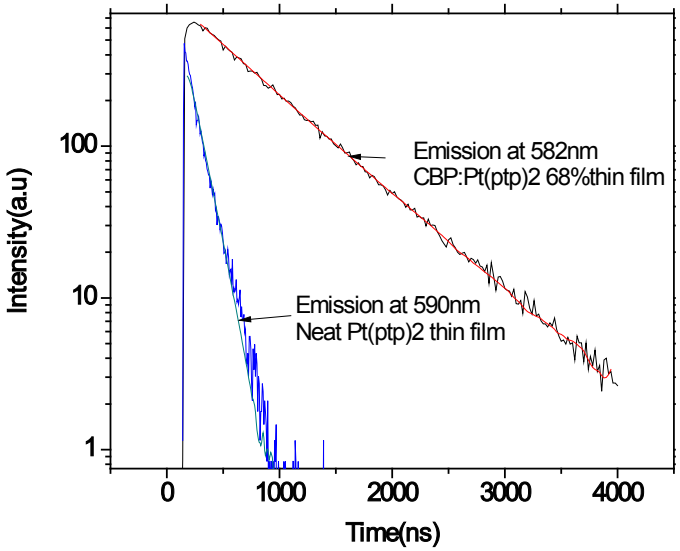

Figure 3.12 65% $Pt(ptp)_2$:CBP and neat $Pt(ptp)_2$ thin film lifetime measurement

3.3.3 Photoluminescence Efficiency: Experimental Methods

A quantitative measurement of external PL efficiency is useful for a number of other reasons. For instance, in conjunction with time-resolved PL measurements, it provides a means of determining the radiative and nonradiative decay constants[43][44].

$$Q = \frac{\Gamma}{\Gamma + \mathrm{k}}$$

Γis the radiative constant,k is the nonradiative constant.

The external quantum efficiency is defined by equation:

$$\mathrm{Q} = \frac{\text{number of photons emitted}}{\text{number of photons absorbed}}$$

The PLQY was subsequently determined according to the method outlined by de Mello[43].

$$\Phi_{PL} = \frac{E_i(\lambda) - (1-A)E_0(\lambda)}{L_e(\lambda)A} \text{ where } A = \frac{L_0(\lambda) - L_i(\lambda)}{L_0(\lambda)}$$

$E_i(\lambda)$: The integrated Luminescence as a result of direct excitation of the film

$E_0(\lambda)$: The integrated Luminescence as a result of secondary excitation which is due to reflected excitation light from sphere walls hitting the sample.

A: is the film absorbance

$L_i(\lambda)$ is the integrated excitation when the film is directly excited and $L_0(\lambda)$ is the integrated excitation when the excitation light first hits the sphere wall as previously explained.

$L_e(\lambda)$ is the integrated excitation profile for an empty sphere.

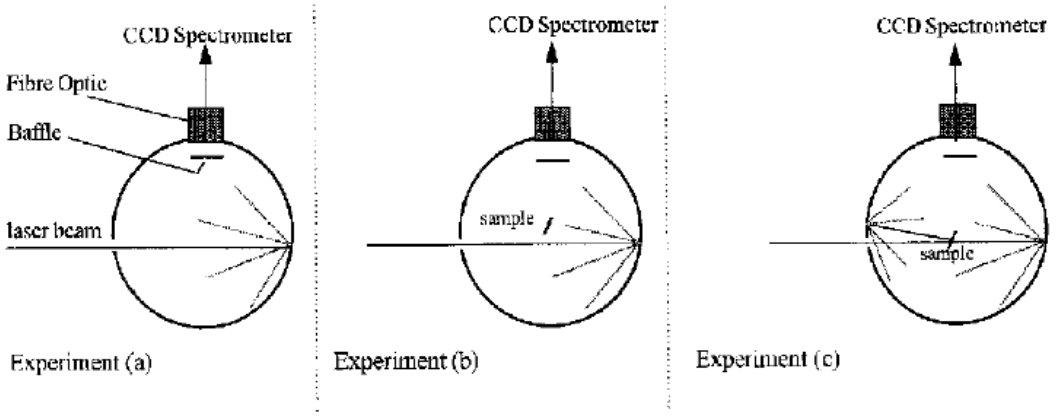

Figure 3.13 Diagram illustrating the three configurations of the sphere required for the efficiency measurement: a) the sphere is empty: b) the sample is in place and the laser beam is directed onto the sphere wall; c) the sample is in place and the laser beam is directed onto the sample. Reproduced from reference [44].

3.3.4 Experimental Results

$E_i(\lambda)$, $E_0(\lambda)$, $L_e(\lambda)$, $L_0(\lambda)$, $L_i(\lambda)$ were all measured in a sequence for each film. The calculated quantum yields are listed in Table 3.1.

Table 3.1 PLQY at different dopant concentrations of $Pt(ptp)_2$ in CBP

Film	Quantum yield
5% thin film(40nm)	25.2% Excitation at 330nm
65% thin film(40nm)	40.7% Excitation at 350nm 51.7% Excitation at 405nm
100% thin film(40nm) 100% thin film(100nm)	23% Excitation at 415nm(where the PLE peaks is) 60% Excitation at 420nm(were the PLE peak is)

As the concentration of $Pt(ptp)_2$ in the CBP increases from 5% to 65%, the quantum yield of 40nm thin film increased from 25.2% to 51.7%. This quantum efficiency trend is contrary to most of phosphorescent molecules, for example, Ir(ppy)3, Pt(OEP), which yield a much lower quantum efficiency at elevated concentrations due to triplet-triplet annihilation and self-quenching. "Self-sensitization" can be a candidate for the overcome of these effect in high concentration $Pt(ptp)_2$ thin films proposed by Dr. Mohammad Omary in which more experimtal data are needed.

For the neat film, the only energy mechanism is direct excitation and for the 65% doped thin film both host-guest energy transfer and direct energy excitation are taking place. Host-guest energy transfer is reported as an efficient energy transfer due to the transfer of electrogenerated excitons from the host to highly emissive and stable dopants which reduces the possibility of non-radiative decay. There is a competition between host-guest energy transfer and direct excitation of the dopant in the 65% film which yields the highest quantum efficiency of 51.7%. As the concentration goes up to 100%, host-guest energy transfer system was fully substituted by direct excitation which is a less efficient mechanism and only 23% quantum yield was exhibited.

Note that a linear dependent of the quantum yield on thickness can be concluded from simple math calculation. (40nm neat film is 23% and 100nm neat film is 23% × (100/40) = 57.5%~60%). The higher quantum yield of the100nm neat thicker film appears to be due to thickness.

3.4 Thin Film Refractive Index and Composition

3.4.1 Instrument Illustration [38]

Ellipsometry is a contactless, non-invasive technique for measuring changes in the polarization state of light reflected from a surface from which based on Fresnel's relations the optical constants, dielectric constants and film thickness are determined [Ref]. Consider plane-polarized light incident on a plane surface, as illustrated in Fig 3.14. The light spot is typically on the order of millimeters in diameter, but can be focused to about 100μm. The incident polarized light can be resolved into a p- component, which is parallel to the plane of incident and a s-component which is perpendicular to the plane of incidence.

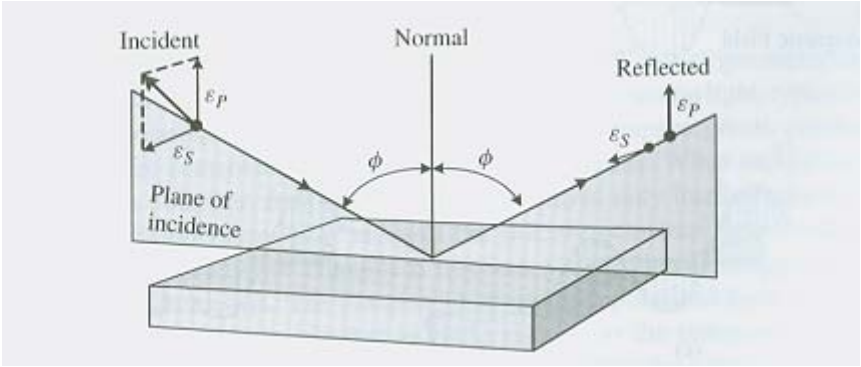

Figure 3.14 Schematic of polarized light reflection from a plane surface. Φ is the angle of incidence. Reproduced from reference [38].

Spectroscopic ellipsometry (SE) is non-destructive and surface-sensitive, with the capability of detecting thicknesses ranging from a single atomic layer to thousands of angstroms. It facilitates direct determination of the real and imaginary components of the complex index of refraction, extinction coefficient, and film thickness simultaneously [18-22]. The physical underpinnings of the technique are well understood and documented [23]. In summary, plane-polarized light impinges a sample at a certain angle, and the change of polarization of the reflected beam is analyzed. The optical constants are determined from the

measured relative phase change Δ and the relative amplitude change, ψ, introduced by reflection from the surface [23]. More specifically, ψ and Δ provides the ratio between the *s*-polarized (r_s) and *p*-polarized (r_p) light reflected off the surface of interest;

$$\rho = \frac{r_p}{r_s} = \tan(\Psi).e^{i\Delta}$$ which

directly relates to the complex index of refraction through Fresnel's Relations;

$$r_p = \frac{\overline{n}\cos\phi_l - \cos\phi_t}{\overline{n}\cos\phi_l + \cos\phi_t} \qquad r_s = \frac{\cos\phi_l - \overline{n}\cos\phi_t}{\cos\phi_l + \overline{n}\cos\phi_t}$$

where r_p and r_s are the *p* and *s* components of the reflected polarized light, and $\overline{n}$ is the complex index of refraction. Both Ψ and Δ are wavelength dependent. Once the real (*n*) and imaginary components (*k*) of the complex index of refraction have been measured, the thickness determination is rather straightforward since the amplitude of the electrical component of the propagating light wave is:

$$\mathrm{E}_x = \mathrm{E}_0 \exp\left[-\frac{\omega k}{c} d\right] \exp\left[i\omega\left(t - \frac{dn}{c}\right)\right]$$

where *d* is thickness and *t* is time.

3.4.2 Experiment Result of $Pt(ptp)_2$

The ellipsometric measurements were performed in wavelength region of 300–1000 nm at the incident angles of 60, 65, 70 and75 degrees. Below is the experimental and fitting data using the Cauchy model. Figures 3.15 and 3.16 show that the refractive index is 1.8 for the 58nm neat $Pt(ptp)_2$ thin film, and 1.8 for the 98nm CBP:Pt(17%) thin film. From this result, the refractive is independent of both film thickness and doping concentration. In other words, the refractive index of this specific film in the whole OLED stack should not influence

the outcoupling efficiency.

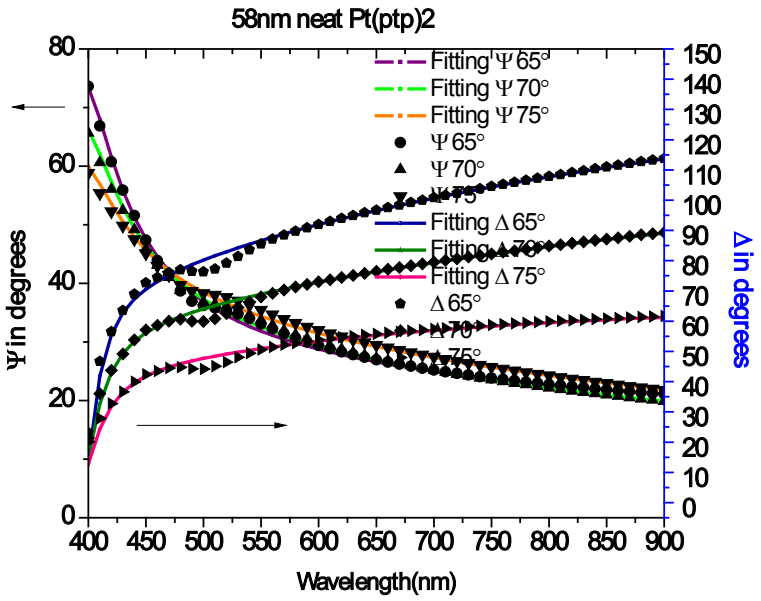

Figure 3.15 58nm neat $Pt(ptp)_2$ Experimental and fitting data

.

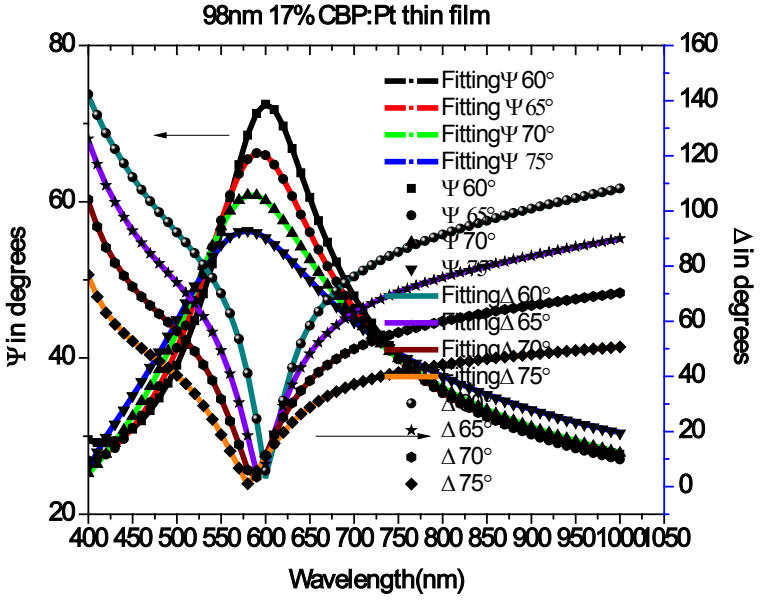

Figure 3.16 98nm CBP:Pt 17% Experimental and fitting data

3.5 References:

[1]C.Adachi,M.A.Baldo,M.E.Thompson,S.R.Forrest,J.Appl.Phys. **90**, 5048(2001).

[2]S.Lamansky,P.Djurovich, D.Murray, F.Abdel-Razzaq, H. E.Lee, C.Adachi, P.E.Burrows, S.R.Forrest, M.E.Thompson, J.Am.Chem.Soc. **123**, 4304(2001).

[3]M.Ikai,S.Tokito, Y.Sakamoto, T.Suzuki, Y.Taga, Appl.Phys.Lett. **79**, 156(2001,).

[4]M.K.Nazeeruddin, R.Humphry-Baker, J.Am.Chem.Soc **125**, 8790(2003).

[5] Tanaka, D., Sasabe, H., Li, Y.-J., Su, S.-J., Takeda, T. & Kido, J.. Jpn. J. Appl. Phys.**46**, 10(2007)

[6] Su, S.-J., Gonmori, E., Sasabe, H. & Kido. Adv. Mater. **20**, 4189 (2008).

[7]Edited by Hartmut Yersin:*High efficient OLED with Phosphorescent Materials 46,*(Wiley-VCH,Weinheim,German,2007).

[8]V.M.Miskowski,V.H.Houlding,Inorg Chem **28**, 1529(1989)

[9]C.M.Che,L.Y.He,C.K.Poon,T.C.W.Mak,Inorg Chem **28,** 3081(1989).

[10]J.Biedermann,G.Gliemann,U.Klement,K.J.Range,M.Zabel,Inorg Chem,**29,** 1884(1990)

[11]H.Kunkely,A.Vogler,J Am Chem Soc,**112**, 5625(1990).

[12]V.M.Miskowski,V.H.Houlding,Inorg Chem **30**, 4446(1991).

[13]V.H.Houlding,V.M.Miskowski,Coord Chem Rev **111**, 145(1991).

[14]K.T.Wan,C.M.Che,K.C.Cho,J Chem Soc,Dalton Trans 1991,1077

[15]H.Wiedenhofer,S.Schützenmeier,A.von Zelewsky,H.Yersin,J.phys Chem **99**, 13385(1995)

[16]W.B.Connick,L.M.Henling,R.E.Marsh,H.B.Gray,Inorg Chem **35,** 6261(1996,)

[17]W.Humbs,H.Yersin,Inorg Chim Acta **265**, 139(1997)

[18]K.P.Balashev,M.V.Puzyk,V.S.Kotlyar,M.V.Kulikova ,Coord Chem Rev **159**, 109(1997)

[19]W.Paw,S.D.Cummings,M.A.Mansour,W.B.Connick,D.K.Geiger,S.D.Cummings,R.Eisenberg,Coord Chem Rev,**171**, 125(1998).

[20]M.Hissler,J.E.McGarrah,W.B.Connick,D.K.Geiger,S.D.Cummings,R.Eisenberg,Coord Chem Rev **208**, 115 (2000).

[21]H.Yersin,D.Donges,W.Humbs,J.Strasser,R.Sitters,M.Glasbeek,Inorg Chem **41**, 4915 (2002),.

[22]J.A.Gareth Williams,Stephanie Develay,David L.Rochester,Lisa Murphy.Coordination Chemistry Reviews **252,** 2596 (2008).

[23] D. Eastwood, M. Gouterman, J. Mol. Spectrosc. **35**, 359 (1970).

[24] (a) Dungey, K. E.; Thompson, B. D.; Kane-Maguire, N. A. P.; Wright,L. L. Inorg. Chem. **39**, 5192 (2000),. (b) Chan, S. C.; Chan, M. C. W.;Wang, Y.; Che, C. M.; Cheung, K. K.; Zhu, N. Chem.sEur. J.,**7**, 4180(2001). (c) Lin, Y. Y.; Chan, S. C.; Chan, M. C. W.; Hou, Y. J.;Zhu, N.; Che, C. M.; Liu, Y.; Wang, Y. Chem.sEur. J., **9**, 1263(2003).(d) Ma, B.; Li, J.; Djurovich, P. I.; Yousufuddin, M.; Bau, R.; Thompson, M. E. J. Am. Chem. Soc., **127**, 28(2005).

[25](a) Pettijohn, C. N.; Jochnowitz, E. B.; Chuong, B.; Nagle, J. K.; Vogler, A. Coord. Chem. ReV. **171**, 85(1998). (b) Connick, W. B.; Geiger, D.; Eisenberg, R. Inorg. Chem, **38**, 3264 (1999). (c) Hissler, M.; McGarrah, J. E.; Connick, W. B.; Geiger, D. K.; Cummings, S.D.; Eisenberg, R. Coord. Chem. ReV., **208**, 115(2000).

[26] Sheng-Yuan Chang, Jakka Kavitha, Shih-Wen Li,Chan-Shou Hsu,Yun Chi, Yu-Shan Yeh, Pi-Tai Chou, Gene-Hsiang Lee, Arthur J. Carty, Yu-Tai Tao, and Chin-Hsiung Chien, Inorganic Chemistry, **45**, 137 (2006).

[27]M.A.Baldo,D.F.O'Brien,Y.You,A.Shoustikov,S.Sibley.M.E.Thompson&S.R.Forrest, Nature, **395**, 451(1998).

[28] D. F. O'Brien and M. A. Baldo, M. E. Thompson, S. R. Forrest, Applied physics letters **74**, 442(1999).

[29] B.W. D' Andrade, J. Brooks, V. Adamovich, M.E. Thompson and S.R. Forrest, Adv. Mater. **14,** 1032 (2002).

[30] J. Brooks, Y. Babayan, S. Lamansky, P. I. Djurovich, I. Tsyba, R.Bau and M. E. Thompson, Inorg. Chem., **41**, 3055(2002).

[31] B. Ma, P.I. Djurovich, M.E. Thompson, Coord. Chem. Rev. **249**, 1501 (2005).

[32] Vadim Adamovich, Jason Brooks, Arnold Tamayo, Alex M. Alexander, Peter I. Djurovich,Brian W. D'Andrade, Chihaya Adachi, Stephen R. Forrest and Mark E. Thompson New J. Chem., **26**, 1171(2002)

[33] B.W.D'Andrade, J.Brooks, V.Adamovich,M.E.Thompson, S.R.Forrest, Adv Mater **14**, 1032(2002).

[34] J. Kalinowski, M. Cocchi, D. Virgili, V. Fattori and J. A. G. Williams, Adv. Mater., **19**, 4000 (2007).

[35] S.-Y. Chang, J. Kavitha, S.-W. Li, C-S. Hsu, Y. Chi, Y.-S. Yeh, P.-T. Chou, G.-H. Lee, A. J. Carty, Y.-T. Tao and C.-H. Chien, Inorg. Chem. **45**, 137 (2006).

[36] P. Pyykkö, Chem. Rev., **97,** 597(1997).

[37] Minghang Li, Wei-Hsuan Chen, Ming-Te Lin, Mohammad A. Omary, Nigel D. Shepherd, Organic Electronics **10,** 863 (2009)

[38]Dieter K.Schroder, *Semiconductor material and device characterization*, 3rd edition,

(Wiley-IEEE Press, US,2006)

[39] F. M. Winnik, Chem. Rev., **93**, 587 (1993).

[40]Joseph R.Lakowicz :*Principles of Fluorescence Spectroscopy(*Springer, New York, 1999) 2nd Edition.

[41] I. D. W. Samuel, B. Crystall, G. Rumbles, P. L. Burn, A. B. Holmes, R.H. Friend, Synth. Met.,**54**, 281(1993).

[42] John C. de Mello, H. Felix Wittmann, and Richard t/. Friend, Adv. Mater. **9**, 230(1997).

[43] Lars-Olof Palsson and Andrew P.Monkman, Adv Mater,**14**, 757(2002).

[44] Nataliya Nabatova-Gabain[a], Yoko Wasai[a] and Taiju Tsuboi, Current Applied Physics, **6**, 833(2006)

[45] V. Bulovic´, V. B. Khalfin, G. Gu, and P. E. Burrows, D. Z. Garbuzov, S. R. Forrest, physical review B,**58**, 3730 (1998)

[46]J.Shi, C.W.Tang, Appl phys lett, **70**, 1665 (1997)

CHAPTER 4

NEAR WHITE AND TUNABLE ELECTROPHOSPHORESCENCE FROM BIS[3,5-BIS(2-PYRIDYL)-1,2,4-TRIAZOLATO]PLANTINUM(II)-BASED ORGANIC LIGHT EMITTING DIODES

4.1 Introduction

This chapter describes the effects of stack design and doping concentration variations on the electrical and optical properties of $Pt(ptp)_2$ based OLEDs. First, a description of the experimental procedures used in this study is given, which is followed by a summary of the electro-optical characterization results of devices designed for efficiency optimization. The effects of the electron transport layer (ETL), emissive layer (EML), doping concentration, hole blocking layer (HBL), host, hole transport layer (HTL) and cathode on device performance are illustrated. Delayed phenomena for devices doped 65% and electron mobility calculations from EL transient measurements are also discussed.

4.2 Experimental Procedures

Organic light emitting devices with the standard bottom emission structure were fabricated using sequential thermal evaporation to deposit multiple organic layers. The process flow diagram is shown in Fig 4.1, and details of the individual steps are given below. All devices were fabricated on commercially available glass/ITO substrates from Lumtec Inc., Taiwan. The substrate layout is shown in Fig 4.2.

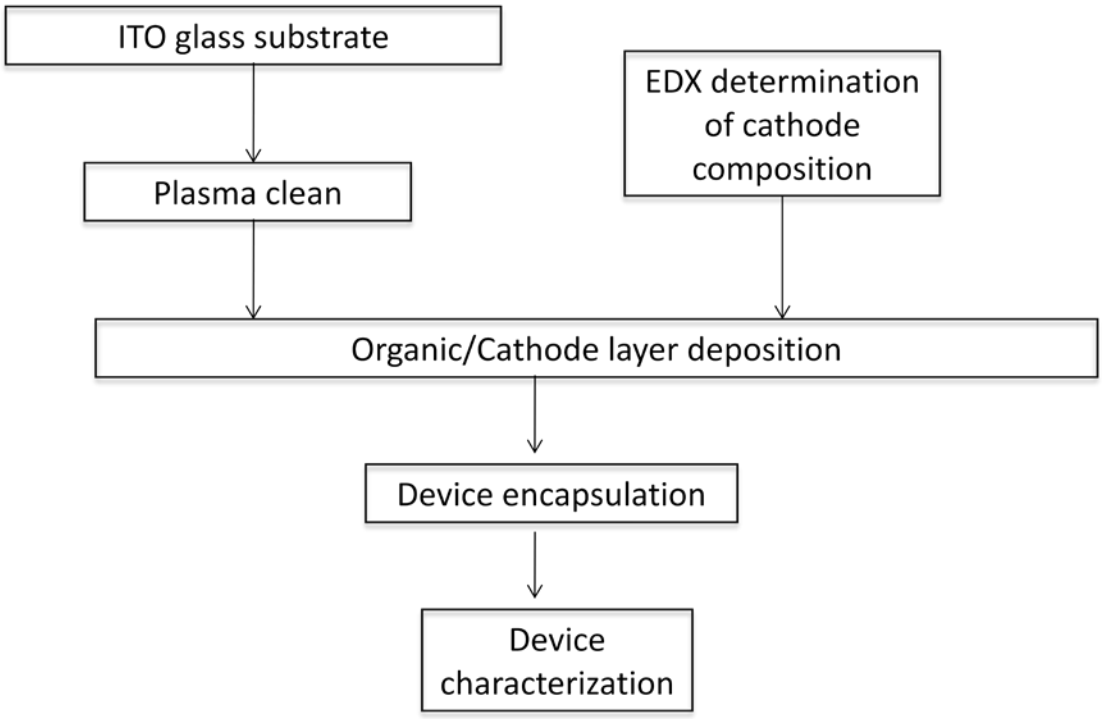

Figure 4.1 Schematic progress flow diagram for the processing of OLEDs.

4.2.1 Substrates Preparation [2]

(a)Dark areas are coated with ITO.

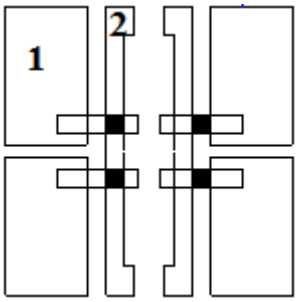

(b)Area 1 is connected to the cathode and area 2 is connected to the anode. The dark areas are the OLED pixels.

Figure 4.2 Substrate layout

The commercial glass/ITO substrates were exposed to a standard cleaning and preparation process prior to device fabrication. Below in Table 4.1 are the parameters of the as-received substrates.

Table 4.1 ITO glasses parameters

Material	Polished soda lime glass
SiO2 Thickness	≧200Å
Glass Thickness	0.7 or 1.1mm
ITO Thickness	1200~1600 Å
ITO Resistance	9~15 Ω/sq
ITO Transparency	more than 84% (at 550nm)

The as-received substrates were sequentially cleaned with DI-water, acetone, and methanol in an ultrasonic cleaner to remove organic surface contaminants.

After blow-drying with nitrogen, the ITO was exposed to a microwave oxygen plasma in order to increase the work function of ITO. A schematic diagram of the plasma equipment used in these experiments is shown in Fig4.3. ,

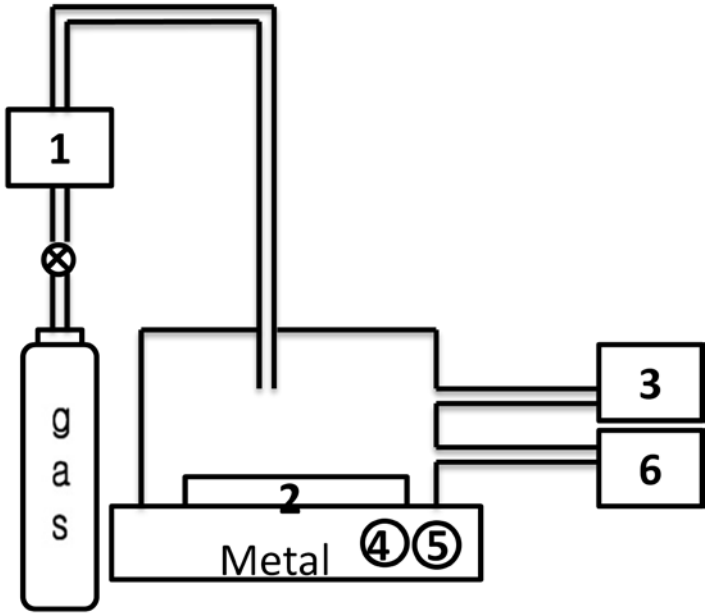

1.Mass flow controller
2.Substrate
3.Vacuum gauge
4.Cooling water-in
5.Cooling water-out
6.Roughing pump

Figure 4.3 Plasma treatment system

A 2.45 GHz plasma generator (115V ac 15 amp service grounded) was used for creating the plasma. The experimental procedure is first evacuate the chamber then flow oxygen to obtain the operation pressure. A plasma power of 460watts, pressure of 380mTorr of oxygen and processing time of 10 minutes were found to optimal for ITO surface modification.

4.2.2 Thin Film Layer Processing

An automated, bell-jar type thermal evaporator was used to deposit thin films and fabricate the devices. Eight sources are controlled by two power suppliers. For the drawing space consideration, only four sources are sketched in Fig 4.4. The power supplies interact with quartz crystal sensors through a feedback loop for precise deposition and co-deposition rate control. One sensor is shared by two adjacent boats, and the distance between sensors and boats is longer than mean free path of the gas phase of all the organic, metal and metal oxide materials. The thicknesses read by the sensors are compared with actual thicknesses determined with a stylus profilometer to derive sensor tooling factors, which are used to produce correct thickness readings.

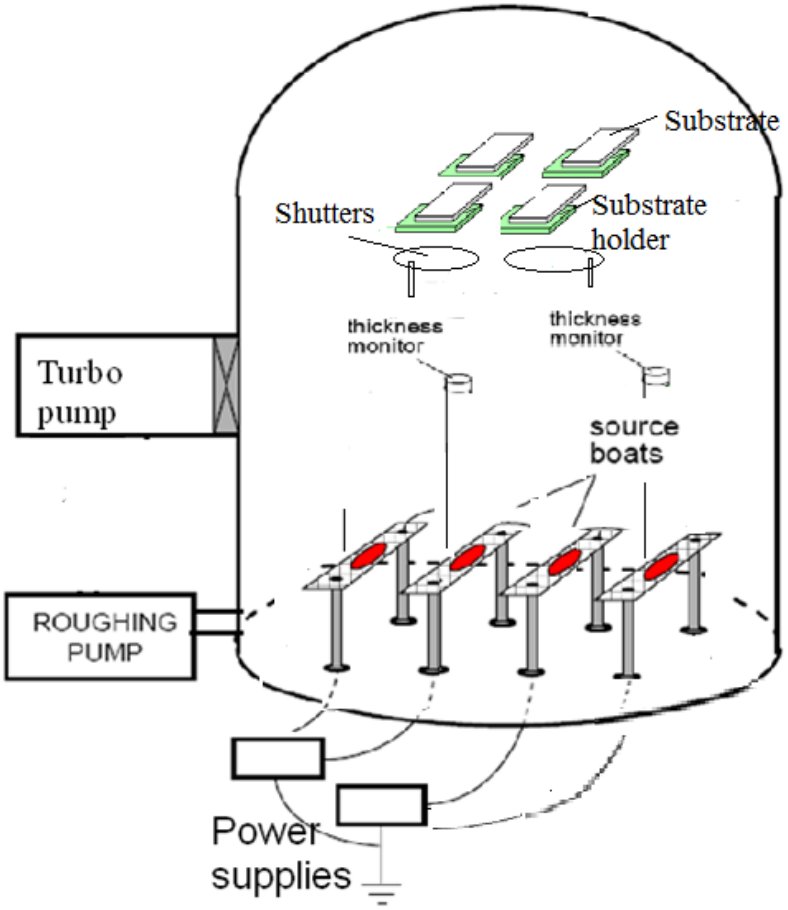

Figure 4.4 Bell-jar type thermal evaporator

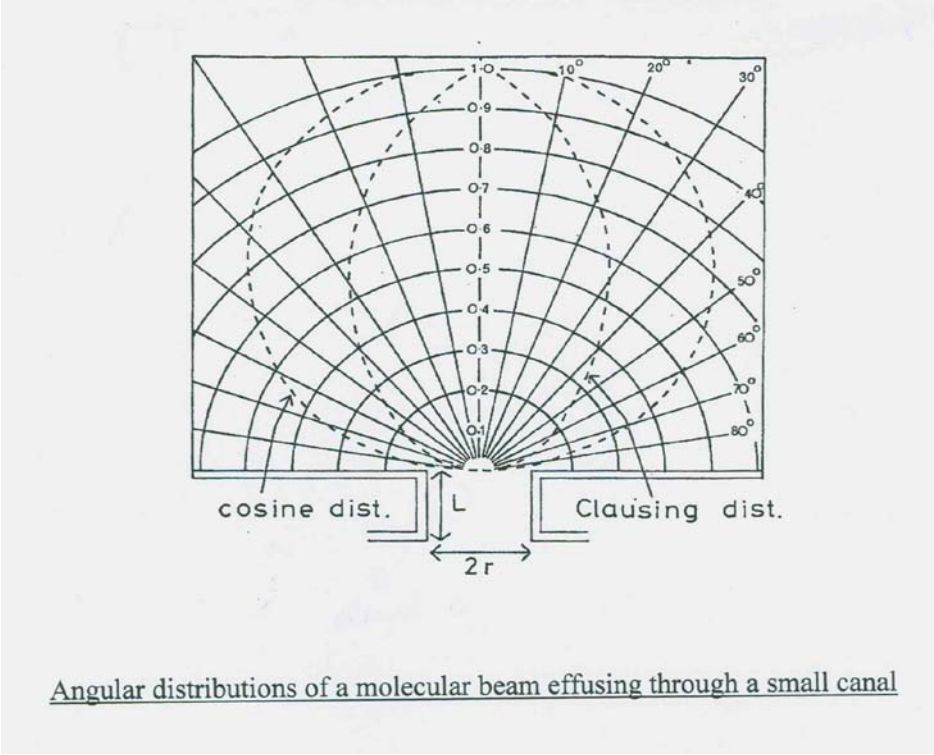

Figure 4.5 Flux distribution of thermal evaporation

Fig 4.5 shows the flux distribution associated thermal evaporation processes. Depending on the dimension of the aperture, either a cosine distribution or the Clausing distribution can be obtained. To ensure a directional flux and to minimize cross-contamination a Clausing distribution is desirable. However, a cosine distribution is obtained from the design of common evaporation boats. All boats were purchased from the R.D.MATHIS company. And the boat selection depending on the material melting temperature of both the boats and material should follow the company instruction boat selection instruction.

As mentioned earlier, the organic light emitting diodes are fabricated by a sequential thermal evaporation of the device layers. The base pressure of the system was 10^{-8} Torr. The cathodes are selected from low work function metals and alloys such as Mg:Ag(10:1) and

LiF/ Al.

4.2.3 Device Encapsulation

A UV curable epoxy-based adhesive (EPO-TEK OG112-4; Epoxy technology Inc) was use to encapsulate devices after fabrication in order to reduce water and oxygen permeation into the device. The UV curing requires exposure to UV light for ~10 mins. A schematic of the encapsulated device is illustrated in Fig 4.6.

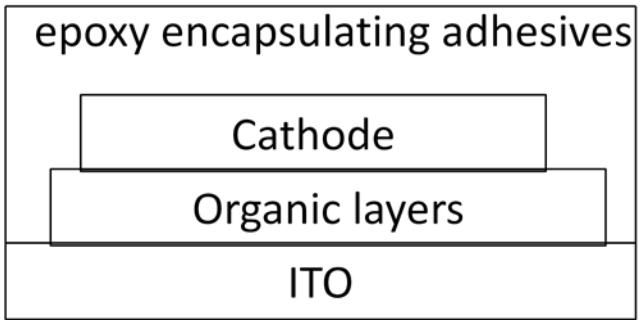

Figure 4.6 The structure of the encapsulated OLEDs

4.2.4 Measurements

The current density-voltage-luminance (J-V-L) characteristics were measured using factory-calibrated Photoscan PR150 integrated via LabView with a Keithley 2420 source measure unti. The composition of the alloy contacts were verified using energy dispersive spectroscopy (EDS). A Veeco, Dektak 150 profilometer was used for film thickness measurements. As shown in Fig 4.7, measurements of six spots at two different were used to compute the average thickness which was used for tooling factor adjustment.

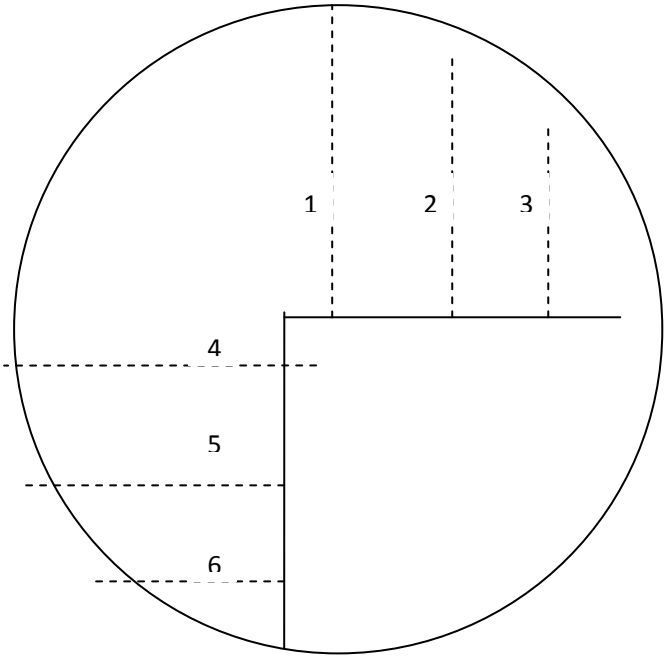

Measured Thickness

Position	Thickness (A)
1	419.7
2	419.3
3	520.2
4	369.4
5	356.2
6	389.2

Average =412.3

Figure 4.7 Thickness measurement and calculation

4.2.5 Transient EL phenomena of Device Lifetime and Mobility Measurement [4]

4.2.5.1 Instrumental Illustration

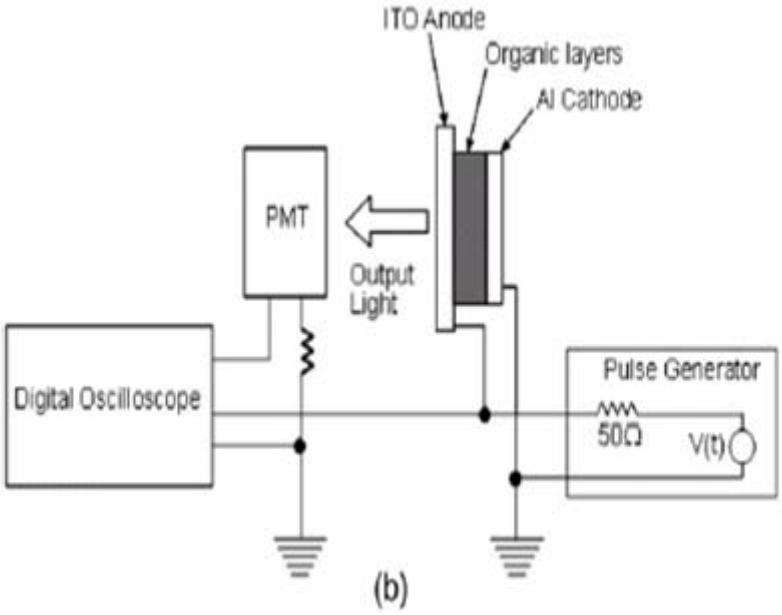

Figure 4.8 Experimental setup for transient EL measurement. Reproduced from reference [4]

Fig 4.8 illustrates schematically the experimental setup for the pulse/transient EL measurements. It consists of a pulse generator, a fast photo detector (photomultiplier (PMT)) and a fast storage oscilloscope. OLEDs were electrically excited by applying a fast square electrical pulse from a 100MHz function generator with accurate repetition, rise and delay time and the response measured with the PMT. The measured OLED capacitance was around 1.9nF. Assuming the OLED equivalent circuit is composed of a series-connected resistor and capacitor, the series resistance is found to be ~140ohms and the overall RC time constant of the experiment setup around 0.266μs. The equivalent circuit of the OLED device was studied using a Solartron SI 1260 impedance analyzer.

4.3 Results and Discussion

4.3.1 Optimization of the HTL Thickness for Higher Power and Quantum Efficiency

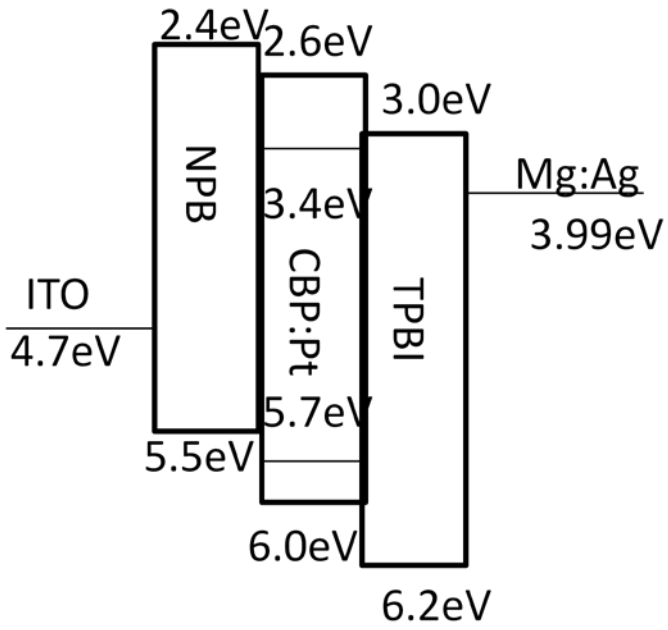

Figure 4.9 Energy bandgap diagram

Fig 4.9 is the energy bandgap diagram of a baseline structure. All of the energy values were taken from references[17] with the exception of Pt complex. The HOMO level of the $Pt(ptp)_2$ was measured by UPS and LUMO level was estimated using the optical energy gap (singlet absorption).This work was done by Unnat S. Bhansali (UTD).

Three devices:

Device 1. ITO/ NPB(40nm) /CBP:Pt(15%) (25nm) /TPBI(30nm) /Mg:Ag

Device 2. ITO/ NPB(25nm) /CBP:Pt(15%) (25nm) /TPBI(30nm) /Mg:Ag

Device 3. ITO/NPB(60nm)/CBP:Pt(15%)(25nm)/TPBI(30nm)/Mg:Ag

were fabricated and measured to investigate the effect of hole transport layer thickness on device efficiency. Electron and hole density are higher at ETL/EML and EML/HTL

interfaces respectively than the bulk. The NPB thickness is expected to influence the location of the recombination zone. The current-voltage (J-V), luminance-voltage (L-V) and efficiency characteristics of the three devices are shown in Fig 4.10-4.12, and the performance parameters for the four devices are tabulated in Table 4.2. From the J-V characteristics in Fig 4.10, more current is injected at the equivalent voltage for device 2 compared to device 1 and device 3, due to the thinner stack with NPB thickness of 25nm. The threshold voltage for device 2 is lower and the luminance higher. Fig 4.13-4.15 shows the EL spectra of the three devices at different voltages. The CIE numbers at each voltage is also included. The emission at 450nm is attributed to NPB. The electron injection barrier between the CBP and NPB ($\approx$0.2eV) is less than the hole injection barrier at this interface, resulting in electron leakage from EML into the NPB layer especially at higher voltage, even though the hole and electron motilities of the CBP are 10^{-3} and 10^{-4} cm²/V s, respectively. The changing NPB contribution to the spectrum leads to color instability issues as well. Artificially expanding the hole injection and travel path from 25nm to 50nm at the anode side, shifts the recombination zone from close to the interface of CBP/TPBI to close to the interface of NPB/CBP. The results suggest that recombination in the middle of CBP:Pt layer is most likely for the 40nm NPB (device 1), which exhibits the highest external quantum efficiency of 4.09% at 2.94cd/m^2. The higher efficiency numbers for device 1 indicate that amongst the three structures, the charge balance is best for device 1. A peak EQE of only 1.37% of obtained from device 2 despite the largest device current, which suggests that a large number of unbalanced charge was transported through the stack but did not participate in emission, but instead contributed to significant nonradiative ohmic losses. From the EL

spectrum of device 2 shown in Fig 4.14, there is still some electron leakage into the NPB layer especially at higher driving voltages. For device 3, extending the NPB layer thickness to 50nm results in pushing the recombination zone closer to the interface of NPB/CBP, however, the peak 3.18% EQE of device 3 compared to 4.09% for device 1 indicates the onset of charge imbalance.

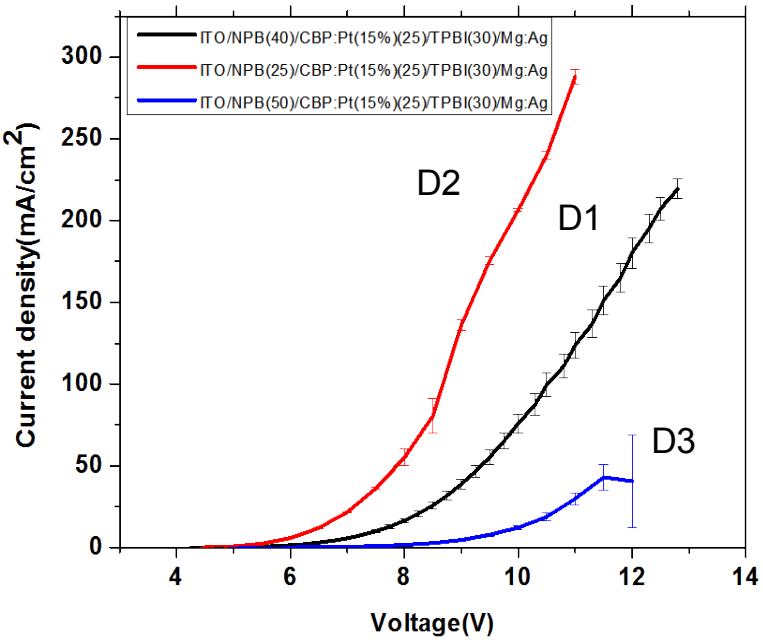

Figure 4.10 J-V characteristics of the three devices

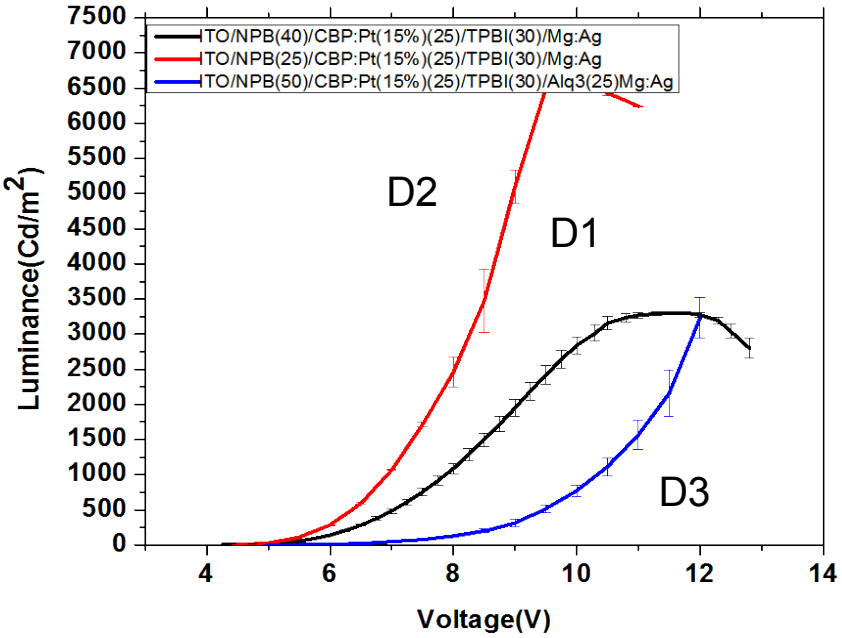

Figure 4.11 L-V characteristics for the three devices

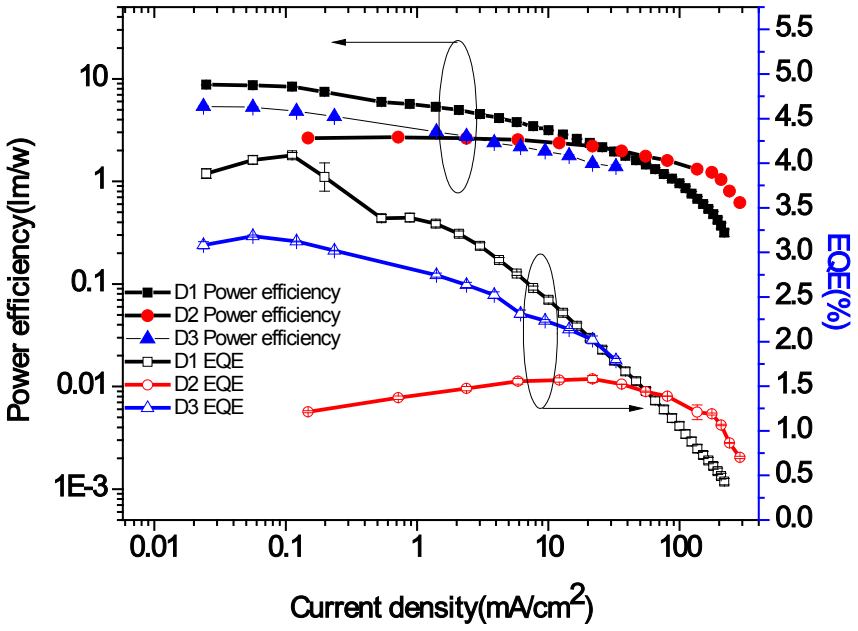

Figure 4.12 Power efficiency and EQE as a function of current density for the three devices

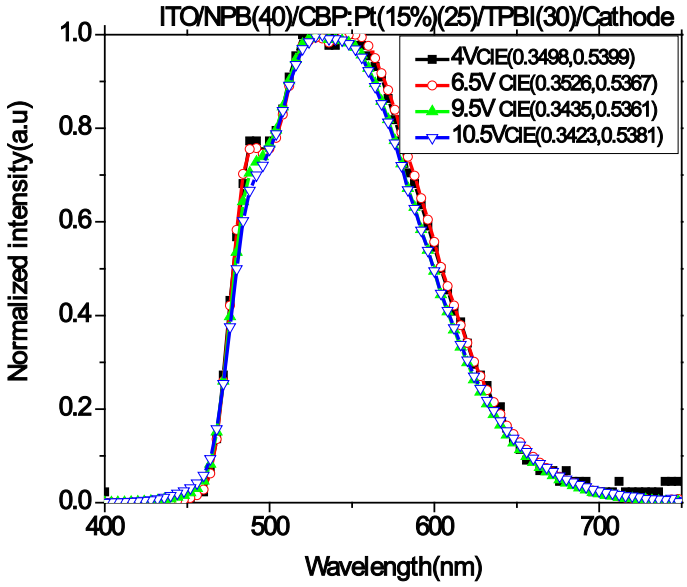

Figure 4.13 EL spectra of device 1

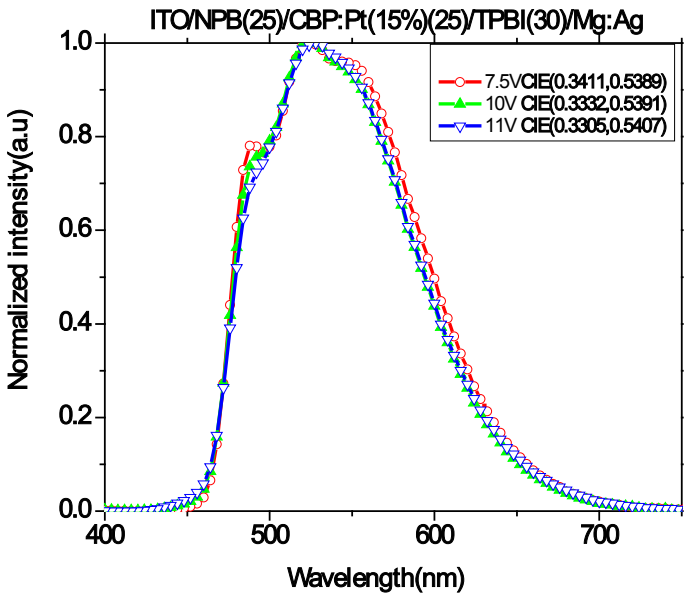

Figure 4.14 EL spectra of device 2

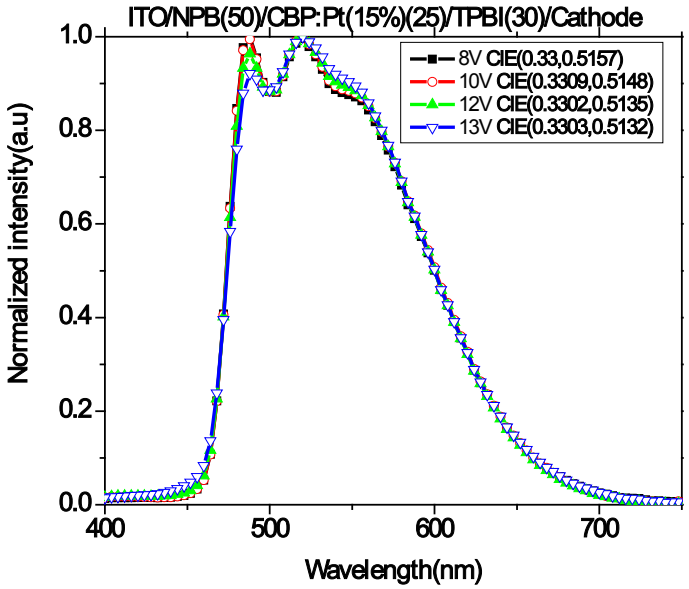

Figure 4.15 EL spectra of device 3

Table 4.2 OLED characteristics as a function of NPB thickness. ITO/ NPB(xnm) /CBP:Pt(15%) (25nm) /TPBI(30nm)/ Mg:Ag

NPB thickness (nm)	Luminance at peak PE (Cd/m^2)	Voltage (V)	Peak External quantum efficiency(%)	Peak Power efficiency (lm/W)	EQE at 1000 Cd/m^2)	Power efficiency at 1000 Cd/m^2)	Turn on Voltage
40	2.94	4.25	4.09	8.74	2.18	2.6	4.25
25	30.9	5	1.37	2.69	1.58	2.21	4.5
50	1.67	5	3.18	5.4	2.14	1.78	5

4.3.2 Optimization of the EML Thickness for Power and Quantum Efficiency

A series of devices with EML of 25, 8, 50nm were fabricated and measured. The J-V-L and efficiency characteristics of three devices and the EL spectrum of device 3 are illustrated in Fig 4.16-4.18. The performance parameters are listed in Table 4.3.

Device 1.ITO/ NPB(40nm) /CBP:Pt(15%) (25nm) /TPBI(30nm) /Mg:Ag

Device 2.ITO/ NPB(40nm) /CBP:Pt(15%) (8nm) /TPBI(30nm) /Mg:Ag

Device3.ITO/NPB(40nm)/CBP:Pt(15%)(50nm)/TPBI(30nm)/Mg:Ag

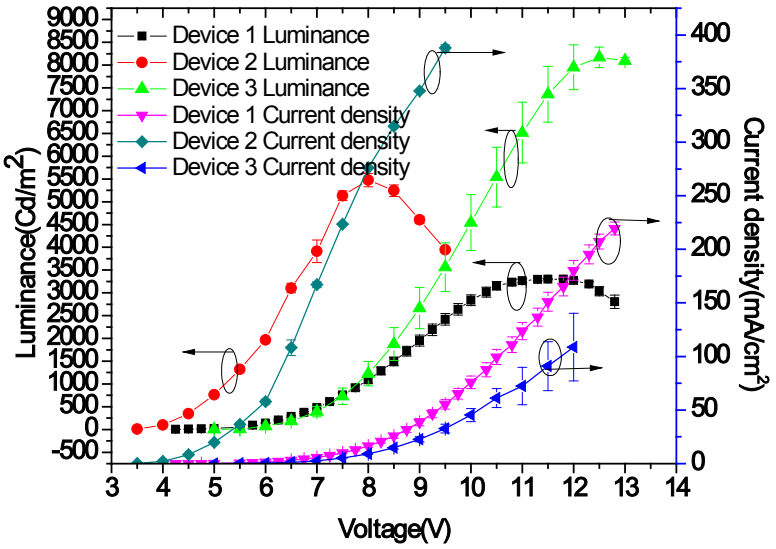

Figure 4.16 J-V-L characteristics of the three devices

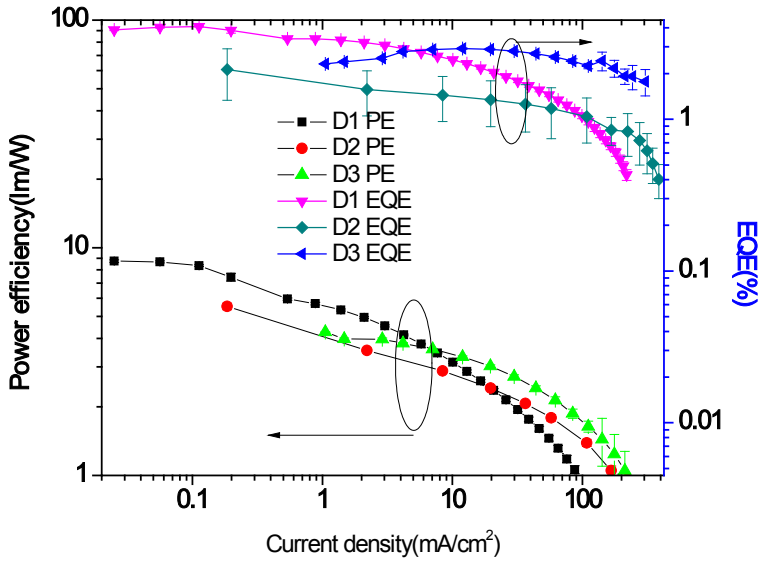

Figure 4.17 Power efficiency and EQE versus current density

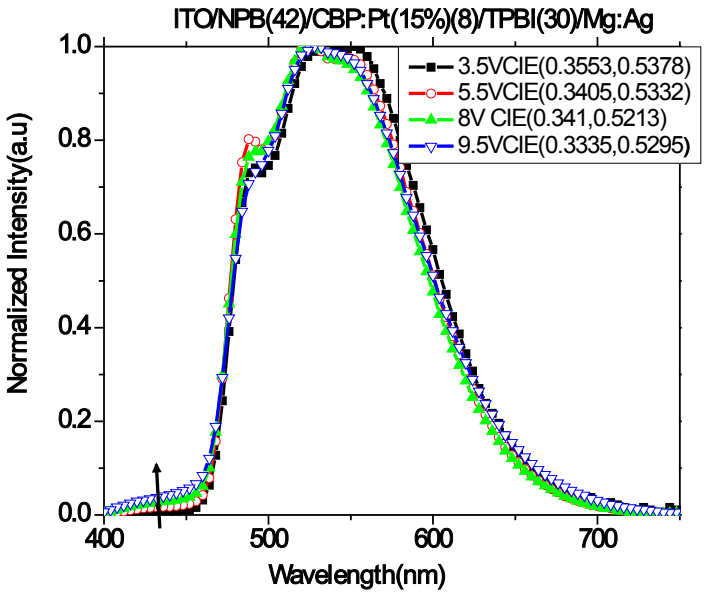

Figure 4.18 EL spectra of device 3

Table 4.3 The OLED characteristics as a function of the CBP:Pt thickness. ITO/ NPB(40nm) /CBP:Pt(15%) (xnm) /TPBI(30nm)/ Mg:Ag

EML thickness (nm)	Luminance at peak PE (Cd/m^2)	Voltage (V)	Peak External quantum efficiency(%)	Peak Power efficiency (lm/W)	EQE at 1000 Cd/m^2)	Power efficiency at 1000 Cd/m^2)	Turn on Voltage
25	2.94	4.25	4.09	8.74	2.18	2.6	4.25
8	11.3	3.5	2.12	5.53	1.25	2.07	3.5
50	2.15	5	2.92	4.26	2.9	3.22	5

From J-V-L curve, it is observed that Device 3 has a smaller current due to its larger total thickness compared to Device 1 or Device 2. Device 3 had the thickest emission layer and contained the largest volume of emission component giving the highest luminance of 8000Cd/m^2 at 13.5V. From the efficiency aspect, both device 1 and device 3 had good charge balance which yielded 4.09% EQE and 2.92% EQE respectively. However, device 3 has a total thickness of 120nm which increase the turn on to 5V and the power efficiency was reduced to 4.26lm/W compared to 8.74lm/W for device 1. The thin emissive layer of Device 2 resulted in a recombination zone that expanded into NPB layer, which can be identified from the characteristic peak of NPB emission at 450 nm in the EL spectra in Fig 4.18. The varying relative intensity of the NPB emission suggests expansion of the recombination zone from the $Pt(ptp)_2$ doped regions at lower current densities and voltages into the NPB layer at higher operating bias or current, causing slight changes in the EL spectra and CIE coordinates.

Another two devices with different thickness of EML are illustrated here for

comparison. The two device structures are as below:

Baseline(device1): ITO/NPB(40nm)/mCP(10nm)/CBP:Pt(65%)(25)/TPBI(30nm)/Mg:Ag

Baseline with 12.5EML (device 2):

ITO/NPB(40nm)/mCP(10nm)/CBP:Pt (65%)(12.5)/TPBI(30nm) / Mg:Ag

The band diagram for the two devices is drawn in Fig 4.19. The J-V-L, efficiency characteristics and EL spectra are illustrated in Fig 4.20-4.23, and the performance parameters are listed in Table 4.4. Device 1 displays a peak EQE of 10.85 ±0.25% and peak power efficiency of 26.00±0.43 lm/W. In contrast, , device 2 whose EML thickness is half that of Device 1 exhibits a peak EQE of 5.64±0.59% and peak power efficiency of 8.81±0.30 lm/W. There is a factor of 2 reduction in the EQE and a factor of 3 reduction in the power efficiency. The threshold voltage which is 1V larger for the thinner device (Device 2) indicates that it may not be the desired thickness that we intended. From the IV curve in Fig 4.20 Device two which has larger current density at equivalent voltage is also contrary to the thickness effect. The lower turn on voltage and larger current density were expected for the thinner device.

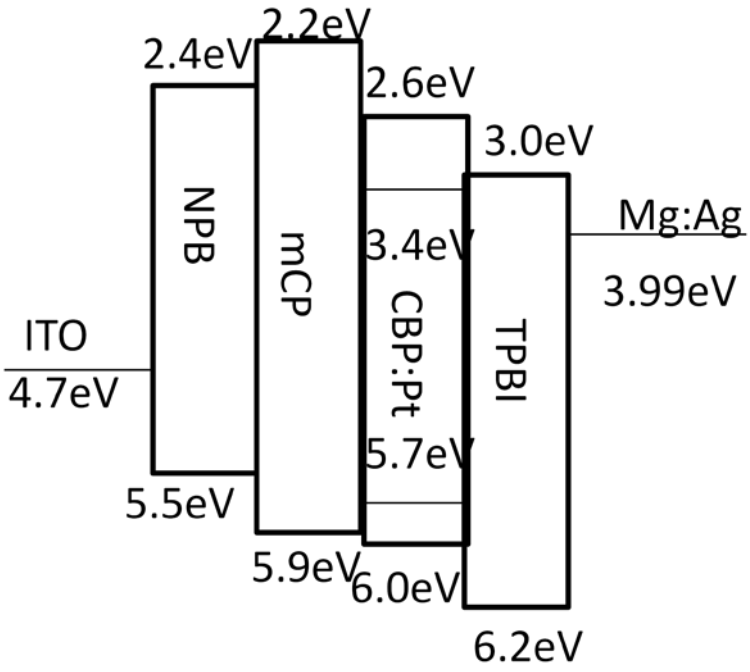

Figure 4.19 Band diagram

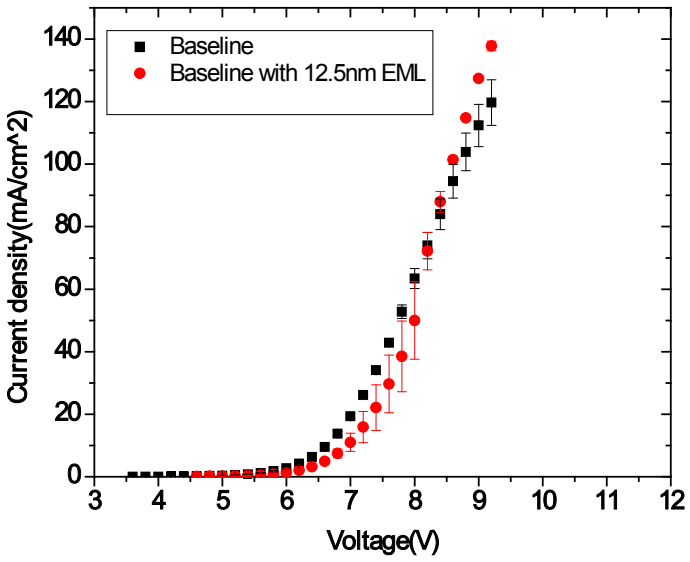

Figure 4.20 IV curve of two devices

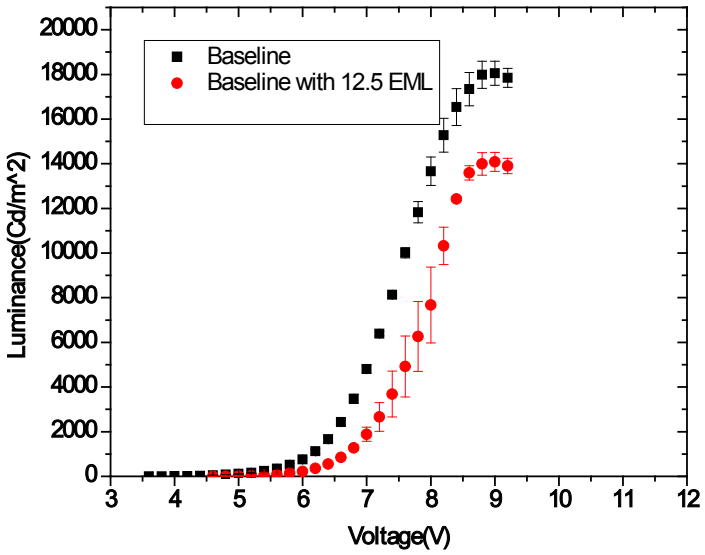

Figure 4.21 Luminance vs voltage for two devices

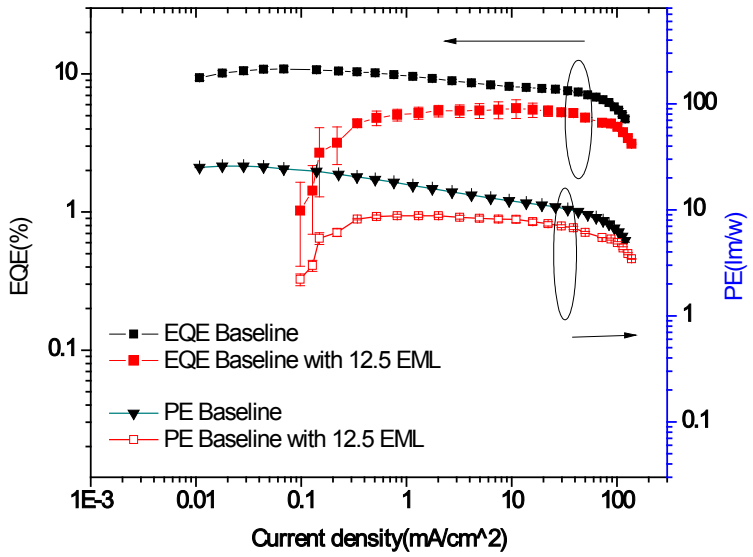

Figure 4.22 Efficiencies vs current density for two devices

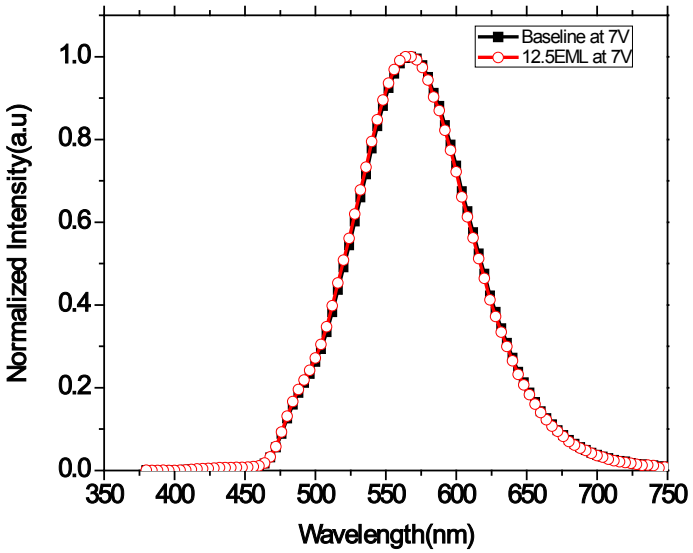

Figure 4.23 EL spectra of two devices

Table 4.4 The OLED characteristics as a function of the CBP:Pt thickness. ITO/ NPB(40nm) /mCP(10nm)/CBP:Pt(65%) (xnm) /TPBI(30nm)/ Mg:Ag

Device ID	PE_{peak} (lm/W)	PE_{1000} (lm/W)	EQE_{peak} (%)	EQE_{1000} (%)	CIE_{peak} (x, y)	CIE_{1000} (x, y)	V_T (V)
Device 1	26.00± 0.43	13.8±0. 17	10.85 ±0.25	8.61±0.11	(0.4511, 0.5169)	(0.4499,0 .5181)	3.6V
Device 2	8.81±0. 30	8.31±0. 08	5.64±0.59	5.42±0.43	(0.4327, 0.5246)	(0.4362,0 .5251)	4.6

4.3.3 Optimization of the Doping Concentration for Higher Power and Quantum Efficiency [8]

---

*This entire chapter is reproduced from Minghang Li,1 Wei-Hsuan Chen,Ming-Te Lin, Mohammad A. Omary,and Nigel D. Shepherd "Near-white and tunable electrophosphorescence from bis[3,5-bis(2-pyridyl)-1,2,4-triazolato]platinum(II)-based organic light emitting diodes ", Organic electronics,10:863(2009)

A series of devices with the structure: ITO/NPB(40nm)/ CBP:Pt (x%) (25nm)/TPBI(40nm)/Mg:Ag were fabricated for this study. Similar to the photoluminescence, a shift from monomer- to excimer - dominated emission with increasing dopant concentration is observed in the electroluminescence, as the normalized spectra in Figure 4.24 show. The CBP emission in the spectrum of the sample doped at 3% suggests that this doping level is insufficient for optimal energy transfer from the host to the dopant. We interpret the NPB shoulder in the electroluminescence of the samples doped at 25 and 45 % to mean that the carrier mobility associated with the dopant is strongly influencing the carrier transport properties of the emissive layer, and thus the extent of the recombination zone. As Figure 4.25 shows, a decrease in the electrical threshold voltage and an increase in the current at a given voltage generally accompanies the dopant concentration increase. The luminance as a function of voltage dependence is shown in Figure 4.26.

In the 5-15% doping range, the average brightness was ~7200 cd/m2 at 9V. We expect that the incorporation of a hole injecting and/or electron-blocking layers into the device structure might lower the turn-on voltages seen. A doping concentration of 5% produced peak luminous and power efficiencies of 15 cd/A and 9.8 lm/W, respectively.

Interestingly, the power efficiency at high luminance was higher for the 7.5% device, decreasing from a peak value of 8.07lm/W to only 7.29 lm/W at 1000 cd/m2; the EQE likewise exhibited a small decrease from 4.91% to 4.89%. The dependence of the luminous and power efficiencies on doping concentration for the full series of devices studied in this work is presented in Figure 4.27. As Figures 4.27 and 4.28 shows, the reduction in power efficiency and external quantum efficiency parameters under high current, brightness, and voltage conditions is relatively moderate compared to the sharp reduction in efficiency that characterizes typical electrophosphorescent devices. Figure 4.29 is representative of the CIE and CRI dependence on drive voltage. For this dopant concentration (7.5 %) the color rendering index is 36 at 6 V and 35 at 10 V. The electroluminescence spectral features are voltage-independent and, as Figure 4.29 depicts, the ratio of monomer to excimer emission is essentially constant for the voltage range used in this study; i.e., we see little or no evidence of preferential saturation of monomer compared to excimer excited states with increased device current, or vice versa. In general all of the devices in this work exhibited better color stability of than reported for other square planar Pt(II) complexes [9-14]. The CRI increased with doping concentration and the maximum value obtained was 56. To the naked eye the emission appeared to be white with a green hue. Table 4.5 is a summary of the pertinent electro-optical performance metrics for OLEDs based on $Pt(ptp)_2$ in this work, showing both peak values as well as values at 1000 cd/m2. This luminance level is deemed an appropriate reference level for OLEDs by the U. S. Department of Energy [15], although device performance data at this high luminance level is rarely seen in the published literature for electrophosphorescent OLEDs. The overall data in Table 4.4 and Figure 4.30 shows that

OLEDs based on $Pt(ptp)_2$ in this work exhibit less significant roll-off in performance metrics at this high luminance, albeit to a different extent in devices with different doping levels.

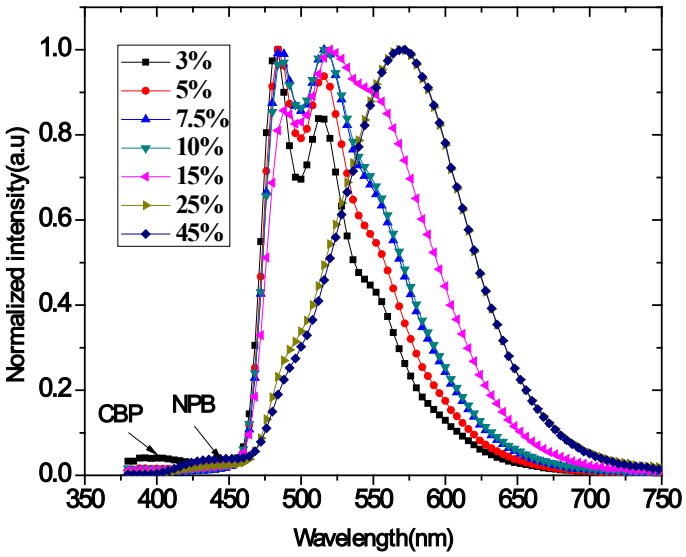

Figure 4.24 Electroluminescence spectra of different volume percentages $Pt(ptp)_2$ in CBP.

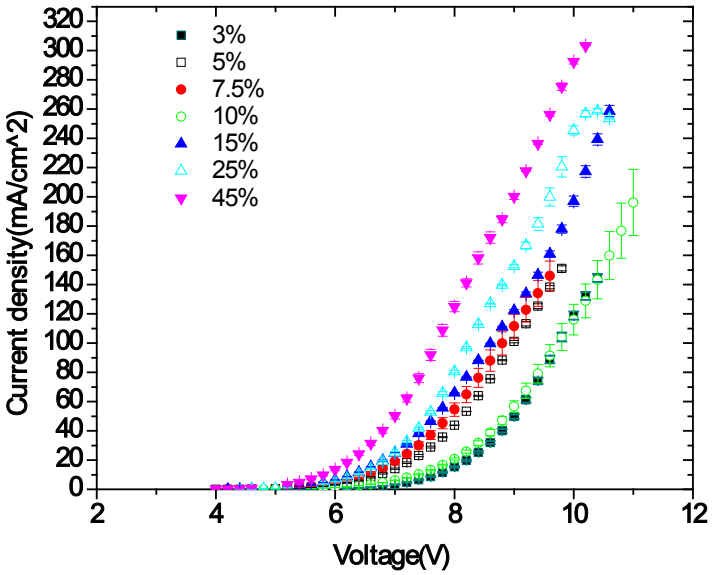

Figure 4.25 Current-voltage curves for devices with different dopant concentration.

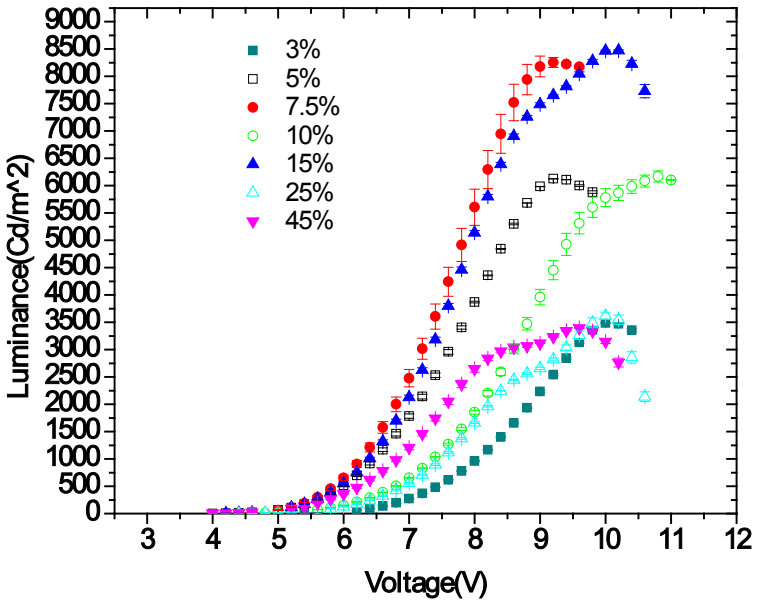

Figure 4.26 Luminance-voltage curves for devices with different dopant concentration.

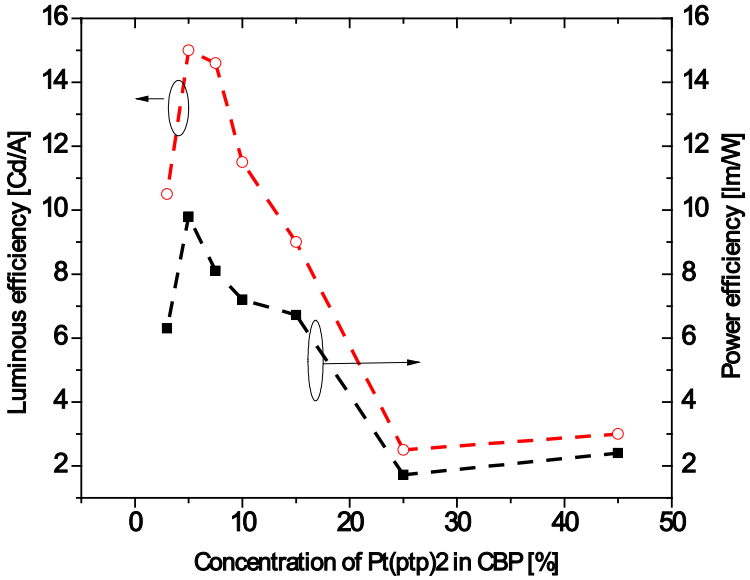

Figure 4.27 Luminous efficiency (solid squares) and power efficiency (open squares) as a function of Pt (ptp)2 doping percent.

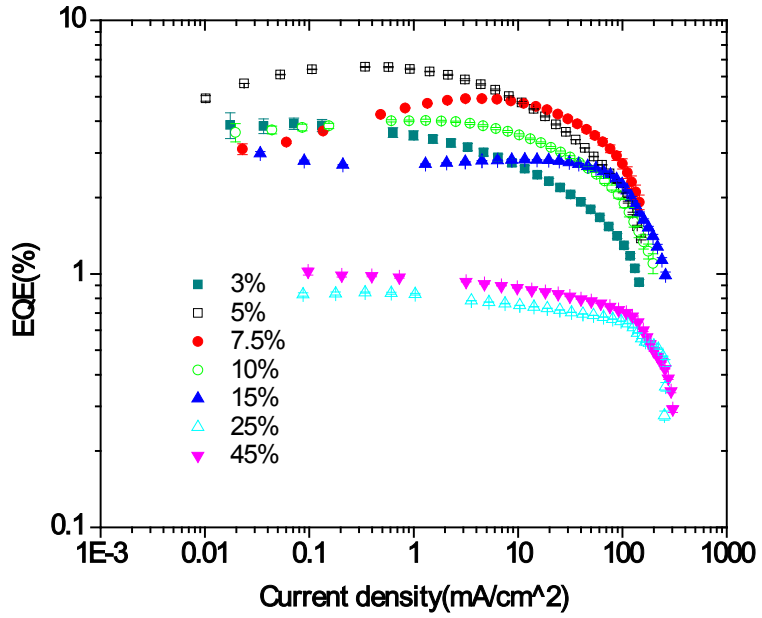

(a)

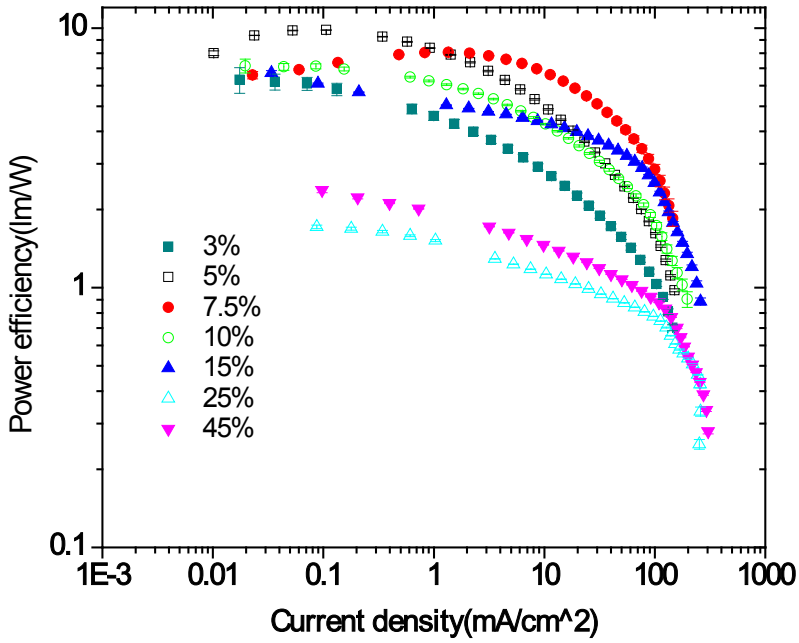

(b)

Figure 4.28 External quantum efficiency (a) and power efficiency (b) as a function of current density.

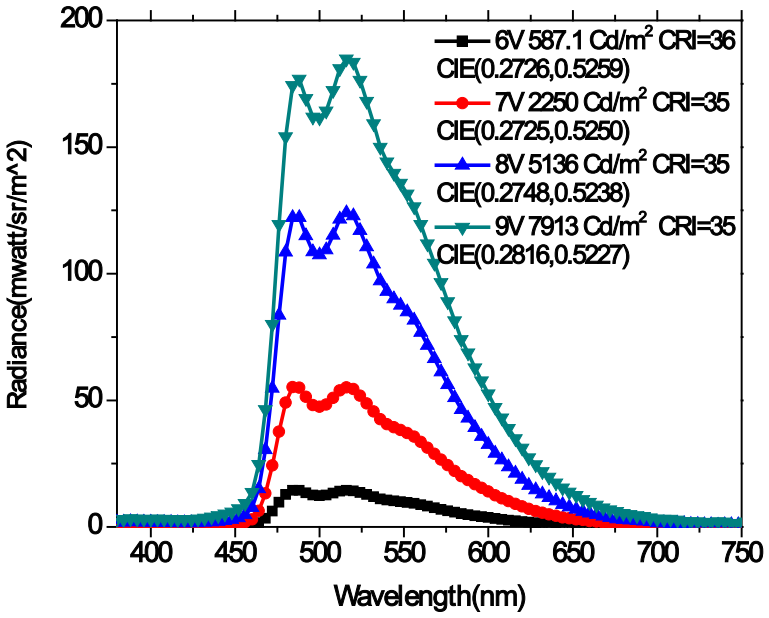

Figure 4.29 Electroluminescence spectra as a function of drive voltage.

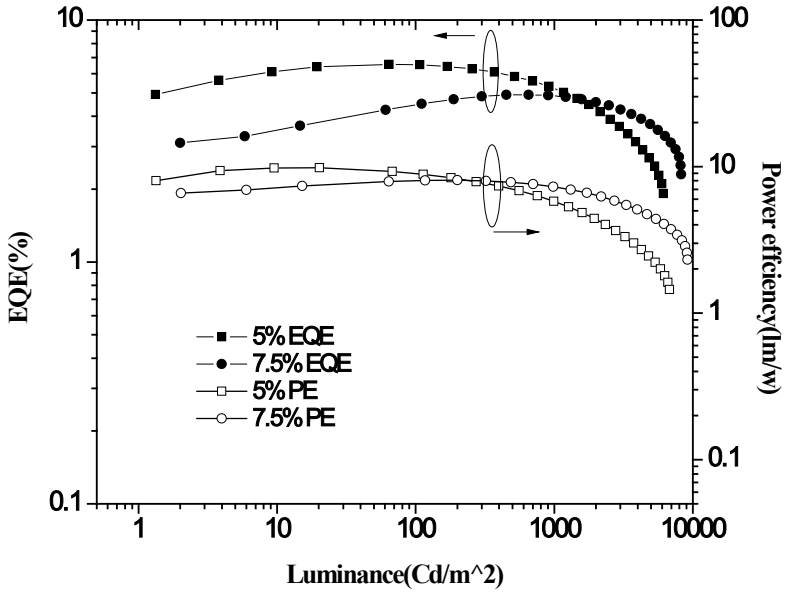

Figure 4.30 External quantum efficiency and power efficiency as a function of luminance for devices doped at 5 and 7.5%.

Table 4.5 Summary of electro-optical parameters showing peak values as well as values at 1000 cd/m2.

Device ID	PE_{peak} (lm/W)	PE_{1000} (lm/W)	EQE_{peak} (%)	EQE_{1000} (%)	Brightness	CIE_{peak} (x, y)	CIE_{1000} (x, y)	CRI_{peak}	CRI_{1000}	V_T (V)
$Pt(ptp)_2$ 3%	6.32	2.47	3.92	2.46	3480	(0.229 ,0.496)	(0.225,0.472)	26	27	5V
$Pt(ptp)_2$ 5%	9.83	5.81	6.55	5.32	6130	(0.248,0.517)	(0.245,0.514)	27	30	4V
$Pt(ptp)_2$ 7.5%	8.07	7.29	4.91	4.89	8250	(0.274,0.526)	(0.272,0.526)	32	32	4.2 V
$Pt(ptp)_2$ 10%	7.16	4.27	4.03	3.53	6170	CIE(0.276, 0.513)	CIE(0.268, 0.509)	38	35	4.4
$Pt(ptp)_2$ 15%	6.72	4.26	2.98	2.82	8470	CIE(0.333, 0.536)	CIE(0.326, 0.533)	45	41	4.2
$Pt(ptp)_2$ 25%	1.72	0.87	0.84	0.69	3620	CIE(0.469, 0.508)	CIE(0.418, 0.518	47	51	4
$Pt(ptp)_2$ 45%	2.38	1.13	1.02	0.79	3390	CIE(0.462, 0.509)	CIE(0.436, 0.510)	51	56	4

4.3.4 Optimization of the Exciton and Electron Blocking Layer (EBL) for Higher Power and Quantum Efficiency [16]

In the electroluminescence of the samples doped at 25 and 45 % in Fig 4.24, the shoulders for 25% and 45% doped devices at 450nm is due to NPB, and indicate that an electron blocker is needed for higher concentrations since the recombination zone is

expanded to NPB layer. Therefore, another series of devices with mCP as EBL were fabricated and measured.

The OLED stack consisted of 40 nm of N,N'-diphenyl-N,N'-bis(1-naphthyl)-1,1'-biphenyl 4,4'-diamine (NPB) as the hole transport layer (HTL) followed by a 10 nm layer of 3,5'-*N,N'*-dicarbazole-benzene (MCP) as the electron/exciton blocking layer (EBL), 25 nm of the emissive layer (EML) with varying dopant concentrations in the host material 4,4'–bis(carbazol–9–yl) biphenyl (CBP) and a 30 nm layer of 1,3,5-tris(phenyl-2-benzimidazolyl) -benzene (TPBI) as the electron transport layer (ETL). The devices were capped with a 100 nm film of co-deposited Mg:Ag alloy in a 10:1 atomic ratio, as the cathode. A wide range of dopant concentrations from low (≤ 5%) to neat (100%) for the emissive layer and the trends in performance as well as the EL spectra of these devices is discussed below.

The EL emission characteristics represent a monotonic increase in the excimer to monomer ratio as the doping concentration is increased. As the EL spectra shown Fig. 4.31 shows, the structured monomer emission in the blue region (λ= 480 nm) dominates at low doping concentrations (5%) and a progressive increase in the excimer emission (broadening at longer wavelengths) is observed as the doping concentration is increased up to 65%. Extended excimer emission is observed for neat films (100% $Pt(ptp)_2$) of the molecule, causing a red-shift (orange emission) in the EL spectra attributed to stronger Pt(II)···Pt(II) intermolecular interactions caused by ordered stacking of the Pt(II)-bis(pyridyltriazolate) square-planar units. Good agreement between the PL and the EL characteristics are observed. The performance of these devices is summarized in Table 4.5. The J-V-L and efficiency curves are depicted in Fig 4.32-4.34. Similar to device series without an EBL, as the doping

concentration increases, a decrease in the electrical threshold voltage and an increase in the current density at equivalent voltage are observed (Fig 4.32). It has been proposed that the reduced roll-off in EQE at higher brightness levels and the increase in the EQE with increasing doping concentrations up to 65% is a result of self-sensitization in $Pt(ptp)_2$ [15], which is consistent with the reduction in radiative lifetimes at similar doping levels. EQE as high as 13.2% for the devices with 65% $Pt(ptp)_2$:CBP as the emissive layer indicates good exciton confinement and charge balance. For the 65% doped devices the power efficiency, EQE and luminous efficiency yield at 1000Cd/m² are 76%, 94% and 94% of their highest values which are obtained at low current density and brightness near the turn on voltages shown in Table 4.6. The carrier recombination zone is assumed to be well confined within the EML since no emission from either MCP or TPBI is observed.

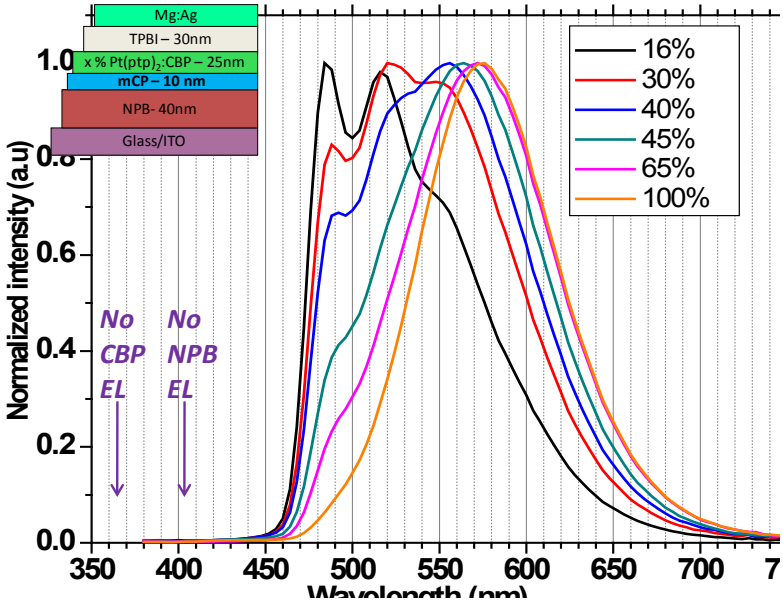

Figure 4.31 Electroluminescence spectra of different volume percentages Pt(ptp)2 in CBP.

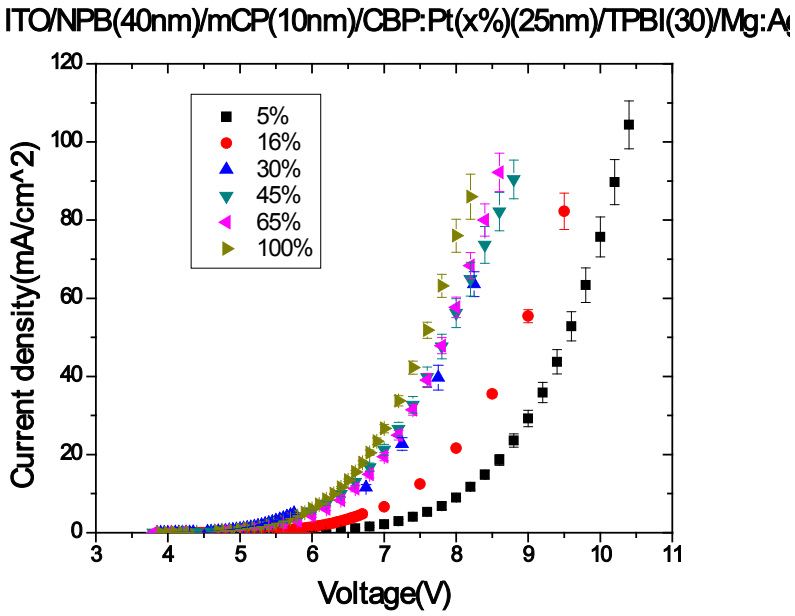

Figure 4.32 Current-voltage curves for devices with different dopant concentration.

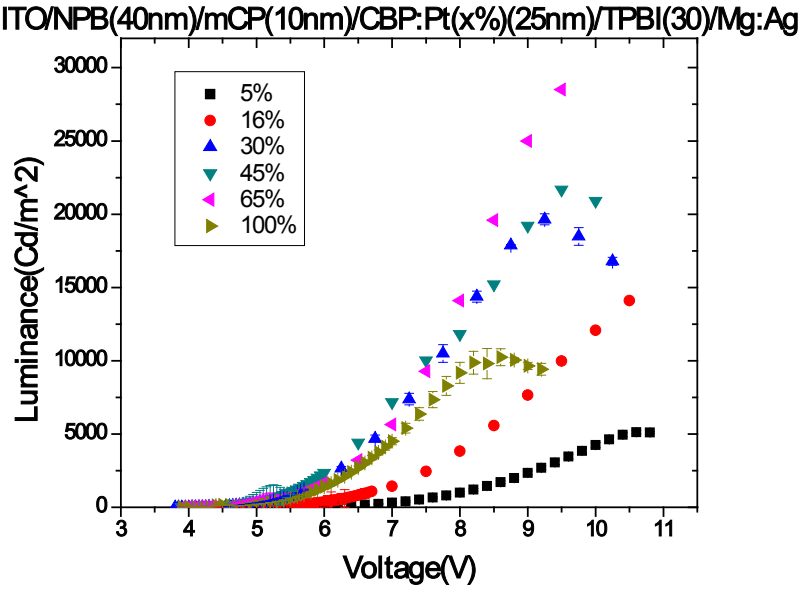

Figure 4.33 Luminance-voltage curves for devices with different dopant concentration.

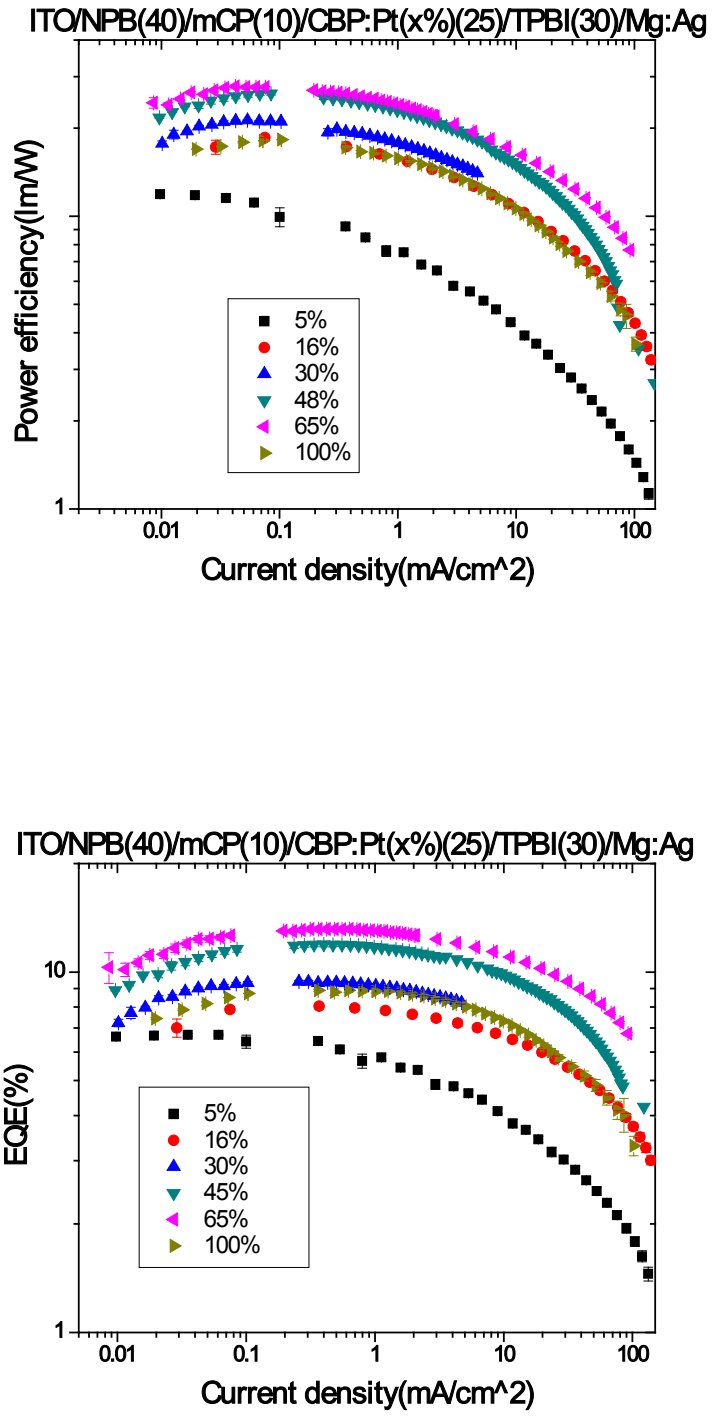

Figure 4.34 External quantum efficiency (a) and power efficiency (b) as a function of current density.

Table 4.6 Performance metrics for doping levels varying from 5% to 100% with the device structure shown in the inset of Fig 4.31. Device efficiencies are reported at peak performance and at 1000 cd/m^2.

x %	PE_{peak} (lm/W)	PE_{1000} (lm/W)	EQE_{peak} (%)	EQE_{1000} (%)	CIE_{1000} (x, y)	LE_{peak} (cd/A)	LE_{1000} (cd/A)	V_t (V)
5%	11.90 ±0.25	4.34±0.04	6.70±0.07	4.11±0.02	(0.2339,0.4868)	18.40± 0.07	11.00± 0.18	4.1
15%	18.14 ±0.05	11.02±0.04	9.39±0.05	7.83±0.02	(0.2898 ,0.5216)	27.48± 0.12	23.16± 0.15	4.1
30%	21.30± 0.06	14.55±0.08	9.41±0.06	8.39±0.09	(0.341,0.5352)	29.20± 0.20	26.10± 0.23	3.8
45%	26.30± 0.30	19.90±0.19	11.92± 0.14	11.07± 0.11	(0.4108,0.5277)	37.51± 0.42	34.94± 0.33	3.9
65%	27.80± 0.16	21.10±0.12	13.16± 0.04	12.40± 0.07	(0.4428,0.5175)	40.51± 0.16	38.26± 0.19	3.9
100%	18.30± 0.30	12.90±0.11	8.90±0.11	8.17±0.07	(0.4908, 0.4935)	25.69± 0.18	23.77± 0.21	3.9

4.3.5 Optimizing the EBL for Better Power and External Quantum Efficiency (II)

If mCP is omitted from the structure, the EL spectrum has a significant contribution from NPB and the quantum efficiency of the devices drops by roughly a factor of around 3 for 15% doping, and a factor of 10 at 25% and 45% doping as is shown in table 4.6 and 4.7. This can be explained since in a poorly charge-balanced structure, where the exciton generation and charge carrier recombination usually occurs at the interfaces and in this case the difference in triplet energy of NPB (E_T = 2.29 eV) and $Pt(ptp)_2$ (E_T = 2.14 eV) is only 0.15 eV, possibly allowing endothermic energy transfer as well. A thin layer (10 nm) of mCP was introduced between the HTL and the EML as an exciton blocker since it has a high triplet energy (E_T = 2.9 eV). The mCP was a bigger barrier for exciton diffusion to the NPB layer and eliminated the NPB emission which resulted in better device performance and stability shown in Fig 4.35 and Fig 4.36.

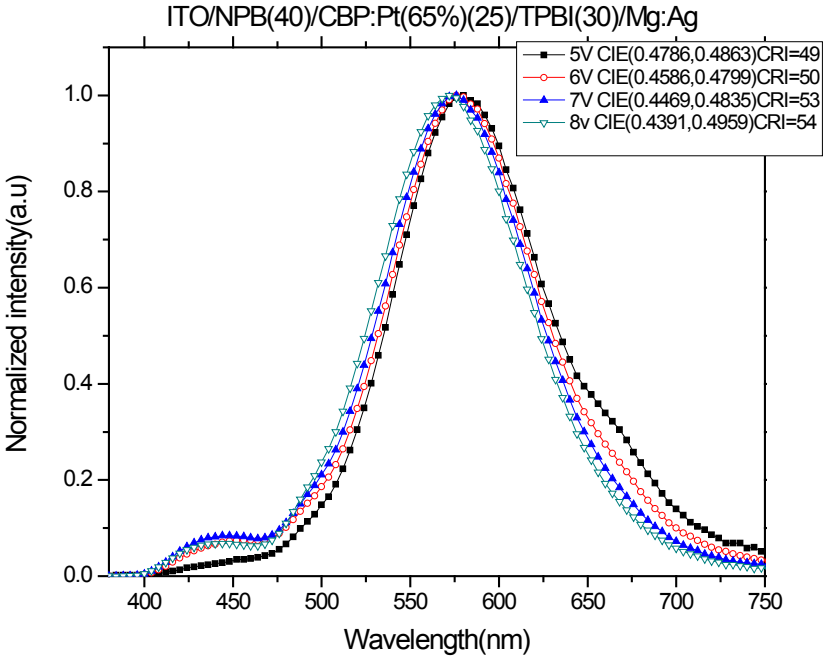

Figure 4.35 EL spectra as a function of applied bias for device : ITO/NPB(40nm)/CBP:Pt(65%)(25nm)/TPBI(30nm)/Mg:Ag

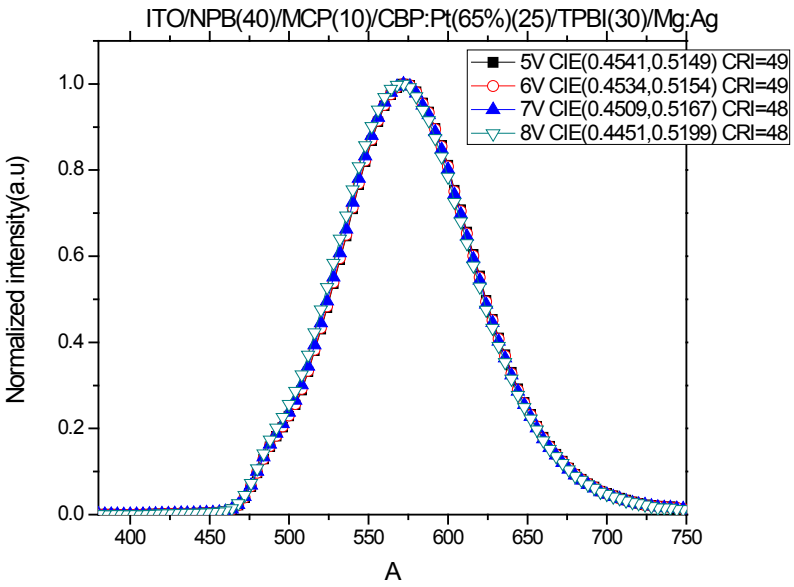

Figure 4.36 EL spectra as a function of applied bias for device : ITO/NPB(40nm)/mCP(10nm)/CBP:Pt(65%)(25nm)/TPBI(30nm)/Mg:Ag

4.3.6 Optimization of the ETL for Higher Power and Quantum Efficiency [16]

Four devices structures were fabricated and measured to understand and evaluate the difference between 1,3,5-tris(phenyl-2-benzimidazolyl) -benzene (TPBI) and 2,9-dimethyl-4,7-diphenyl-1,10-phenanthroline (BCP) as ETL.

Device 1: ITO/NPB(40nm)/CBP:Pt(15%)(25nm)/TPBI(30nm)/Mg:Ag

Device 2: ITO/NPB(40nm)/CBP:Pt(15%)(25nm)/BCP(30nm)/Mg:Ag

Device 3: ITO/NPB(40nm)/mCP(10nm)/CBP:Pt(10%)(25nm)/TPBI(30nm)/Mg:Ag

Device 4: ITO/NPB(40nm)/mCP(10nm)/CBP:Pt(10%)(25nm)/BCP(30nm)/Mg:Ag

From the bandgap diagrams in Fig 4.37, there is a smaller electron injection barrier from TPBI into the EML($\approx 0.4eV$) compared to BCP ($\approx 0.6eV$). Larger turns on voltages are found in both device 2 and device 4 compared to device 1 and device 3 as shown in Table 4.6.

BCP can block holes from migrating from the doped CBP to the cathode, due to the large HOMO difference between CBP and BCP ($\approx$0.5eV). Both BCP(E_T=2.5eV) and TPBI (E_T =2.9eV) are reported as efficient high triplet energy blockers, which can prevent exciton from diffusing out of EML[17]. The triplet energy of $Pt(ptp)_2$ is 2.14eV, and the triplet energy difference between BCP and $Pt(ptp)_2$ is only 0.36eV, which may possibly allow endothermic energy transfer (triplet energy will be transferred from dopant back to host). More current is injected into device 1 compared to device 2 at equivalent voltage as is shown in Fig 4.38. Device 1 displays a higher power efficiency of 8.74 lm/W and EQE of 4.09% compared to device 2. Better charge balance for device 1 may be attributed to the higher electron mobility of TPBI compared to BCP[18]. After adding 1,3-*bis*(9-carbazolyl)benzene (mCP) as EBL both device 3 and device 4 displayed a much higher power and external quantum efficiency than devices 1 and 2. mCP is reported as an efficient electron and exciton blocker and has been used successfully to eliminate electron/exciton leakage from the EML which contained Pt complex as dopant[19]. The use of mCP as EBL improves the device performance significantly. Device 3 exhibited a peak power efficiency of 17.2lm/W and external quantum efficiency of 9.39% as shown in Fig. 4.41. Device 4 also got improvement in both efficiencies and gave a peak power efficiency of 10.8lm/W and EQE of 5.84%.

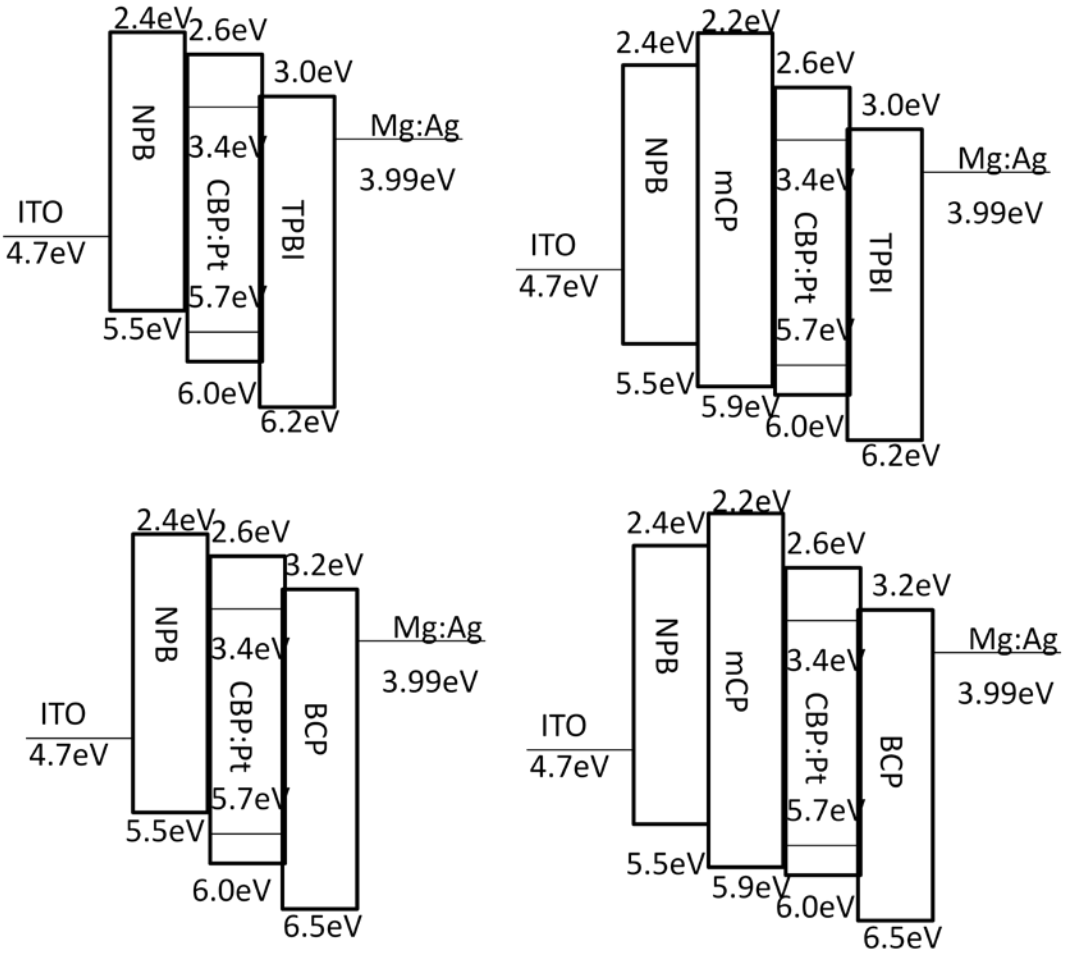

Figure 4.37 Band diagram

Table 4.7 Performance metrics for four devices

Device ID	PE_{peak} (lm/W)	PE_{1000} (lm/W)	EQE_{peak} %)	EQE_{1000} (%)	V_T
Device 1	8.74	2.6	4.09	2.18	4.25V
Device 2	1.76	1.34	1.65	1.16	5
Device 3	17.2	7.83	9.39	6.60	4.4
Device 4	10.8	5.04	5.84	4.04	4.6

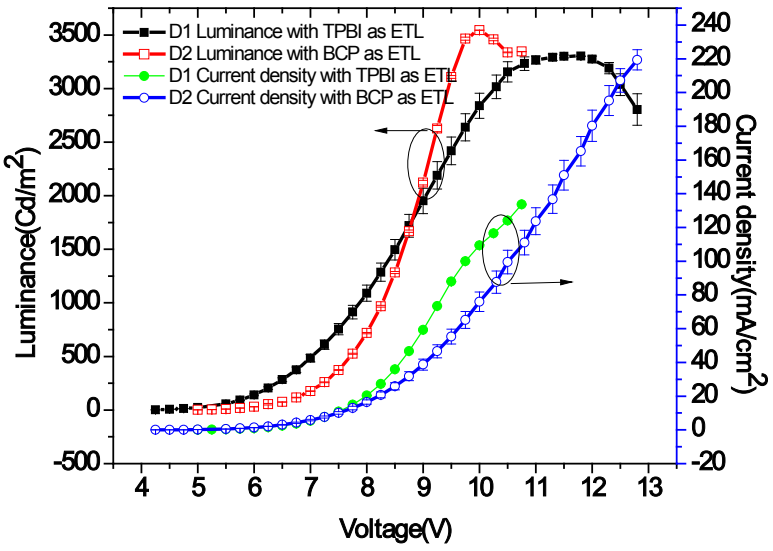

Figure 4.38 J-V-L behavior of Device 1 and Device 2

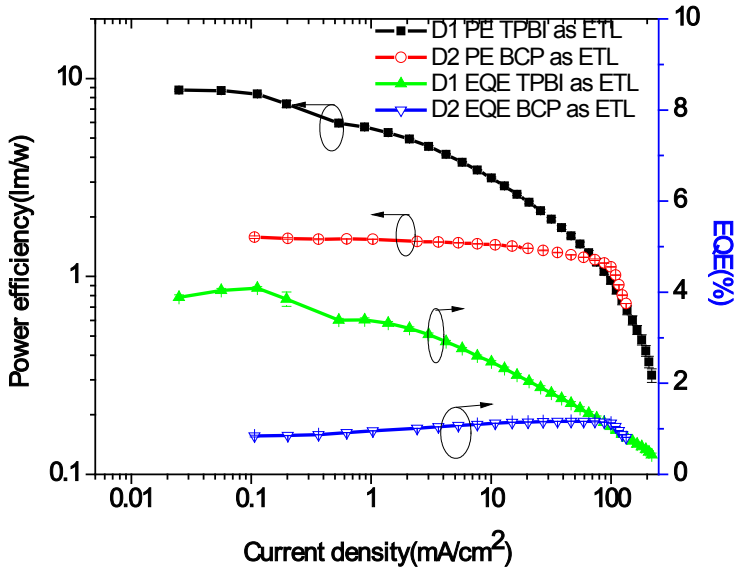

Figure 4.39 Efficiency behavior of Device 1 and Device 2

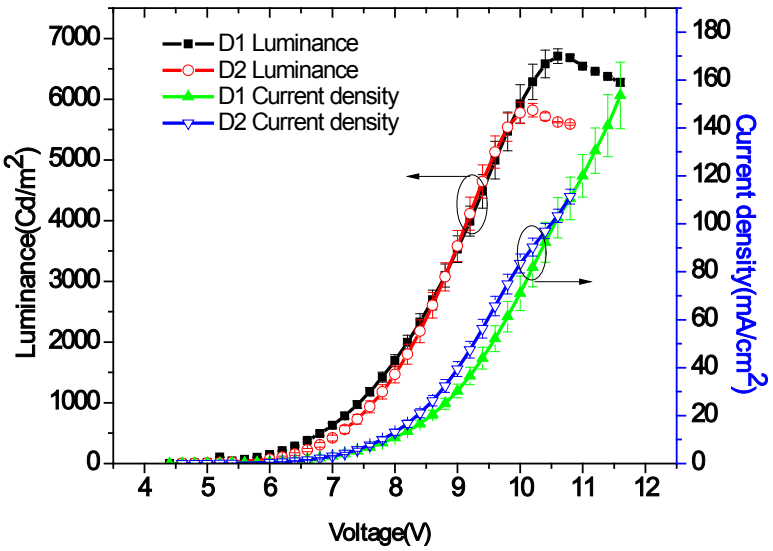

Figure 4.40 L-J-V behavior of Device 3 and Device 4

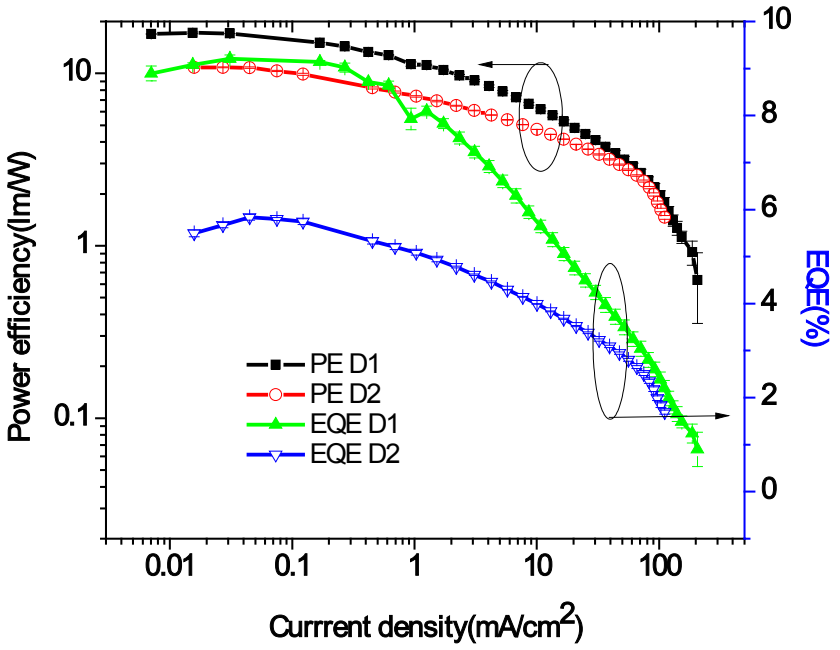

Figure 4.41 Efficiency behavior of Device 3and Device 4

4.3.7 Optimizing the Host for Better Power and External Quantum Efficiency

Two structures were fabricated and evaluated to investigate the effect of different hosts in terms of efficiencies.

Device 1:ITO/NPB(40nm)/CBP:Pt(15%)(25)/TPBI(30nm)/Mg:Ag

Device 2:ITO/NPB(40nm)/mCP:Pt(15%)(25)/TPBI(30nm)/Mg:Ag

The band diagram for the two devices is shown in Fig 4.42. The J-V-L, efficiency characteristics and EL spectrum were illustrated in Fig 4.43-4.47 and the performance parameters are listed in Table 4.8.

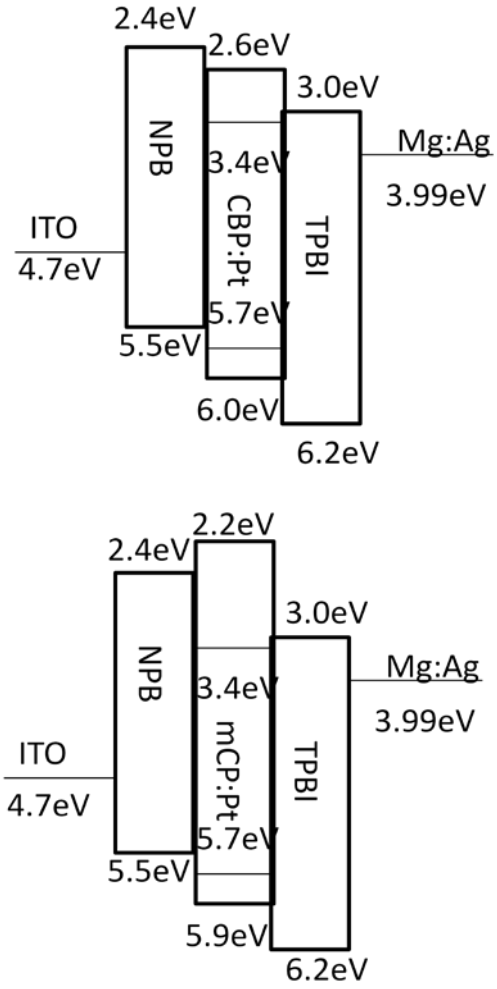

Figure 4.42 Band diagrams of two devices

Table 4.8 Performance metrics for two devices

Device ID	PE_{peak} (lm/W)	PE_{1000} (lm/W)	EQE_{peak} %)	EQE_{1000} (%)	V_T
Device 1	8.74	2.6	4.09	2.18	4.25V
Device 2	4.41	0.97	4.08	1.65	6.5V

The maximum peak and power efficiency for device 1 are 8.74lm/w and 4.09%,

respectively, which dropped to 4.41lm/w and 4.08% for device 2 as shown in Table 4.7. The use of the mCP as the host in the place of CBP produced a much lower power efficiency. The huge electron injection barrier of 1.2eV between the LOMO of TPBI and mCP is likely responsible for the high turn-on voltage of 6.5eV, and consequent reduction in efficiency. The different solubility of $Pt(ptp)_2$ in the different hosts caused the EL spectral changes shown in Fig 4.43, which also contributed to the efficiency difference.

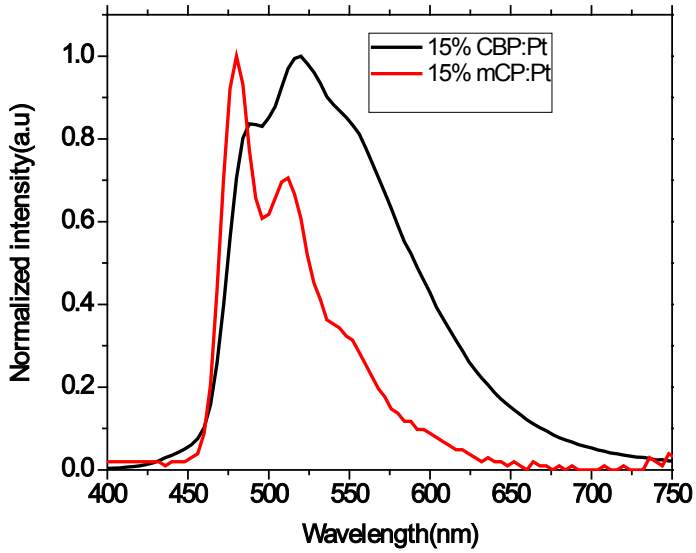

Figure 4.43 EL spectrum of the two devices indicating that $Pt(ptp)_2$ has different solubility in different hosts.

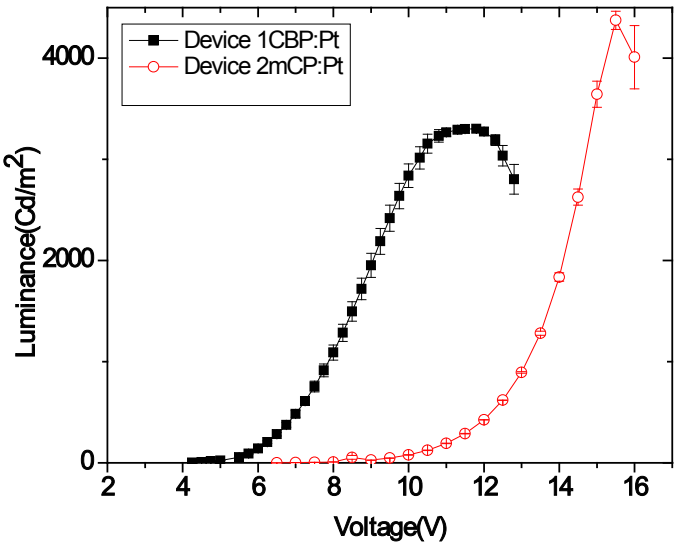

Figure 4.44 L-V behavior of the two devices

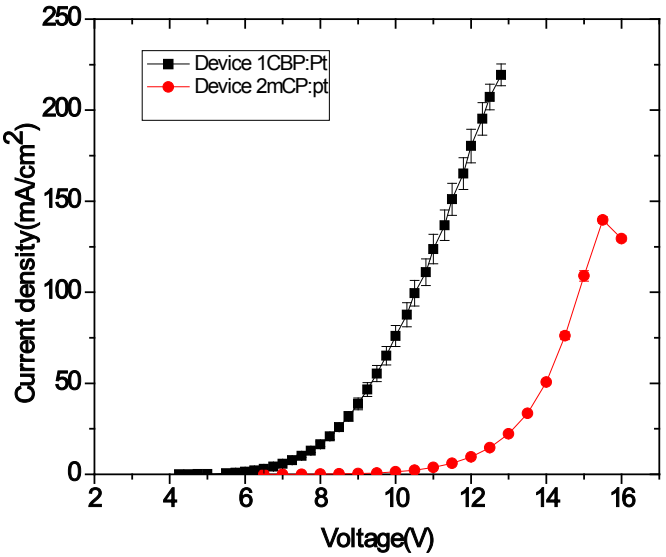

Figure 4.45 J-V characteristics of the two devices

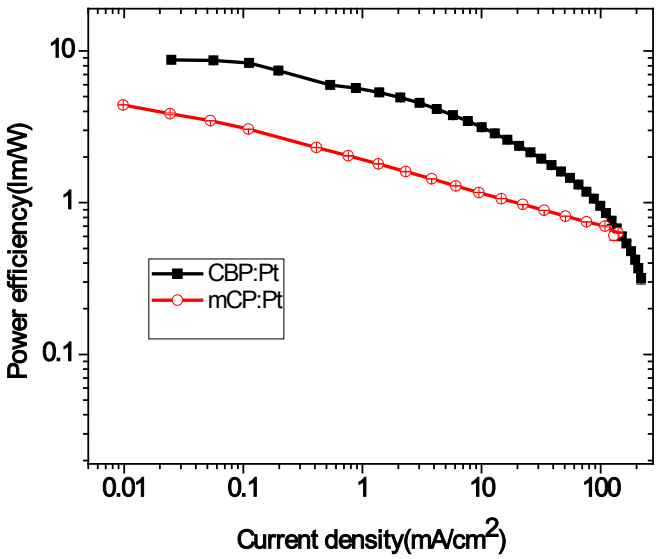

Figure 4.46 Power efficiency as a function of current density of the two devices

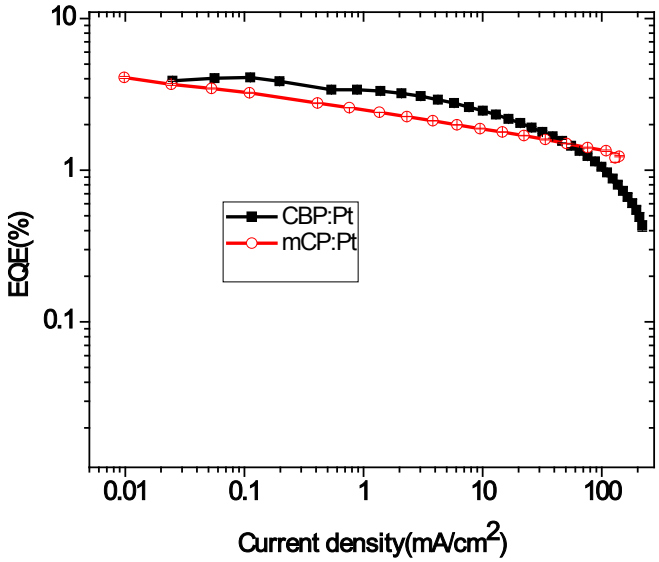

Figure 4.47 EQE as a function of current density of the two devices

4.3.8 Optimizing the Cathode for Better Power and External Quantum Efficiency

Six devices were made to compare different cathode performance and optimize the LiF thickness. Only one parameter in the structure is changed at a time as shown in Fig 4.48. The J-V-L efficiency characteristics and EL spectra are illustrated in Fig 4.49-4.52. The performance parameters are summarized in Table 4.9.

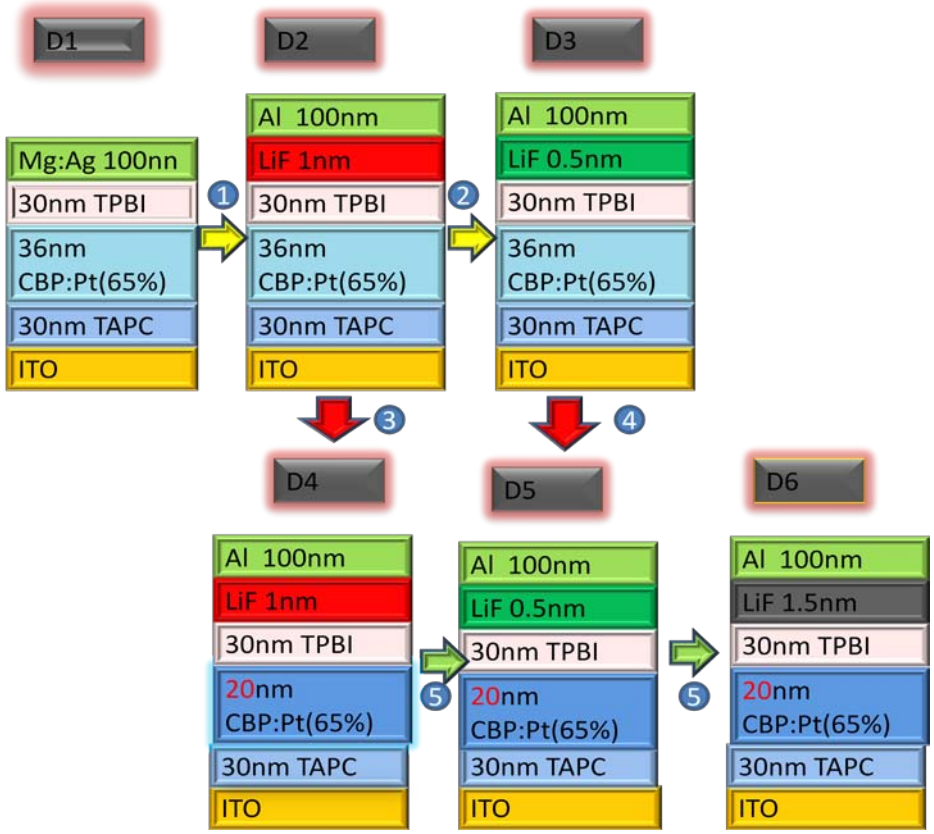

Figure 4.48 Six devices to optimize the cathode for better power and external quantum efficiency

Table 4.9 Power efficiency and EQE metrics

Device ID	PE_{peak} (lm/W)	PE_{1000} (lm/W)	EQE_{peak} (%)	EQE_{1000} (%)	CIE_{peak} (x, y)	V_T (V)
D1 Best pixel	35.5 ±0.5 (36)	23.0 ±0.4	14.9±0.05 (15.1)	13.8±0.2	0.4833 ,0.5042	3.4V
D2 Best pixel	44.7±0.5 (45.5)	35.1±0.5	19.7±0.1 (19.87)	18.9±0.2	0.469 ,0.5 137	3.4V
D3 Best pixel	45.1±0.9 (46.5)	32.6±1	20.8±0.2 (20.9)	19.3±0.7	0.4874,0.5 007	3.4V
D4 Best pixel	37.4±0.9 (38.7)	23.2±1	14.3±0.2 (14.7)	13.4±0.9	0.4757,0.5 107	3V
D5 Best pixel	29.9±0.3 (31.02)	17.6±0.2	13.8±0.02 (13.8)	11.5±0.1	0.4748,0.5 114	3.6V
D6 Best pixel	35.6±1 (37.7)	23.7±0.9	12.9±0.5 (13.6)	11.7±0.5	0.4762,0.5 103	3.2V

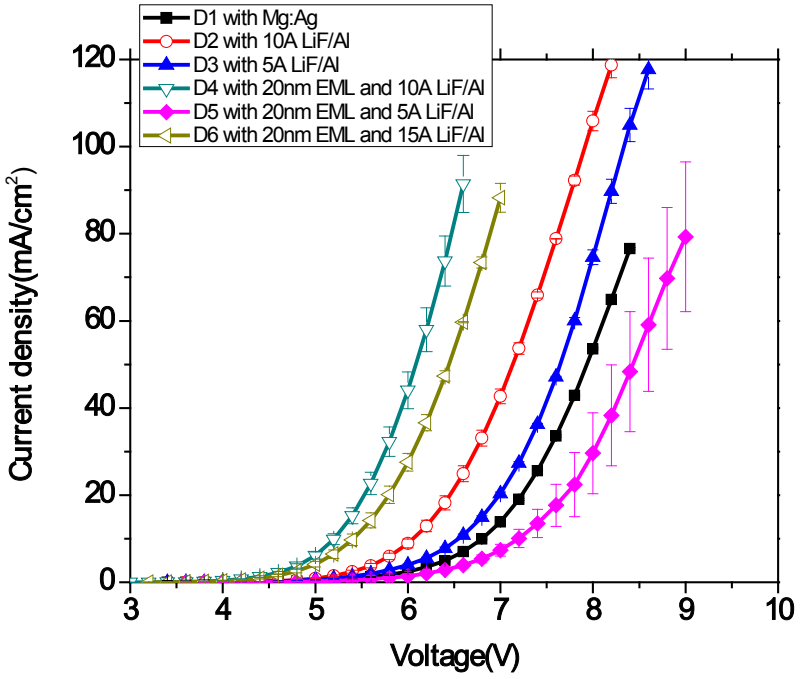

Figure 4.49 J-V characteristics

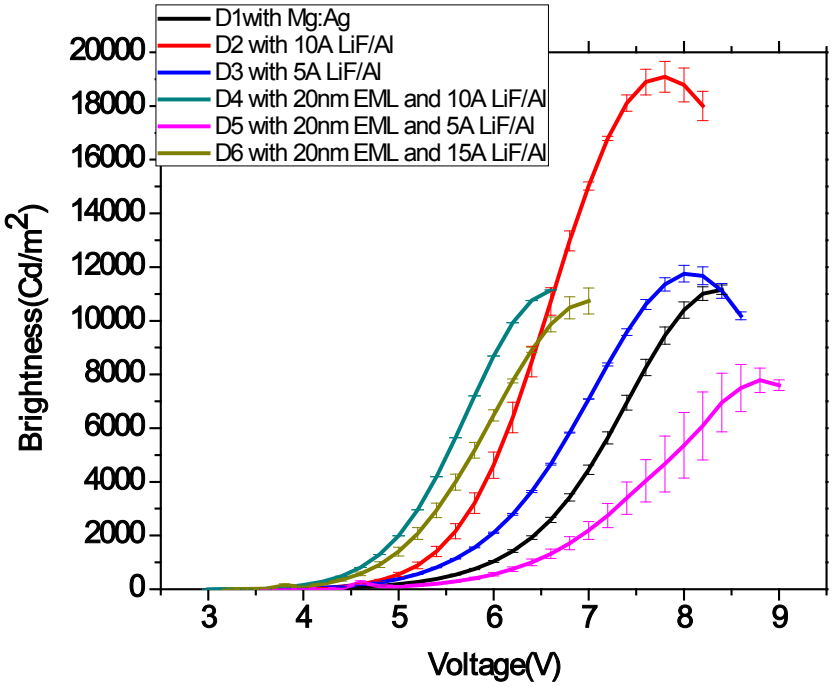

Fig 4.50 L-V characteristics

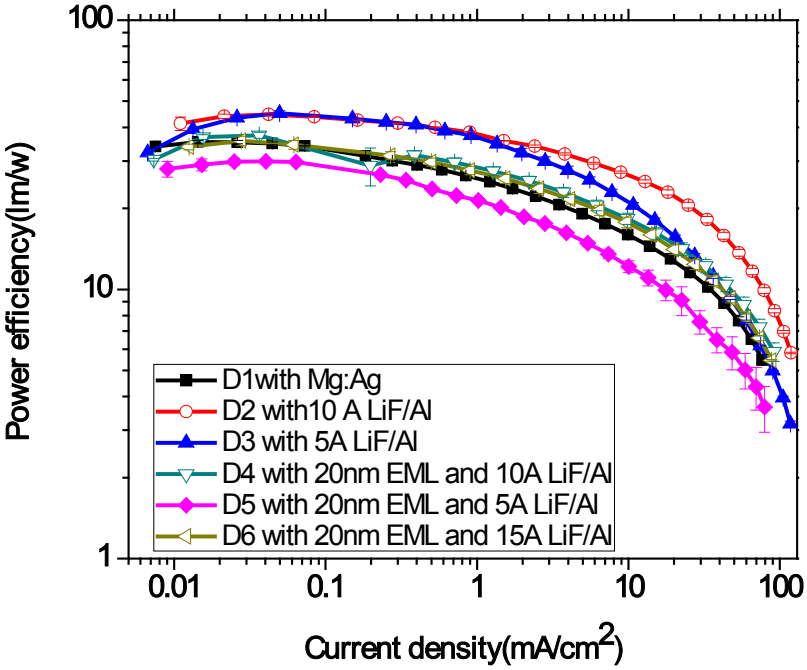

Figure 4.51 Power efficiency as a function of current density

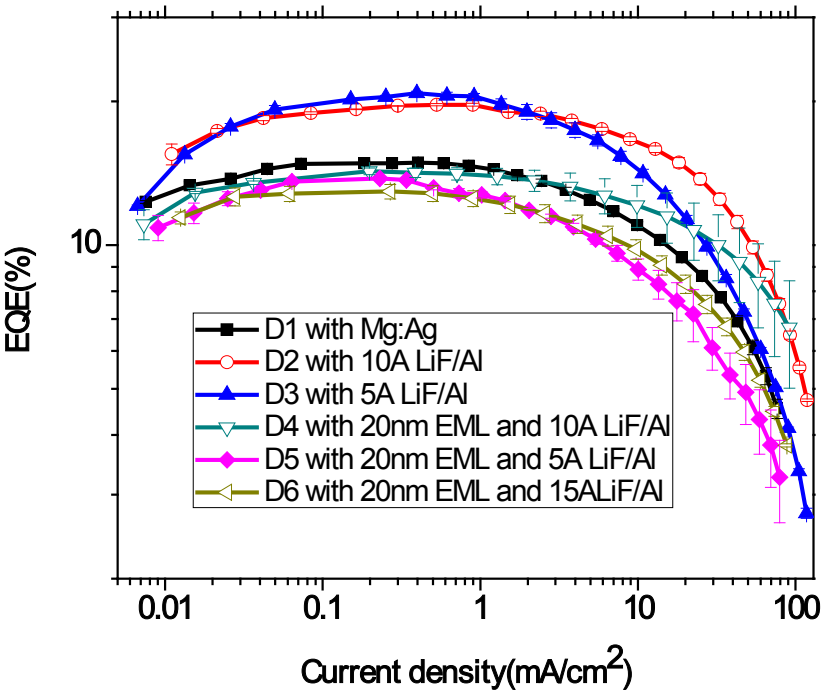

Figure 4.52 EQE as a function of current density

As can be seen from the current-voltage curves in Fig 4.48 of Device 1 and Device 2, more current have been injected into the stack from LiF/Al than Mg:Ag as a cathode. This may result from the reduction of the electron injection barrier by dipole formation. Also as the LiF thickness is increased, the slope of the current density curve also increases, indicating more current is flowing through the stack. Among all of the different LiF cathode thicknesses devices with 10Å LiF exhibited the highest brightness as is shown in Fig 4.50. In the case of LiF/Al cathode, a number of mechanisms have been proposed in the literature for enhanced electron injection including the tunneling effect [20], band bending at the organic/metal interface [21], lowering of the work function of Al [22], etc. For the same organic layers structure, the maximum device power and external quantum efficiency performance increased from 35.5lm/W and 14.9% with Mg:Ag cathodes to 45.1lm/W and 20.8 % by using 5Å LiF and 100nm Al as the cathode. This record efficiency may be due to two reasons: firstly, as concentration goes up as high as 65%, self-quenching can be minimized by reduced dopant triplet states. Secondly, radiative lifetime is reduced at higher concentration. Also, devices with 10Å LiF as cathode shows even less severe efficiency roll-off than the 5Å LiF devices shown in both Fig 4.51 and 4.52. From this series of devices, it is observed that NPB/MCP with a single layer of 1, 1-bis[(di-4-tolylamino)phenyl] cyclohexane (TAPC), better hole transport as well as an exciton and an electron blocking is obtained. The hole mobility for TAPC is almost 3 orders of magnitude higher than that of NPB at comparable electric fields (~0.1 MV/cm), which presumably contributes to good charge balace. The LUMO level is -2.0 eV (a good electron blocker) and the triplet energy, E_T = 2.87 eV, produces

better exciton blocking.

4.4 EL Transient Lifetime and Mobility Measurement

4.4.1 Mobility t_d Study [23]

Fig 4.53 shows the oscillograms of an applied voltage pulse with zero dc forward offset, and the transient EL response of the device under investigation. The delay time t_d is defined as the time difference between the applied voltage pulse and the onset of the EL. Several physical device processes can be identified by the difference between the rise of the voltage pulse and the onset of the EL signal, such as, the transport of charge carriers, accumulation at the interface, and formation of excitons. The delay time (t_d) can be divided into two components: (i) the charge injection delay or charging time of the OLED (t_{inj}) and (ii) the charge transport delay time (t_{trans}). The EL delay time can be represented as

$$t_d = t_{inj} + t_{trans} \quad (1)$$

where

$$t_{inj} = RC\ln\left(\frac{V_{max}}{V_{max} - V_{th}}\right) \quad (2)$$

Here V_{max} is the height of the applied rectangular voltage pulse and V_{th} is the threshold voltage for charge injection [24]. Once the delay time at the applied field is known, the carrier mobility is calculated using the following transit time and field relation [23]:

$$t_d = t_{inj} + t_{trans} = t_{inj} + \frac{d_e}{(\mu_e + \mu_h)E} \quad (3)$$

Where d_e is the distance the electrons travel before they meet holes, μ_e and μ_h are the

electron and hole motilities, respectively, and E is the internal electric field. The transient EL method is suitable only for the case where the mobility of one charge carrier is more than that of the other charge carrier. It is assumed that (a) the mobility of one of the carriers is much higher than the other ($\mu_e >> \mu_h$) and (b) the internal field is uniform throughout the whole device thickness. Now equation (3) can be written as

$$t_d = t_{inj} + \frac{dd_e}{\mu_e(V - V_{bi})} \quad (4)$$

where d is the thickness of the organic layer, V is the applied external voltage and V_{bi} is the built-in potential.

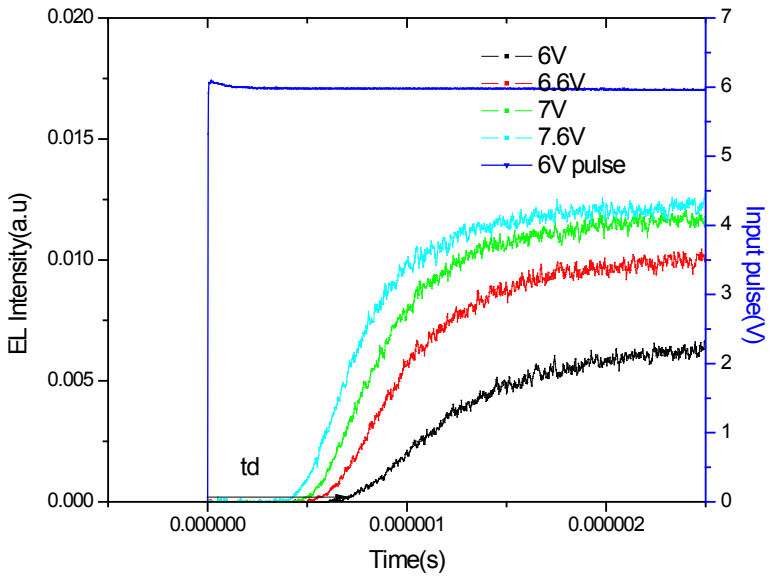

Figure 4.53 Input voltage pulse and transient EL response of the device on the time scale. Td is the delay time between the input voltage pulse and the onset of EL.Device structure is ITO/TAPC(50nm)/CBP: $Pt(ptp)_2$ (65%)(30nm)/TPYMb(30nm)/Mg:Ag

4.4.2 Result and Discussion

TAPC has high hole mobility ~(1.0×10^{-2} cm^2 V^{-1} s^{-1})[24], therefore, holes that are injected will quickly reach the TAPC/CBP interface. Due to the high hole mobility in TAPC it can be considered as a part of the ITO anode and the voltage drop across the TAPC can be

assumed to be negligible. On the other side, electron mobility of TPYMb~($1.0 \times 10-5\,cm^2 V^{-1} s^{-1}$), TPYMb cannot be assumed as part of the cathode. The holes and electrons meet with each other at the interface of TAPC and CBP, the total voltage will drop across the EML and ETL. The monitored wavelength is the peak wavelength of the EML which is located at 575nm. In this case, equation (4) can be written as: $t_d = t_{inj} + \frac{d_e^{\,2}}{\mu_e (V - V_{bi})}$, where d_e is the thickness of EML and ETL, $t_{inj} = 2.7E-7s$ (RC time constant of system setup), V_{bi} is the built–in voltage and can be estimated as the difference of the work function of the two electrodes. We assume the work function of ITO to be 4.8eV and that of Mg:Ag to be 3.99eV, and with d_e=60 nm, V=6V, t_d=6.6E-7s(from Fig 4.52), V_{bi}=0.81eV, the calculated effective electron mobility in TPYMb/CBP: $Pt(ptp)_2$ is μ_e=1.54E-9$m^2V^{-1}s^{-1}$ =1.54E-5$cm^2V^{-1}s^{-1}$.

The EL response of the diodes to the pulse was recorded for different device structures at different bias. Fig 4.54 shows the typical EL transients for a 10μs pulse and duty of 50% at 295K which are normalized to the maximum emission. The two device structures are ITO/NPB(40nm)/Pt(25nm)/TPBI(30nm)/Mg:Ag and ITO /NPB (40nm) / CBP:Pt (65%) (25nm)/TPBI(30nm)/Mg:Ag respectively. In order to achieve an acceptable signal to noise ratio, the pulse height is 8V. The decay time for the neat device is 448 ns and the decay time for the device doped at 65% is 522ns as shown in Fig 4.54. Similarly Fig 4.55 shows the transient decay time of the neat device and 30% doped CBP device with mCP as EBL. The decay time for the neat device is 436ns and the decay time for the 30% device is 944ns.

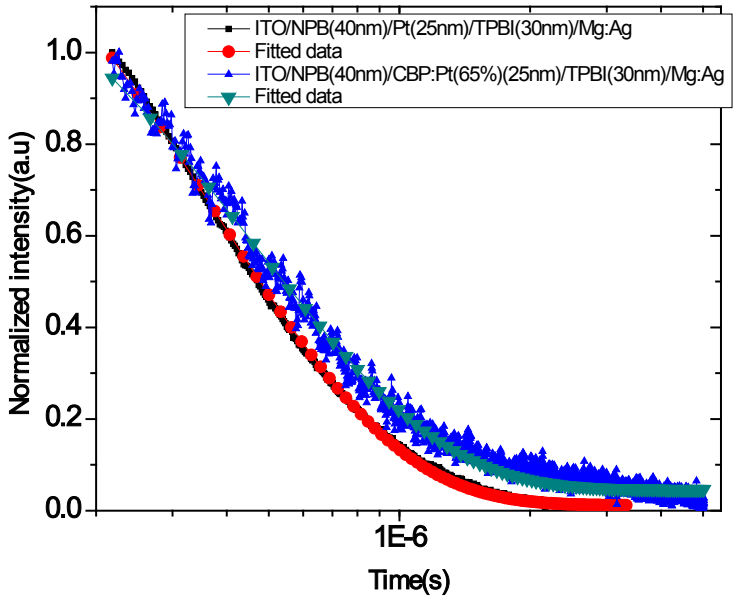

Figure 4.54 EL transient decay time 1

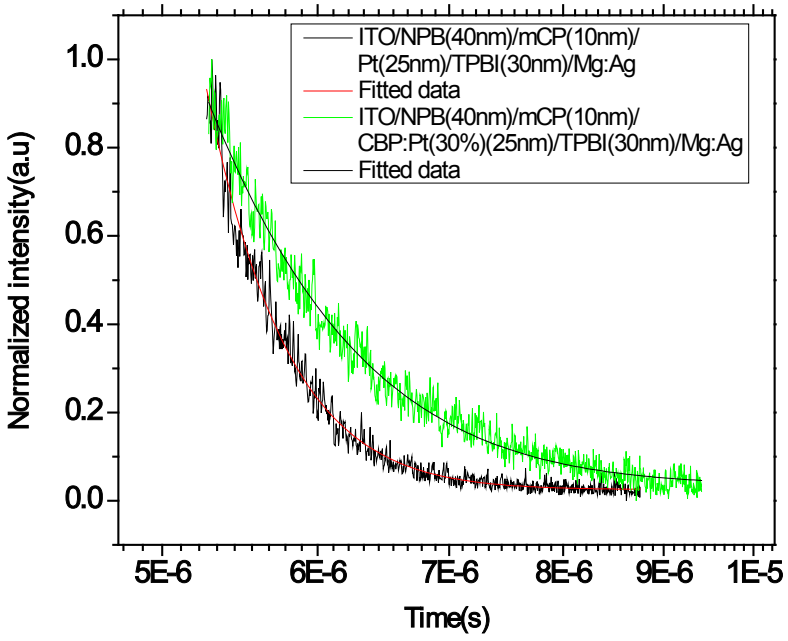

Figure 4.55 EL transient decay time 2

The transient EL for the structure ITO /NPB (40nm)/mCP(10nm)/CBP:Pt(65%) (25nm)/TPBI(30nm)/Mg:Ag was shown in Fig 4.56. Initially, the EL decays rapidly corresponding to the discharge of the OLED which is modeled as a capacitor. After 1 μs, the

EL is found to rise again and decay slowly without external applied bias.

The second rise is due to charge trapping at the mCP/CBP:Pt interface, because this phenomena is not observed in the 65% device without mCP as EBL. This phenomenon can be explained as follows: first, the highly doped CBP layer with large electron penetration and a thin mCP layer with LOMO as low as 2.2eV will lead to significant buildup of negative charge in the interface between mCP and CBP during the device operation. Some holes remain trapped in the bulk after voltage turn-off. When the bias is turned off, the electrons diffuse back into the EML and recombine with trapped holes they meet. From Fig 4.56 the time position of the second rise stays the same for different applied bias, suggesting the diffusion of electrons from the same set of the traps responsible is the origin of the delay. EL decay was also measured at different monitor wavelength shown in Fig 4.57, and the peak emission wavelength of 65% device at 570nm gives the highest intensity.

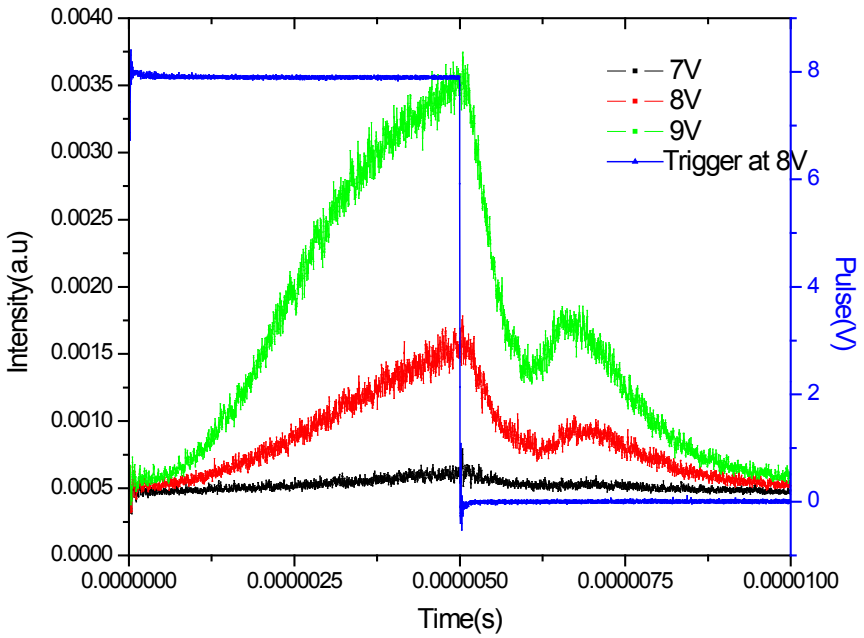

Figure 4.56 Transient EL at different applied bias

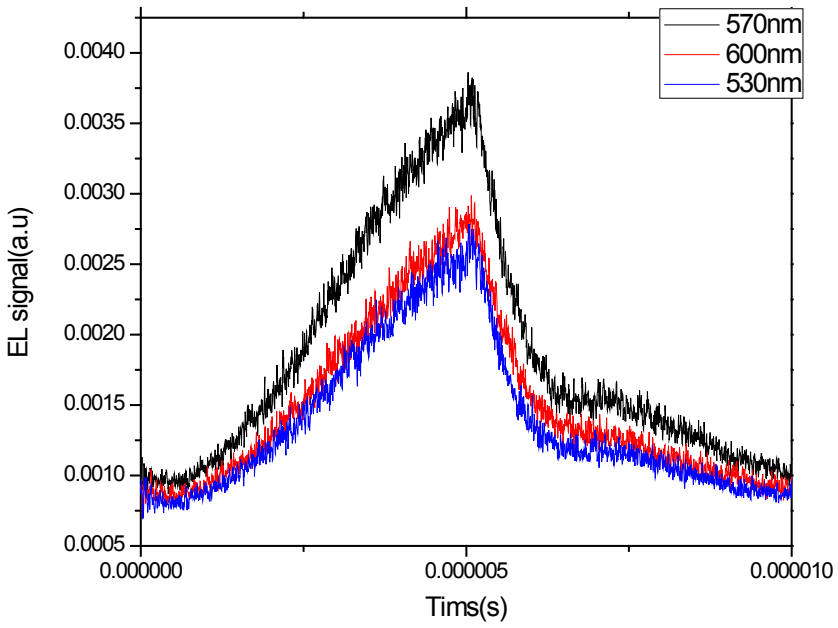

Figure 4.57 Transient EL at different monitor emission wavelength

4.5 References:

[1] Hari Singh Nalwa, and Lauren Shea Rohwer (Eds.), *Handbook of Luminescence, Display Materials and Devices*, (ASP Press, California, 2003) vol. 1.

[2] J.-S Lim, P.-K Shin, Applied Surface Science **253**, 3828 (2007)

[3] S.R.Forrest, D.C.Bradley and M.E.Thompson, Adv.Mater:.**15**, 1043 (2003)

[4]P.E.Burrows,V.Khalfin,G.Gu,andS.R.Forrest,Appl.Phys.Lett.**73**, 435(1998)

[5]T.Granlund, L.A.A.Pettersson,M.R.Anderson,and O.Inganas, J.Appl.Phys. **81**, 8097 (1997).

[6] Y.Fukuda, T. Watanabe, T. Wakimoto , S. Miyaguchi, M. Tsuchida, Synthetic Metals .**111**, 327(2000)

[7] T. Watanabe, K.Nakamura, S.Kawami, Y.Fukuda,T Tsuji, T.Wakimoto, S.Miyaguchi,M.Yahiro, M.-J.Yang, and T. Tsutsui. Synthetic Metals .**122**, 203(2001)

[8] M.Li; W-H.Chen; M-T.Lin; M.Omary; N. Shpherd.Organic electronics. **10**, 863(2009)

[9]. B.W. D' Andrade, J. Brooks, V. Adamovich, M.E. Thompson and S.R. Forrest, Adv. Mater., 14, **1032** (2002).

[10]. J. Kalinowski, M. Cocchi, D. Virgili, V. Fattori and J. A. G. Williams, Adv. Mater., **19**, 4000 (2007).

[11] M. Cocchi. J. Kalinowski, D. Virgili , V. Fattori, S. Develay and J. A. G. Williams, Appl. Phys. Lett., **90**, 163508 (2007).

[12]. S.-Y. Chang, J. Kavitha, S.-W. Li, C-S. Hsu, Y. Chi, Y.-S. Yeh, P.-T. Chou, G.-H. Lee, A. J. Carty, Y.-T. Tao and C.-H. Chien, Inorg. Chem., **45**, 137 (2006).

[13]. E. L. Williams, K. Haavisto, K, J. Li and G. E. Jabbour, Adv. Mater., **19**, 197 (2007).

[14]. V. Adamovich, J. Brooks, A. Tamayo, A. M. Alexander, P. I. Djurovich, B. W. D'Andrade, C. Adachi, S.R. Forrest and M.E. Thompson, New. J. Chem., **26,** 1171 (2002).

[15]Multi-Year Program Plan FY'09-FY'15, Solid-State Lighting Research and Development, U. S. Department of Energy, March 2009.

[16] Mohammad A. Omary*[1], Unnat S. Bhansali[2], Ming-Hang Li[3], Wei-Hsuan Chen[1], Ming-Te Lin[3], Huiping Jia[2], Roy N. McDougald[1], Jr., Nigel D. Shepherd[3], and Bruce E. Gnade[2,] Self-Sensitization in Photo- and Electro-Luminescence of a Pt(II) Square-Planar Complex: Fundamentals and Applications in Orange and Single-Emitter White Organic Light-Emitting Diodes in preparation.

[17]V.Adamovich,S.Cordero,P.Djurovich,A.Tamayo,M.Thompson,B.D'Andrade,S.Forrest,Organic electronics **4**, 77(2003)

[18] Z. Y. Xie, Y. Q. Li, T. C. Wong, F. L. Wong, M. K. Fung, S. T Lee, and L. S. Hung,

Mat. Res. Soc. Symp. Proc. **725,** 11(2002)

[19]B.Ma et al.Adv.Funct.Mater.**16**, 2438(2006)

[20]. L. S. Hung, C. W. Tang, and M. G. Mason, Appl. Phys. Lett. **70**, 152(1997).

[21]. K. Ihm, T. H. Kang, K. J. Kim, C. C. Hwang, Y. J. Park, K. B. Lee, B. Kim, C. H. Jeon, C. Y. Park, K.Kim, and Y. H. Tak, Appl. Phys. Lett. **83**, 2949 (2003).

[22]. S. E. Shaheen, G. E. Jabbour, M. M. Morrell, Y. Kawabe, B. Kippelen, N. Peyghambarian, M. -F. Nabor,R. Schlaf, E. A. Mash, and N. R. Armstrong, J. Appl. Phys. **84**, 2324 (1998).

[23].P.Kumar, S.Jain, V.Kumar, S.Chand, M.Kamalasanan and R Tandon, J.Phys.D:Appl.Phys.**40,** 7313(2007).

[24]. Lee, Jaewon Chopra, Neetu Eom, Sang-Hyun Zheng, Ying Xue, Jiangeng So, Franky Shi, Jianmin , Applied Physics Letters **93**, 123306(2009)

CHAPTER 5

CHROMATICITY TUNING OF WOLEDS BASED ON BIS[3,5-BIS(2- PYRIDYL)-1,2,4-TRIAZOLATO]PLATINUM (II)

5.1 Introduction

This chapter describes the effect of different stack designs on the optical properties of $Pt(ptp)_2$ based WOLEDs. The experimental procedures were the same as described in Chapter 4. WOLEDs using $Pt(ptp)_2$ at different concentrations in dual layers WOLED mixing excimer and exciplex emissions and WOLEDs combing fluorescence and phosphorescence were fabricated with the aim of tuning the color coordinates and color rendering index. A summary of the results of electro-optical characterization of these WOLEDs is given. Depends on the different correlated color temperatures, WOLEDs can be sorted to “Cool WOLEDs” and “Warm WOLEDs”.

5.2 Dual Layer WOLEDs Using a Single Emitter at Different Concentrations.

As discussed in the previous section, devices with single layer of neat $Pt(ptp)_2$ exhibit CRI as high as 50 and EQE of 8.9%. Therefore, the possibility of combining the efficient orange emission of a neat $Pt(ptp)_2$ with the turquoise-blue emission from a low doped $Pt(ptp)_2$ film to obtain white warm light emission was explored. Here, devices were designed with a dual EML structure; blue and orange emissions are generated by two discrete emitting layers as is shown in Fig 5.1. The doping concentration and thickness were designed and optimized in order to obtain a balance of blue and orange emissions, and thus achieve white light. For the structures labeled as Device 1 in Fig 5.1, the EL spectra (Fig 5.2) showed a majority

contribution from the low doped (15%) films, indicating that the recombination zone was located mainly in the CBP:Pt region. At high driving voltage, the EL spectrum became wider and the 584 nm contribution from the neat films increased, which lead to an increase in the percentage of red emission (CIE=(0.30,0.51) at 4V; CIE (0.35,0.51) at 8V). This suggests that the recombination zone expands to incorporate regions of both the doped and neat $Pt(ptp)_2$ layers as the band diagram in Fig 5.3shows. As shown in the previous chapters, the conductivity of the neat film is higher than that of a layer CBP doped with low concentration of $Pt(ptp)_2$. With increasing voltage, the contribution of orange emission increases as more holes are transported through the doped layer and injected into the neat $Pt(ptp)_2$ film.. As shown in Fig 5.4 and 5.5, the device luminance reaches 10000 Cd/m² at a voltage of 10 V, and the peak power efficiency and quantum efficiency were 12.1 lm/W and 5.6% at 4V. The CIE coordinates changed from (0.30, 0.51) at 10 cd/m² to (0.34, 0.51) at 1000 cd/m² (Fig 5.6). In comparison, the CIE for neat devices remained constant at (0.48, 0.50) for a luminance up to1000 cd/m² (Fig 5.7) and greater. The data indicates that more emission from the neat layer and more deep-blue emission are required for balanced color and white emitting WOLEDs. Analysis of the data indicates good stability of all of performance parameters as Table 5.1 shows. Specifically, the power efficiency, CRI, and external quantum efficiency at the operational condition of 1000 cd/m2 for Device 1 are at 60%, 107%, and 84% of their maximum values which are obtained at low brightness near the turn-on voltages. The reduced efficiency roll-offs indicates that that characteristic phosphorescent triplet-triplet annihilation processes that normally degrade electrophosphorescent devices are not as significant in $Pt(ptp)_2$ films and WOLEDs [1].

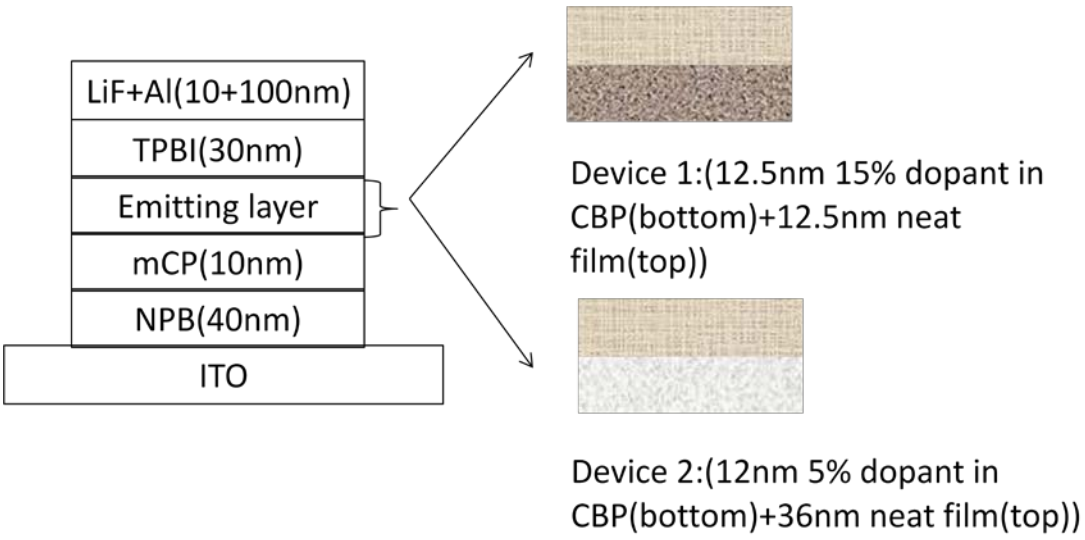

Figure 5.1 Device architectures of WOLEDs using the $Pt(ptp)_2$ as single emitter

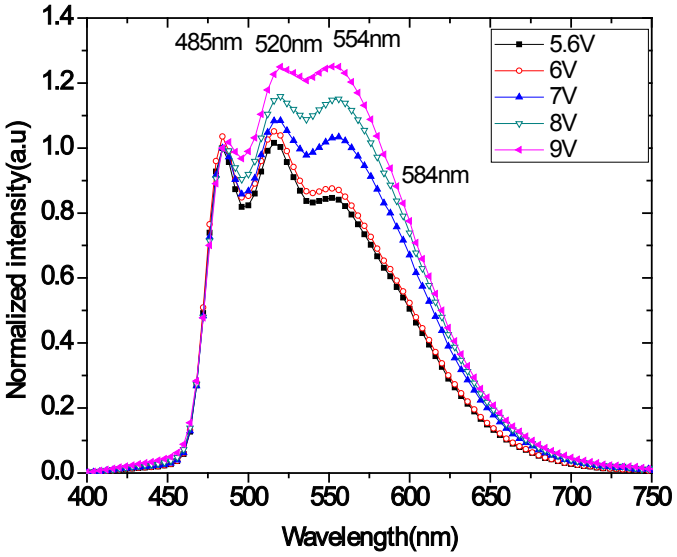

Figure 5.2 The EL spectra for Device 1 with dual emissive layer

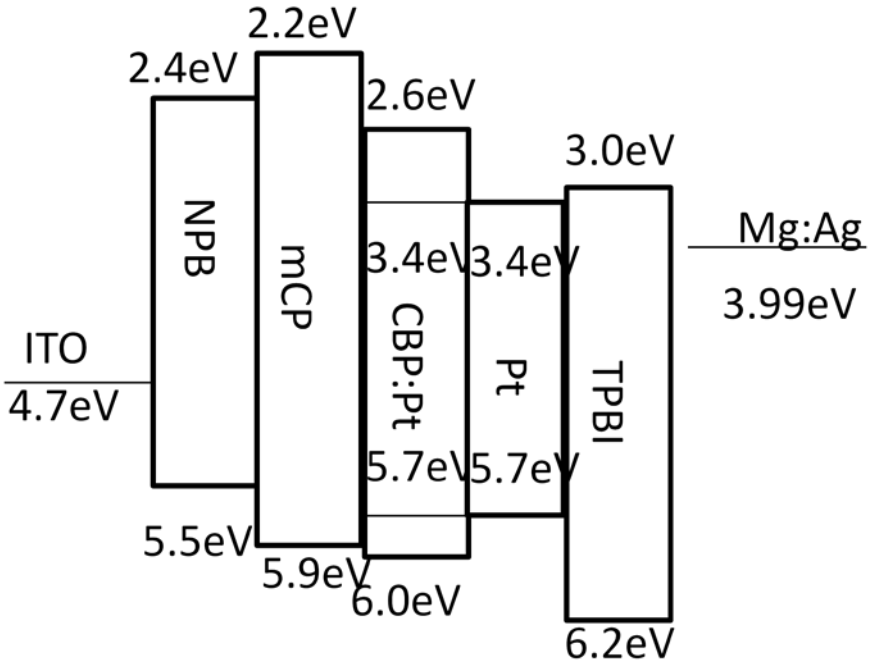

Figure 5.3 Band diagram of dual emissive layer devices

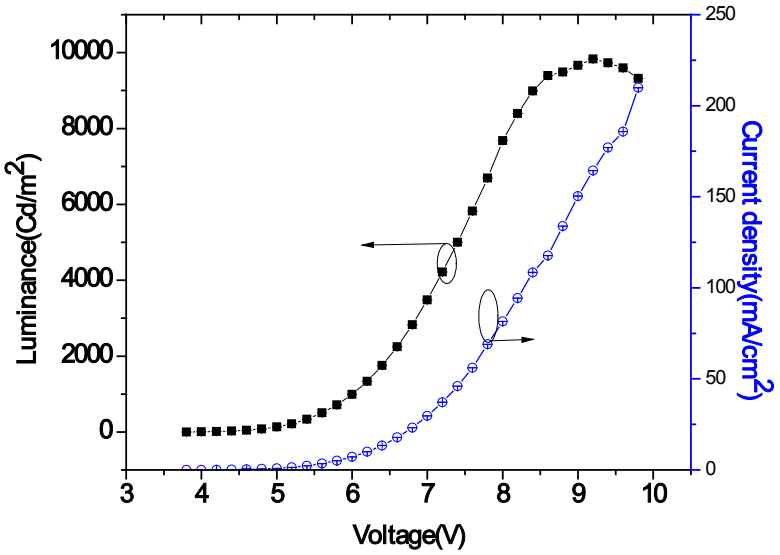

Figure 5.4 J-V-L characteristic of Device 1

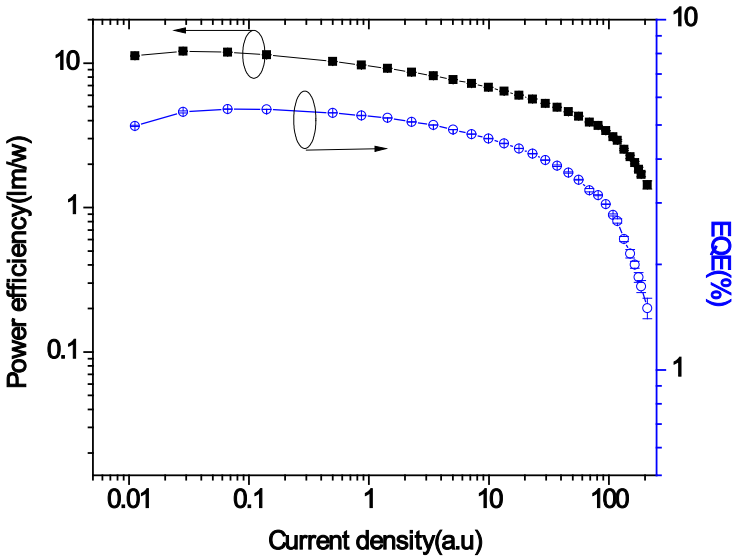

Figure 5.5 Efficiency as a function of current density of Device 1

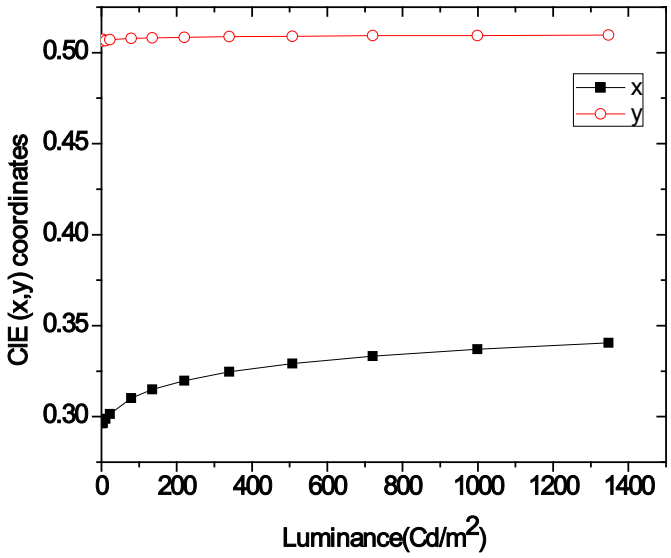

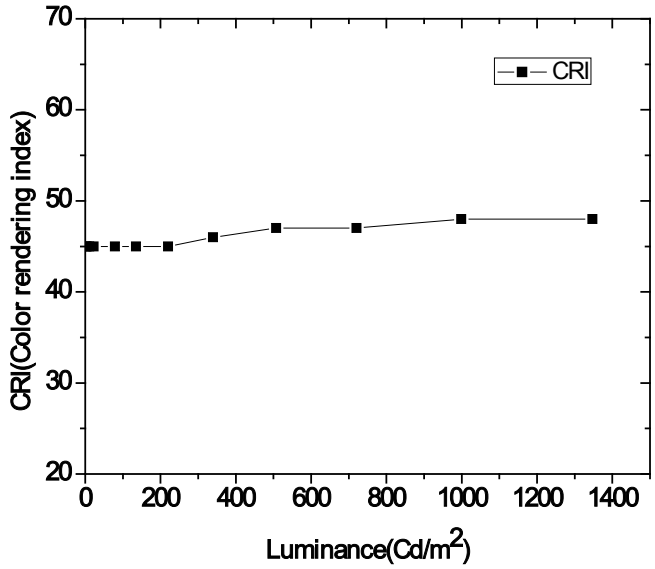

Figure 5.6 (Color online) CIE and CRI vs luminance for Device1

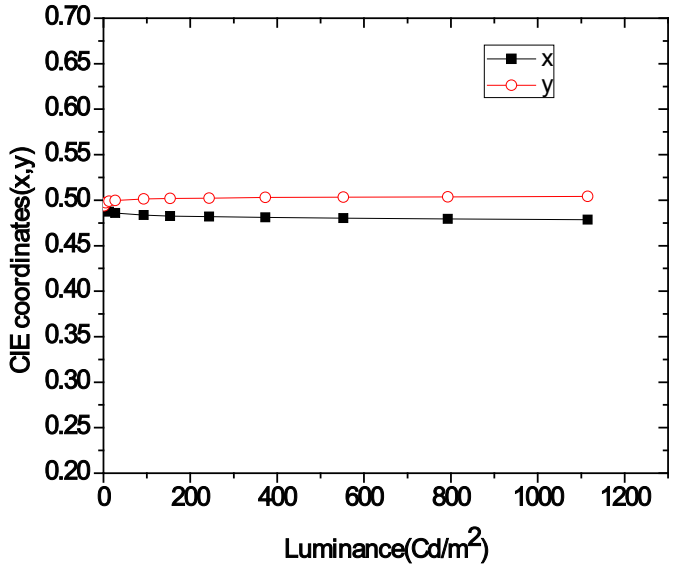

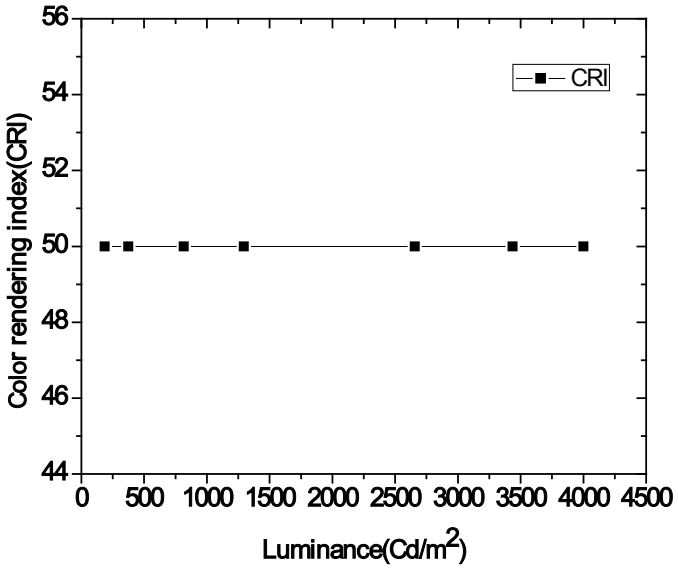

Figure 5.7 (Color online) CIE and CRI vs luminance for neat devices [ITO/NPB(40nm)/mCP(10nm)/CBP: $Pt(ptp)_2$ (25nm)/TPBI(30nm)/Mg:Ag]

Device 2 was fabricated with a thicker neat film layer and a second layer with an even lower concentration of $Pt(ptp)_2$ doped into CBP, in order to achieve more balanced white light emission. The WOLED includes 40 nm of NPB as a hole transporting layer, 10nm mCP as the electron blocking layer, 12 nm of 5% Pt(ptp) doped into CBP, 36 nm of neat $Pt(ptp)_2$ as the second emitting layer and 30 nm of TPBI as electron transport layer. Fig 5.8 shows the EL spectra of the WOLED. The decreasing of orange emission intensity at 588 nm at higher current density indicates that the recombination zone expands from the neat film region at low voltage into the 5% doped CBP region at higher bias, causing slight changing in the CIE coordinates and the CRI. The shoulders at 488 nm and 520 nm in the EL spectra are attributed to the doped layer. Fig 5.9 shows the Current density-voltage-luminance (J-V-Luminance) characteristics and Fig 5.10 is a plot of the efficiencies as a function of current density. The device luminance reached 11,600cd/m² at an applied bias of 10.6 V, and the

maximum quantum efficiency was 12.8 % at 5.4 V (See table 5.1). The CIE coordinates change from (0.49, 0.49) at 50 cd/m² to (0.47, 0.49) at 1000 cd/m², and the CRI changes from 57 to 59 (Fig 5.11). This WOLED structure shows a higher CRI since the $Pt(ptp)_2$ phosphorescence from the neat film layer is more intense, and results in a more balanced warm light. However, the color balance still needs to be adjusted for higher CRI. The correlated color temperature (CCT) as a function of CIE coordinates is shown in Fig 5.12. Based on the color temperature of these WOLEDs, their emission is categorized as "warm".

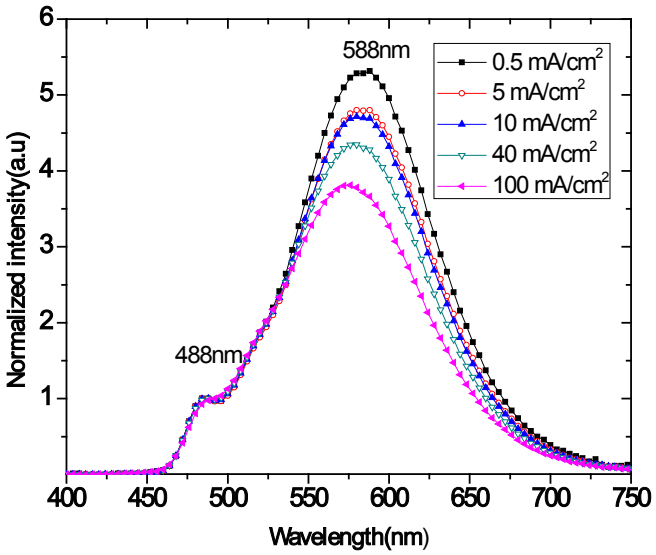

Figure 5.8 Normalized EL spectra vs current density for Device 2

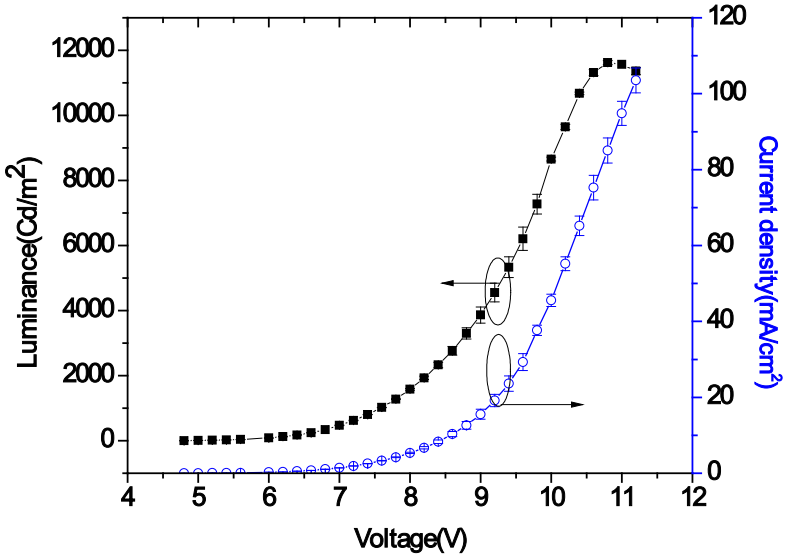

Figure 5.9 J-V-L characteristic for Device 2

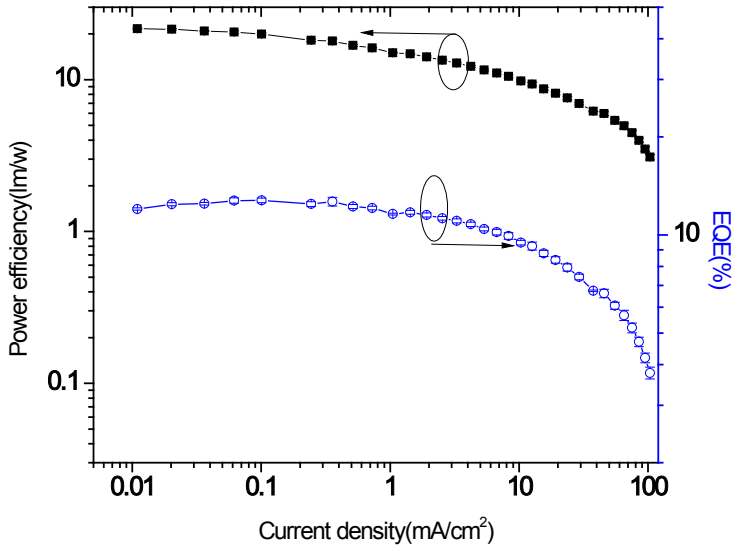

Figure 5.10 Efficiency as a function of current density

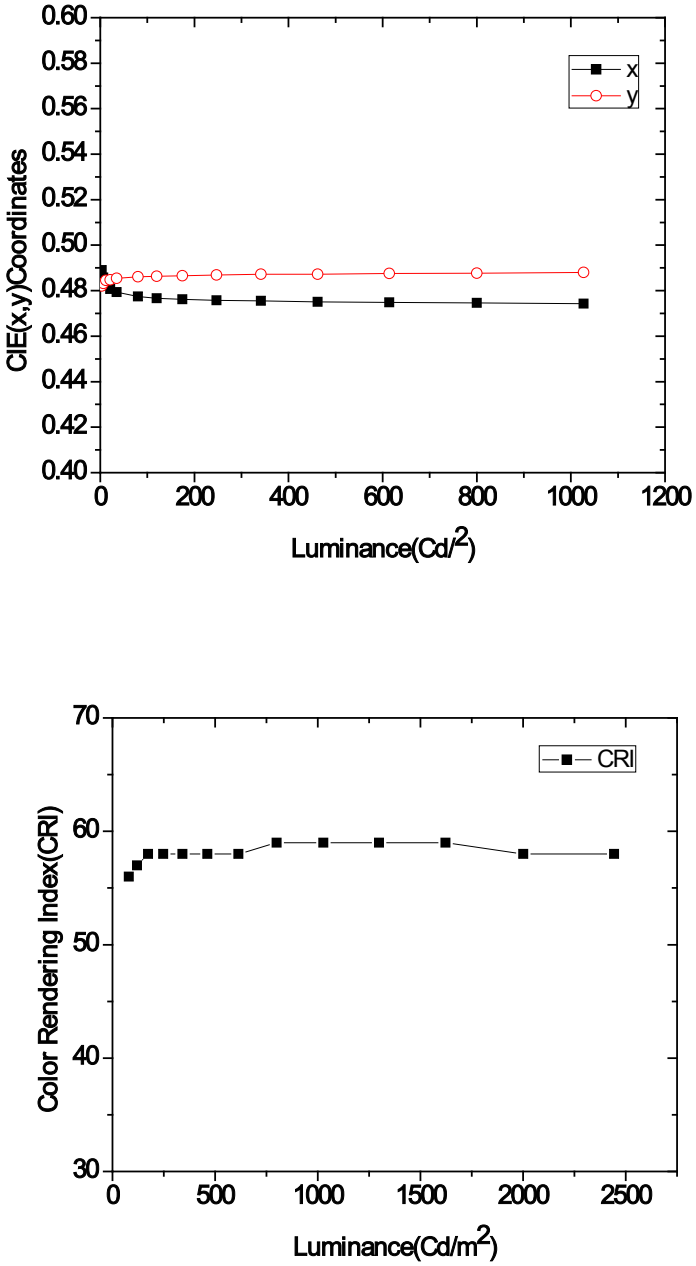

Figure 5.11 (Color online) CIE and CRI vs luminance for Device2

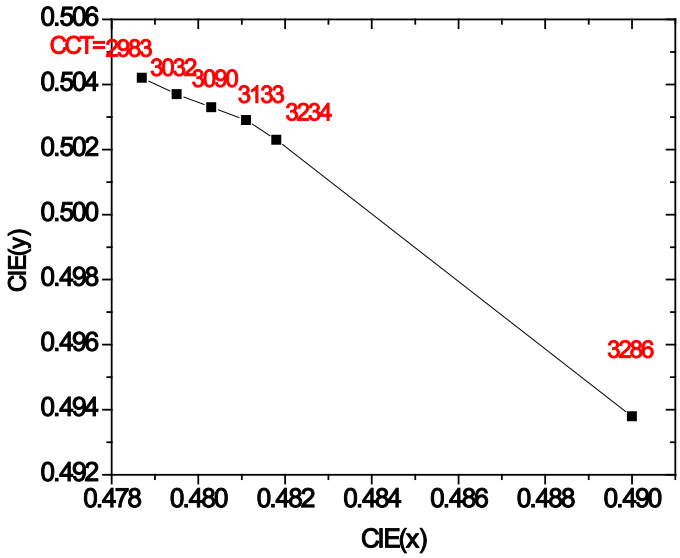

Figure 5.12 CCT vs CIE(coordinates) for Device 1(top) and Device 2(bottom)

Table 5.1 Summary of device characteristics for the two devices. The device structures are shown in Fig 5-1.

Device	**Turn on voltage (V@> 1Cd/m^2)**	**Current density:J(mA/cm^2@turn on V**	**Luminance (Cd/m^2) @ Turn on voltage**	**Peak Quantum efficiency(%)**	**Peak Power efficiency**	**Power efficiency/EQE at 500 Cd/m^2**	**Power efficiency /EQE at 1000Cd/m^2**
Device 1	3.8	0.011	1.5	5.6%	12.1	8.2lm/w /5.0%	7.2 lm/w / 4.7%

Device 2	4.8	0.010	3.5	12.8%	21.7	14.5lm/w /11.5%	12.6lm/W/10.8%

5.3 "Warm" WOLEDs by Mixing of Excimer and Exciplex emissions

The EML reported here consists of $Pt(ptp)_2$ as a dopant and 4,4′′ -tris-(3-methylphenylphenylamino)triphenylamine Mtdata as a host co-evaporated at a 1:20 ratio onto another 5% $Pt(ptp)_2$ doped CBP layer. The hole transport layer is NPB and the electron blocking layer is mCP in this structure. The band diagram and device structure (Device 3) are shown in Fig 5.13. Fig 5.14 shows the PL spectra of 5% $Pt(ptp)_2$ doped into Mtdata. The emission around 605 nm could come from two kinds of emissive states: (1) triplet excimers $^3(AA^*)$= excited homo-molecular dimmers of the acceptor ($Pt(ptp)_2$) that falls apart in the ground state producing excimer phosphorescence or (2) excited hetero-molecular dimers [exciplex $^3(DA)^*$] producing exciplex phosphorescence [2]. Both excimers and exciplex lack a bound ground state and efficient energy transfer from the hosts to light emitting dopants [3] can occur. Fig 5.15 shows the EL spectra of the WOLED. The varying relative emission intensities at 480 nm, 520 nm and 600 nm suggest that the recombination zone expands from 5% $Pt(ptp)_2$ in CBP to 5% $Pt(ptp)_2$ in Mtdata at higher applied bias voltage, causing slight changes in the EL spectra and CIE coordinates. The CIE coordinate changes from (0.34, 0.49) at 50 cd/m² to (0.37, 0.49) at 900 cd/m², while the WOLED shows a large shift in CRI from 53 to 63 (Fig 5.16). From the J-V-L characteristics in Fig 5.17, the turn on voltage is 8 V, which may due to the low electron mobility in Mtdata. Only at higher voltage, electrons can

tunnel through the Mtdata and recombine holes in the CBP:Pt layer. At even higher voltages holes are transported to the Mtdata layer and as a result the emission around 600 nm begins to increase. All the efficiency numbers (shown in Fig 5.18 and table 5.2) are low due to low luminance and high turn-on voltages.

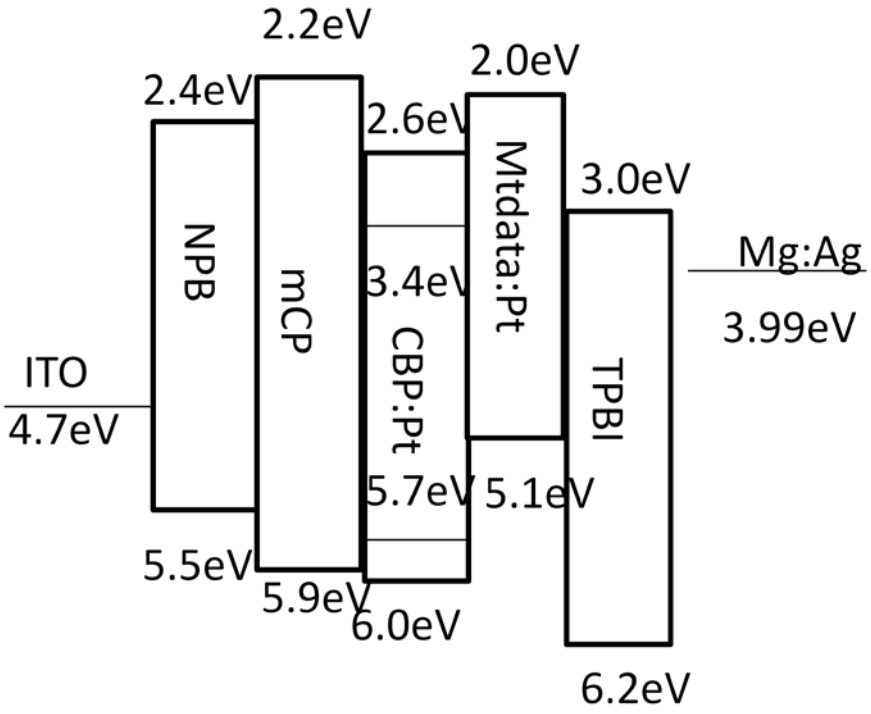

Figure 5.13 Band diagram of warm WOLEDs with different host (Device 3)

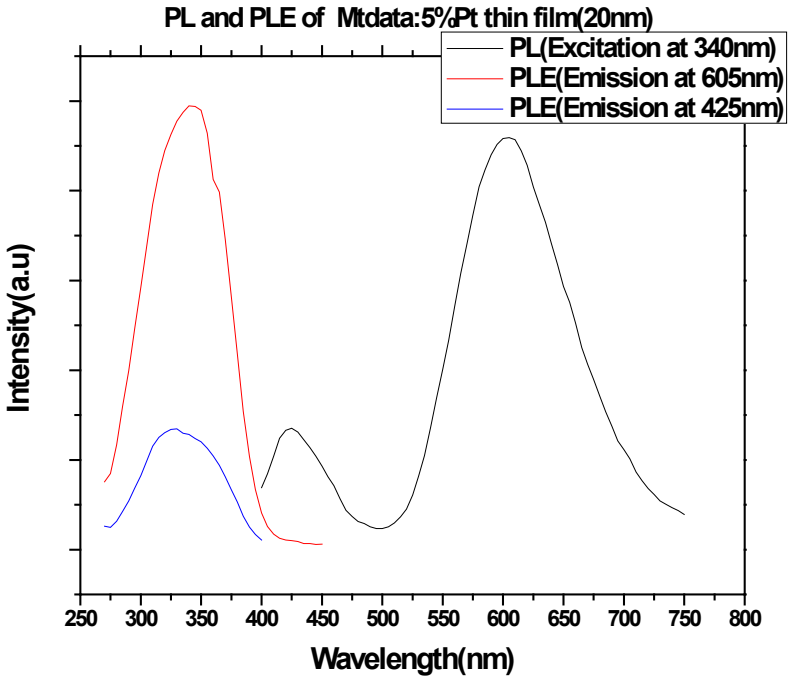

Figure 5.14 The PL spectra of 5% $Pt(ptp)_2$ doped into Mtdata

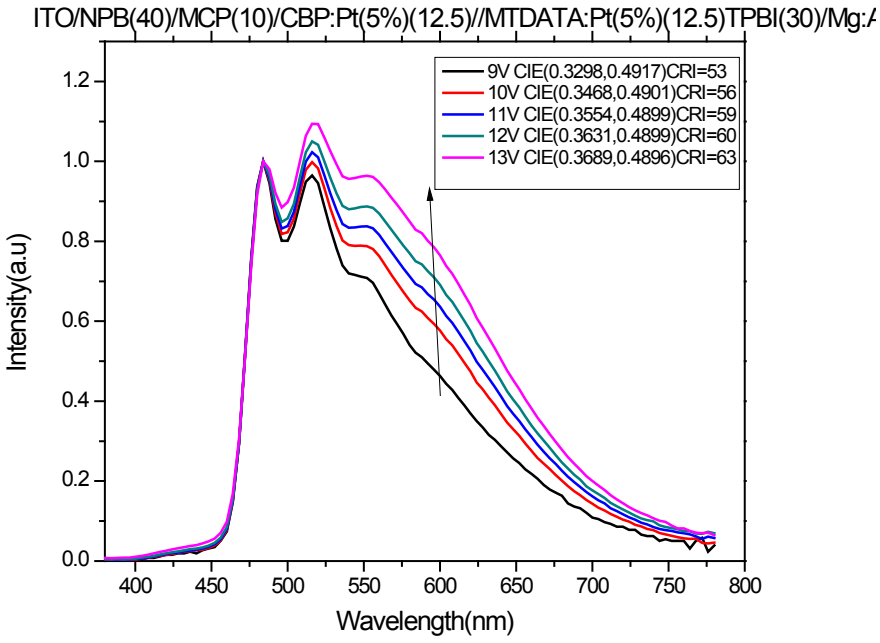

Figure 5.15 Normalized EL spectra vs applied bias for the Device 3

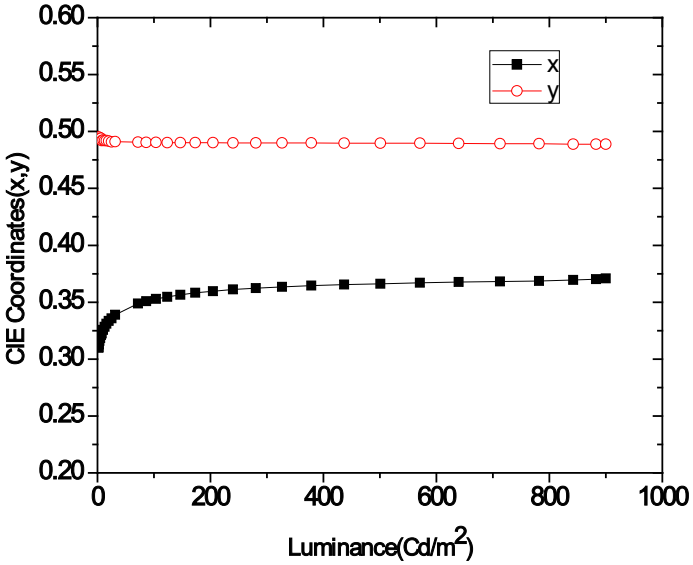

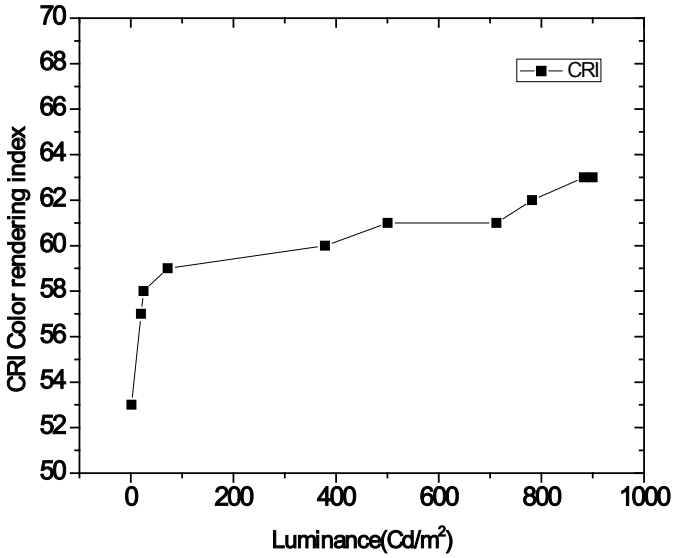

Figure 5.16 (Color online) CIE and CRI vs luminance for Device 3

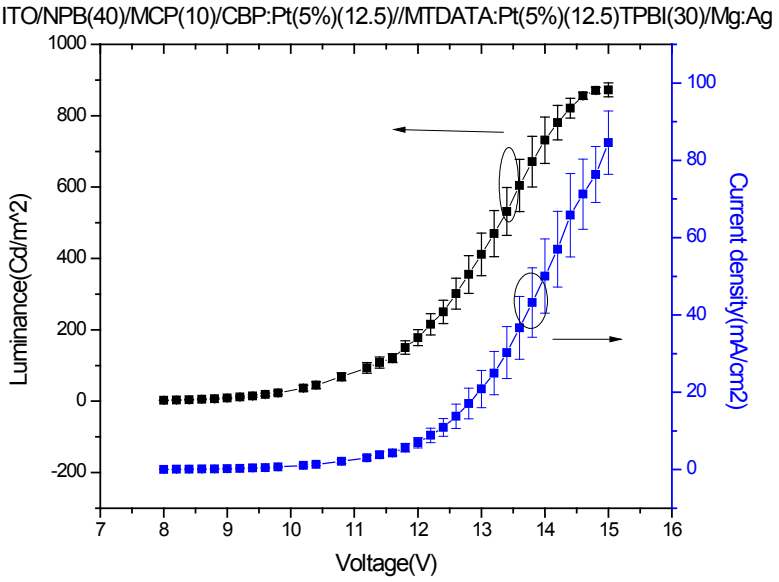

Figure 5.17 J-V-L characteristic for Device 3

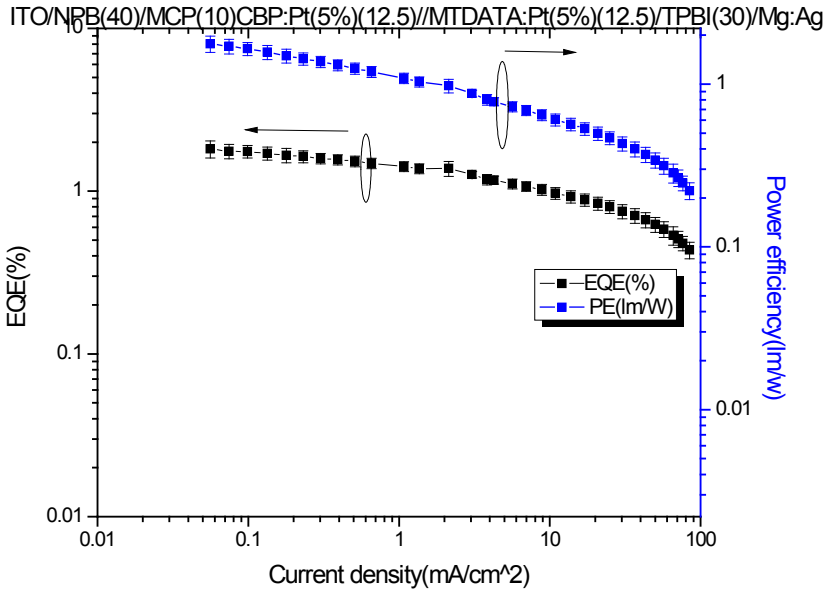

Figure 5.18 Efficiencies as a function of current density

Table 5.2 Summary of device characteristics for the Device 3

PE_{peak} (lm/W)	EQE_{peak} (%)	Brightness	CIE_{peak} (x, y)	CRI_{peak}	Turn on
1.77±0.22	1.81±0.23	6130	(0.3298,0.4917)	53	8

5.4 "Cool" WOLEDs

Sun et al. [2] demonstrated a white emitting structure which combined a fluorescent blue dopant with green and red phosphorescent dopants to yield high power efficiency and stable color balance. Here, a simplified structure based on the work of Bhansali et al [1] combines the deep blue emission layers from BCzVBi as a fluorescent dopant with the broad yellow emission layer from high concentrations of $Pt(ptp)_2$ doped into CBP . Two undoped, spacer CBP layers are included in the structure as shown in Fig 5.19 to provide insights to recombination zone effects [1]. The device fabrication procedures are essentially as have been described previously. The deposition rates for CBP:BCzVBi layers were 3.8 Å/s and 0.2 Å/s respectively and for the CBP: $Pt(ptp)_2$ layers were 0.31 Å/s and 0.25 Å/s respectively. $Pt(ptp)_2$ devices singly at 37% display combined monomer/excimer phosphorescence with a dominant emission wavelength of around 570 nm (yellow) and CIE of (0.41, 0.52). The approach to obtaining white emission here, is mixing the yellow $Pt(ptp)_2$ emission with the blue (λ~450nm) fluorescence emission from BCzVBi. Fig 5.20 is the EL spectra of the WOLED (Device 4). The varying relative emission intensities of BCzVBi and $Pt(ptp)_2$ indicate the expansion of the recombination zone from the fluorophore-doped regions at lower applied bias into the phosphor-doped regions at higher applied bias. The CIE

coordinates change from (0.28, 0.31) at 100 cd/m² to (0.29, 0.33) at 1000 cd/m², while the WOLED shows a shift in CRI from 77 to 75 (Fig 5.21). The J-V-L characteristic is shown in Fig 5.22. The luminance of Device 4 is 8000 cd/m² at an applied bias of 10 V. A maximum power efficiency of 6.7 lm/W at 5.4 V and quantum efficiency of 5.7 % at 6.2 V were obtained as is shown in Fig 5.23. It has been proposed that electron and holes mainly recombine in the top CBP:BCzVBi layer at lower applied bias, and that the recombination zone expands to the CBP: $Pt(ptp)_2$ layer at higher applied bias. The above device based on the work of Bhansali et al [1] was used as a "control" structure for Device 5 wherein the bottom BCzVBi doped CBP layer and the spacer layer on top of it were removed from the OLED stack as is illustrated in Fig 5.24. Compared to the EL spectra of Device 4, Device 5 (Fig 5.25) produced a higher intensity of BCzVBi emission (λ~450nm) at higher current density, indicating the recombination zone expanded from the CBP:$Pt(ptp)_2$ layer to CBP:BCzVBi layer at higher applied bias. Device 5 exhibited a maximum quantum efficiency of 6.82% at 4.8 V and power efficiency of 12.6 lm/W at 4.4V (shown in Fig 5.26). The increase of both power and external quantum efficiency for Device 5 (Table 5.3) suggests that the bottom CBP:BCzVBi layer accounts for the main efficiency reduction. However, the CRI and CIE suffer when this bottom CBP:BCzVBi layer (Fig 5.27 and 5.28) is removed. The CIE coordinates change from (0.31, 0.45) at 100 cd/m² to (0.30, 0.44) at 1000 cd/m², while the WOLED shows a shift in CRI from 69 to 67 (Fig 5.28). By omitting the bottom CBP:BCzVBi and spacer layer, better charge balance with the onset of exciton imbalance of Device 5 compared to Device 4 is achieved. Electrons and holes are prone to pile up at the interfaces of the EML/ETL and EML/HTL and experiments have been done to prove that by

Sun et al in similar structures [2]. The exciton formation probability, which is densities of electrons (n) × densities of holes (p), is also significantly higher at these interfaces compared to the EML bulk. By omitting the bottom CBP: BCzVBi and spacer layer, excitons only form at the interface of EML/ETL. The singlet excitons which are formed in this region will be transferred to fluorescent dopant of BCzVBi and triplet excitons will diffuse to phosphorescent dopant of $Pt(ptp)_2$. Higher EQE and power efficiency have been achieved by device 5 can be explained as by reducing the exciton formation zone to only one ,energy loss in the process of triplet diffusion to phosphorescent dopant and singlet transferring to fluorescent dopant has been reduced. However, comparing EL of device 4 and device 5, significant reduction in the blue emission region is observed as a result of the missing of the bottom CBP:BCzVBi and spacer layer. The CCT categories these devices in the cold WOLED range.

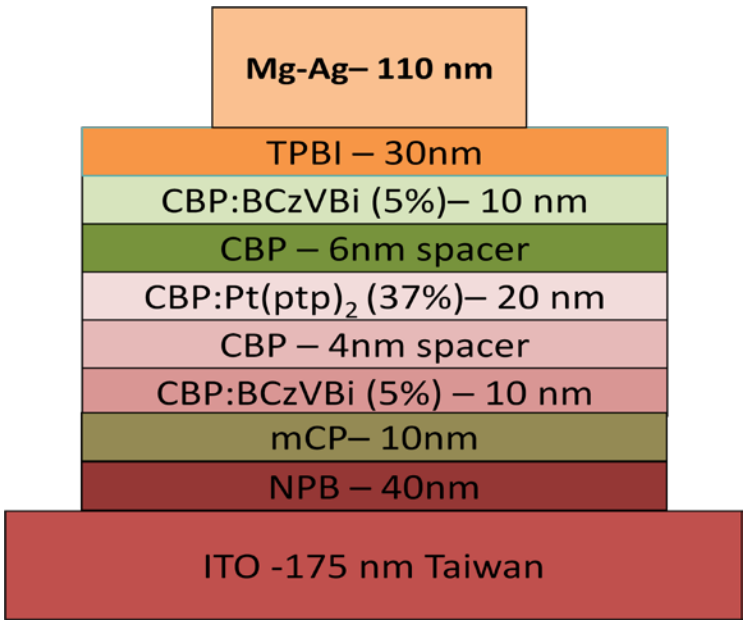

Figure 5.19 Device architectures of Device 4

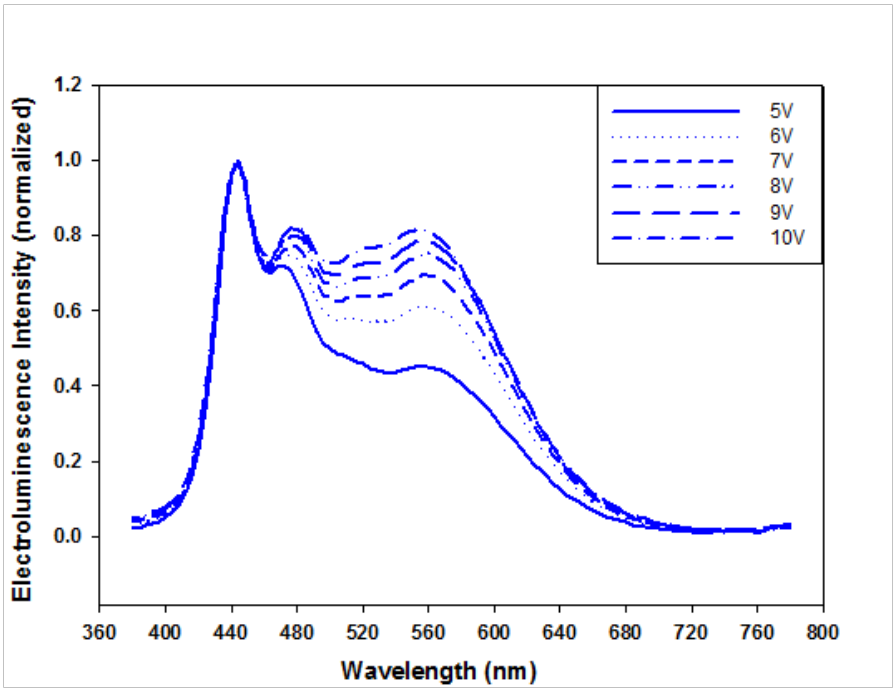

Fig 5.20 EL spectra of Device 4

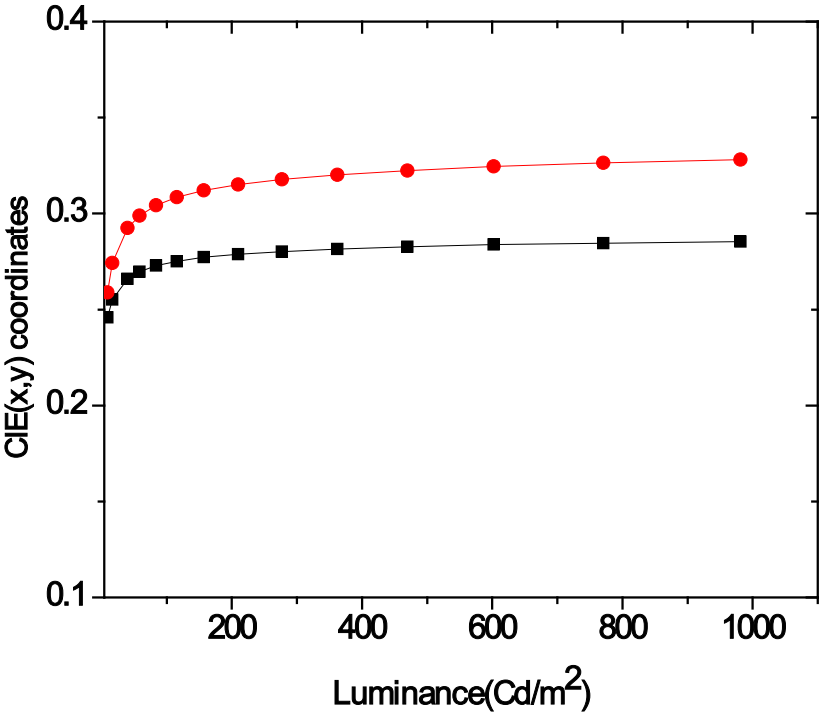

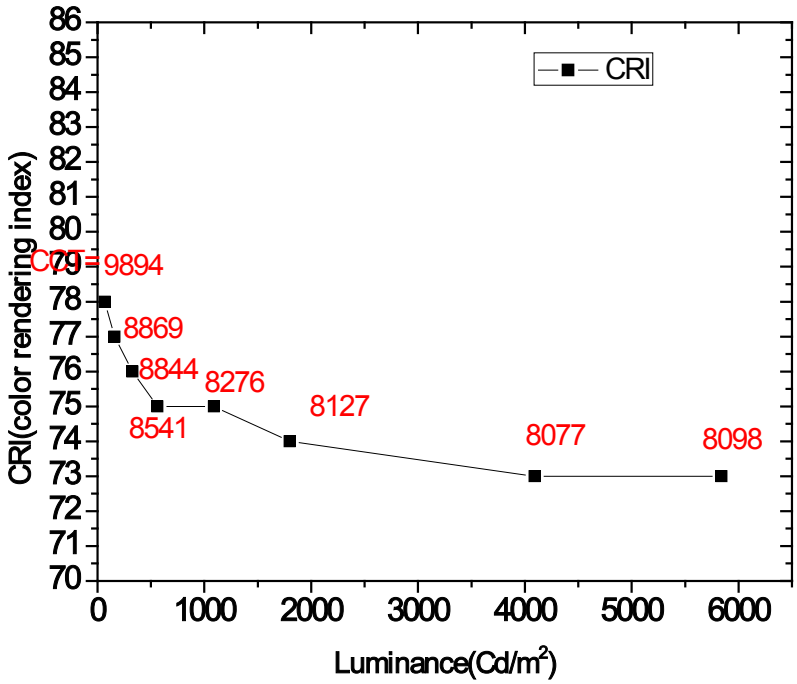

Figure 5.21 CIE coordinates and CRI shifting as a function of voltage for Device 4

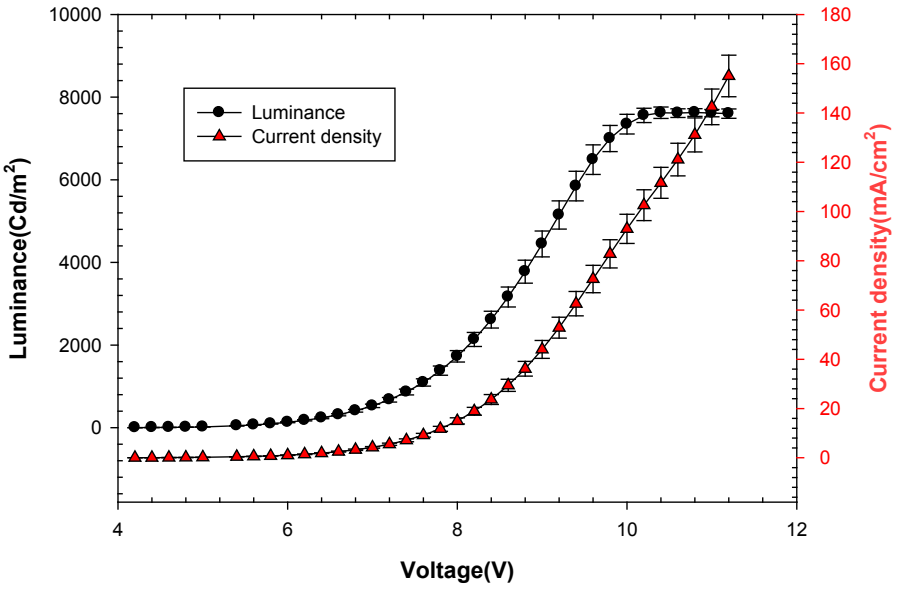

Figure 5.22 J-V-L characteristic of Device 4

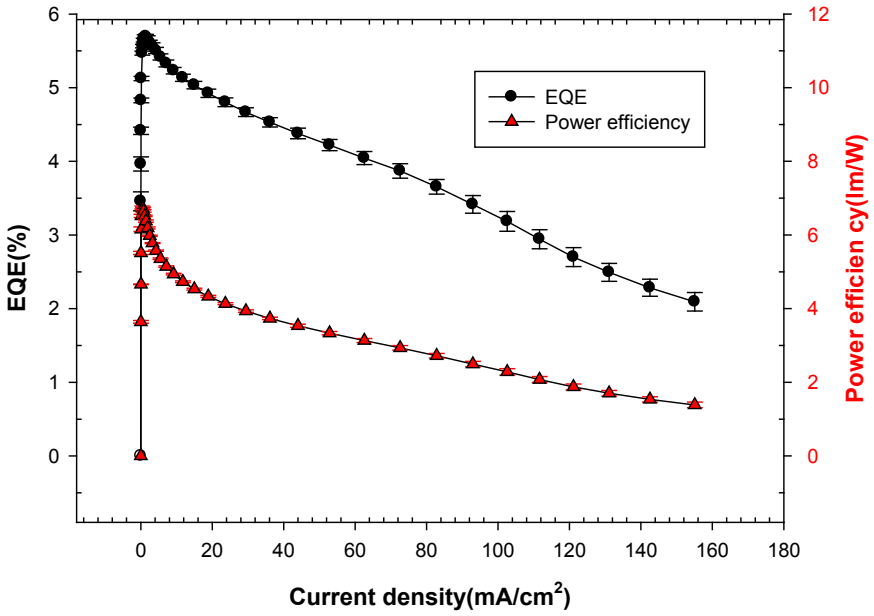

Figure 5.23 Efficiencies as a function of current density for Device 4

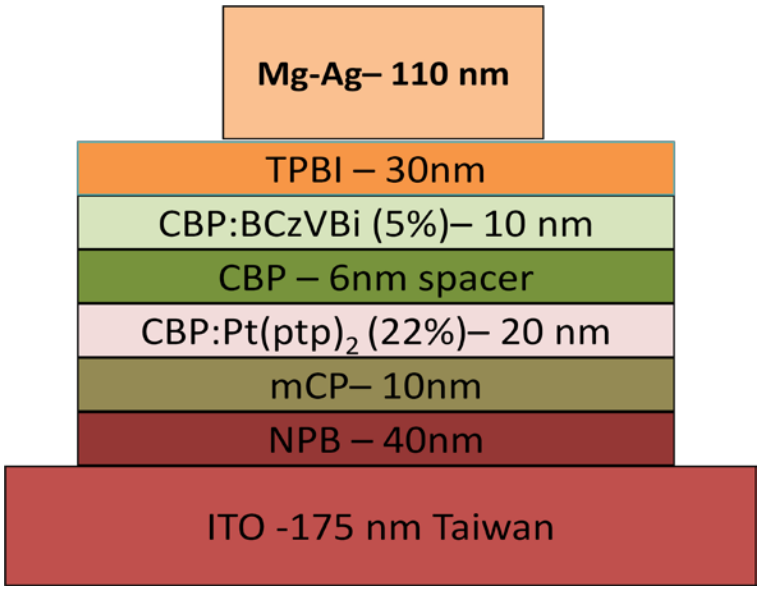

Figure 5.24 Device architectures of Device 5

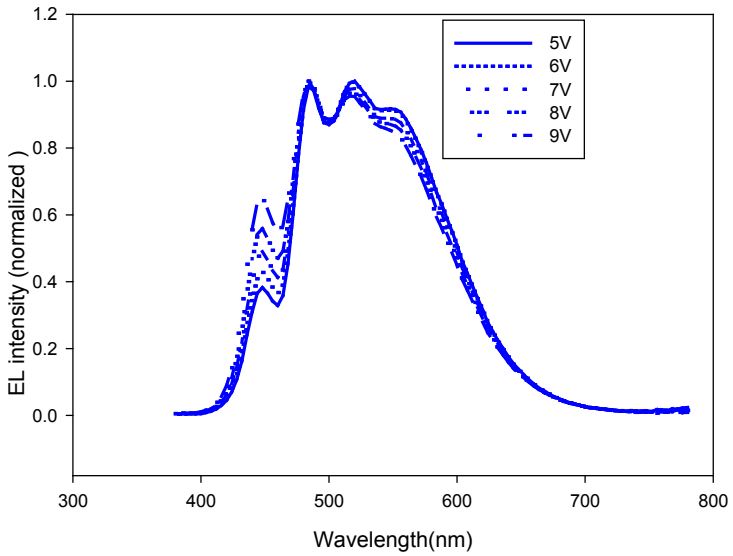

Figure 5.25 Normalized EL spectra vs voltage for Device 5

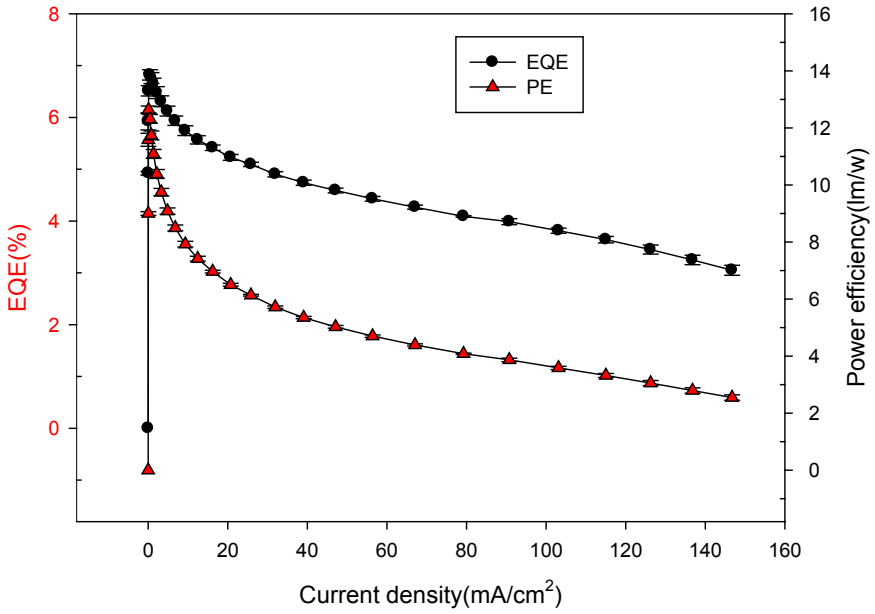

Figure 5.26 Efficiencies as a function of current density for Device 5

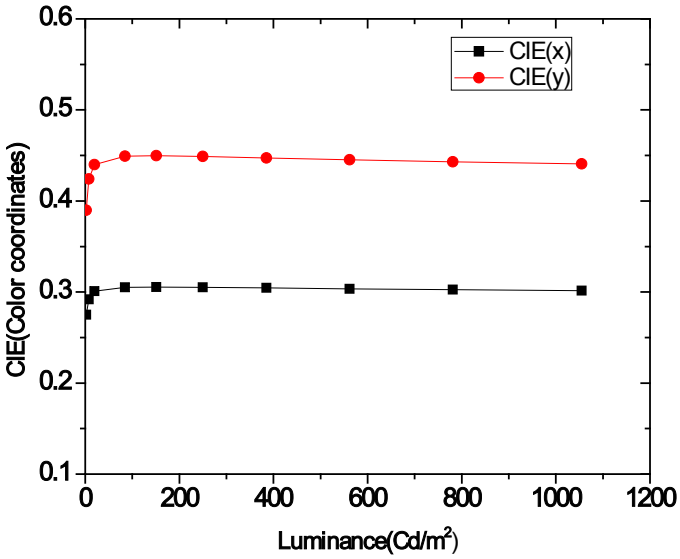

Figure 5.27 CIE (coordinates) as a function of luminance for Device 5

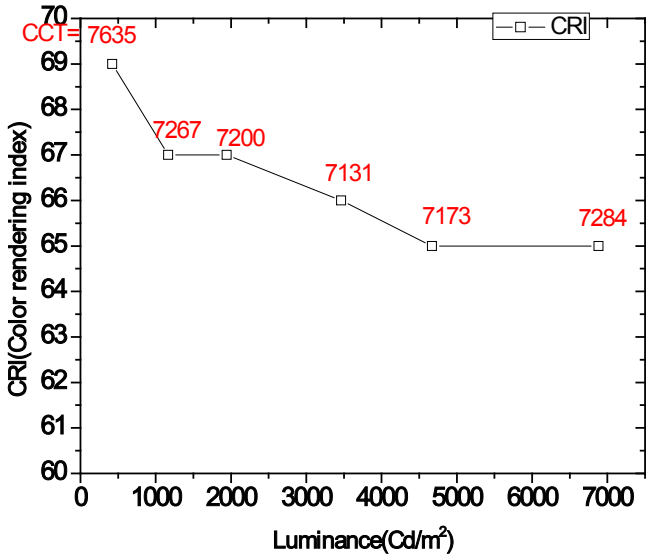

Figure 5.28 CRI and CCT as a function of luminance for Device 5

Table 5.3 Summary of device characteristics for Device 1 and Device 2

Device	**Turn on voltage**	**Current density :J(mA/cm^2 @turn on V**	**Luminance (Cd/m^2) @ Turn on voltage**	**Peak Quantum efficiency(%)**	**Peak Power efficiency**	**Power efficiency/EQE at 500 Cd/m^2**	**Power efficiency /EQE at 1000Cd/m^2**
Device 4	4.2	0.019	1.0	5.7% at 6.2V	6.7lm/w at 5.4V	5.6lm/w/ 5.5%	4.9lm/w 5.2%
Device 5	4.0	0.015	1.7	6.8% at 4.8V	12.6 lm/W at 4.4V	9.8lm/w/ 6.3%	8.5lm/W/5.9 %

5.5 References:

[1]. U.S.Bhansali,H.Jia,M.A.Quevedo Lopez,B.E.Gnade,W-H Chen,and M.A.Omary,Applied Physics Letters **94**, 203501 (2009)

[2].Y.Sun,N.C.Giebink,H.Kanno,B.Ma,M.E.Thompson,andS.R.Forrest,Nature(London)**440**, 908(2006)

CHAPTER 6

CONCLUSION AND FUTURE WORK

6.1 Structural, Chemical, Photoluminescence and Lifetime of $Pt(ptp)_2$ Thin Films

$Pt(ptp)_2$, a non–organometallic/non–cyclometalated square-planar complex without C–Pt bonds has been doped into CBP thin films with varying concentration levels, and it was found that with increased doping the spectral character of the PL red-shifts, and progressively changes from monomer- to excimer-dominated emission. This result is consistent with an increase in the number of paired $Pt(ptp)_2$ molecules with the separation required for excimer formation as the dopant concentration increases. The excited state lifetime decreases from 17.71μs for CBP films doped at 5% to 114ns for neat $Pt(ptp)_2$ films as a result of "self-sensitization" effect, while the quantum yield number increases from 25.2% for 5% doped CBP thin films to 51.7% for the 65% thin film and decrease to 23% for the neat $Pt(ptp)_2$ films which could be due to the two energy transfer mechanism competition. The ellipsometry measurements show that the refractive indices of the doped and undoped films are the same (n=1.801).

6.2 Near-white and Tunable Electrophophorescence From Bis[3.5-bis(2-pyridyl) - 1,2,4-triazolato]Platinum(II)-Based Organic Light Emitting Diodes

The thickness of the CBP: $Pt(ptp)_2$ and TPBI device layers were first maintained at 25nm and 30nm respectively while varying the thickness of the NPB hole transport layer (HTL) from 25nm to 50nm. A NPB thickness of 40nm produced the maximum peak power

efficiency and external quantum efficiency of 8.74lm/W and 4.09% respectively. The maximum numbers were reduced to 2.60lm/W and 2.18% at device drive levels that produced 1000Cd/m². The peak power efficiency for devices with a thicker HTL of 50nm was lower at 5.40lm/W, which decreased to 1.78lm/W under drive conditions that produced 1000Cd/m². The efficiency decrease with increase HTL layer thickness is interpreted as an indication of charge imbalance onset. With the HTL (NPB) thickness set at 40nm, the thickness of emissive layer (EML) was then varied from 8nm to 50nm. A slight improvement in device performance in terms of EQE (2.90%) and power efficiency (3.22lm/W) at 1000 Cd/m², was obtained by increasing the EML from 25nm to 50nm, which suggests good confinement of excitons in the bulk of the thicker emissive layer. The thickness of the HTL, EML and ETL were then maintained at 40nm, 25nm and 30nm respectively while the doping concerntration of $Pt(ptp)_2$ in CBP was varied. Doping levels of ~ 5-10 % were found to be optimal for both EL efficiency and white color coordinates which is due to simultaneous monomer and excimer emissions. The peak power and luminous efficiencies obtained were 9.8 lm/W and 14 cd/A respectively, while the peak external quantum efficiency was 6.6%. It is proposed that higher maximum power efficiency and external quantum efficiency were obtained in these devices featuring 1,3,5-tris(phenyl-2-benzimidazolyl) -benzene (TPBI) as the electron transport layer (ETL) due to the higher triplet energy and better exciton confinement of TPBI.

With all other layer thicknesses and constituents being the same, devices with 3,5'-*N,N'*-dicarbazole-benzene (mCP) as host were compared with devices with CBP as host. Lower turn on voltage and higher efficiency numbers are achieved by CBP as host. Adding

mCP as an electron blocking layer (EBL) while keeping all the other device layers unchanged increased the maximum quantum efficiency of the devices by roughly a factor of 3 with 15% doping, and a factor of 10 with doping between 25% to 45%. Efficiency numbers were also significantly increased by switching the cathode from Mg:Ag to LiF/Al which produced a reduction in threshold voltage.. The excited state lifetime in devices doped at higher decreases and is consistent with thin film radiative lifetimes for similar concentrations. It has been proposed that "self-sensitization" is responsible for the observed decreases [Ref], but more study is required to validate this hypothesis. Delayed EL was observed for devices doped at 65%, which is attributed to charge trapping and interfacial effects.

6.3 Chromatic Tuning of OLEDs Based on Bis[3, 5-bis(2-pyridyl)- 1,2,4-triazolato] Platinum(II)

Dual EML devices composed of neat $Pt(ptp)_2$ thin films emitting orange, and CBP: $Pt(ptp)_2$ thin films emitting blue-green color were fabricated and categorized as warm OLEDs. At 1000Cd/m² a CRI of 59 and CIE of(0.47,0.49) were achieved with a power efficiency of 12.6lm/W and EQE of 10.8%. Dual EML devices composed of both Mtdata and CBP as host produced more balanced white emission with a CRI of 63 and CIE(0.37,0.49). By combing fluorescent emission from BCzVBi and yellow broad-band phosphorescent emission from CBP: $Pt(ptp)_2$ device with two blue fluorescent emission layers as singlet filters,a CRI of 78, and CIE of (0.28,0.31) at 100Cd/m² , and a maximum power efficiency of 6.7lm/W and EQE of 5.7% were obtained.

6.4 Future Work

6.4.1 Enhancing Outcoupling Effect by Micro-Scale Lens [1] .

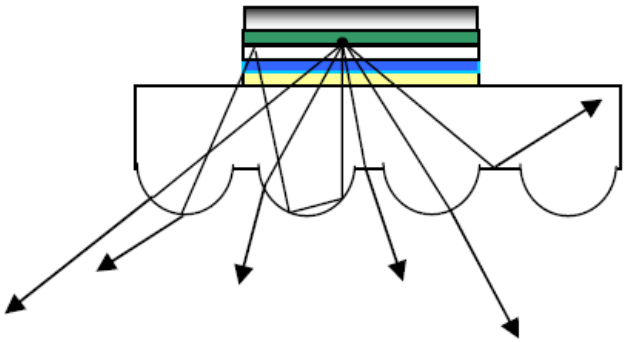

Figure 6.1 Microlens array on high index glass substrate. Reproduced from Reference [1]

Figure 6.1 is a schematic explanation of the method for enhancing light outcoupling from devices using a microlens array on high index glass substrate. Light is generated in the emissive layer. Total internal reflection of the emitting light at the substrate/organic interface could be eliminated, because the refractive index of the substrate is larger than that of the organic material. That is, waveguiding at the substrate/ITO/organic interface can be reduced. With a microlens array, modification of the glass-air interface angles is achieved, and more light is extracted from the device due to the variety of incidence angles and scattering opportunities for the light impinging from the device layers. It has been reported by H. J. Peng et al [1] that depending on the geometric structure and fill factor of the lens array, an increase of over 65% more light can be extracted from the OLED on the microlens substrate compared to a conventional device, without affecting the electrical performance. No color variation is induced by the microlens array.

6.4.2 Residual Potential Measurement for the Trapping Charge at the Interfaces.

An electrostatic voltmeter is used to measure the "residual potential" remaining in a material after a voltage is applied to the material under test in a capacitor setup. A schematic of the set up is shown below in Fig 6.2:

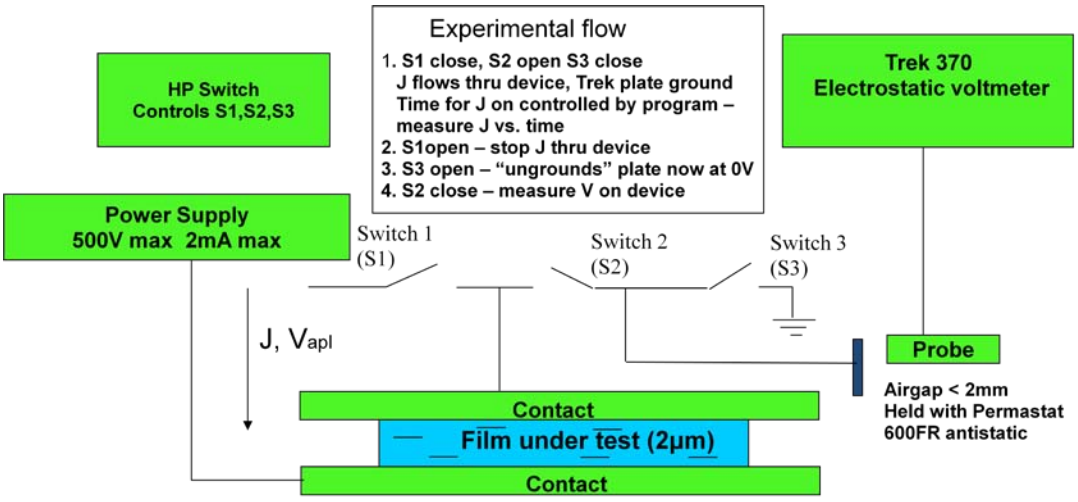

Figure 6.2 Residual potential measurement setup

The experiment follows three steps:

1) S1 close, S2 open, S3 close, current flow through the device ,and trek plats are grounded.
2) S1 open, stop current going through the device
3) S3 open, unground plates are at 0V
4) S2 close, measure V on device.

The potential in the material due to the trapped charge can thus be measured, which contribute to explaining the delayed EL phenomenon for the 65% devices discussed in Chapter 4 .

6.4.3 "Self-Sensitization" Theory

"Self-sensitization" theory which means for both thin films and devices, at higher concentration, emissive rate should be higher. Table 1 and Table 2 are the calculations of emissive rate for both thin films and devices. More data from devices are expected. $\Phi = \frac{kr}{knr + kr} = kr\Gamma$ This concept has been discussed in chapter 2.9.3.kr is the emissive rate and knr is the non-emissive rate, Γ is the radiative lifetime. Φ is quantum yield.

Table 6.1 Thin film emissive rate calculation at different concentrations

Doping (%)	Φ	Γ	kr
5%	0.252	17.71E-6	14229.25
65%	0.517	0.64E-6	807812.5
100%	0.23	0.11E-6	2090909

Table 6.2 Device emissive rate calculation at different concentrations

Doping (%)	EQE	IQE	Γ	kr
30%	0.094	0.47	9.44E-7	4.98E+07
100%	0.089	0.445	4.36E-7	1.02E+08

6.4 References

[1] H. J. Peng, Y. L. Ho, C. F. Qiu, M. Wong and H. S. Kwok SID 04 Digest 11.4, p.158